Макромолекулярная кристаллография на синхротронном источнике

А. Попов (ESRF)

Macromolecular Crystallography is a technique used to study biological molecules such as proteins, viruses and nucleic acids (RNA and DNA) to a resolution higher than ~5 Å. This high resolution helps elucidate the detailed mechanism by which these macromolecules carry out their functions in living cells and organisms.

DNA double helix: A, B, Z

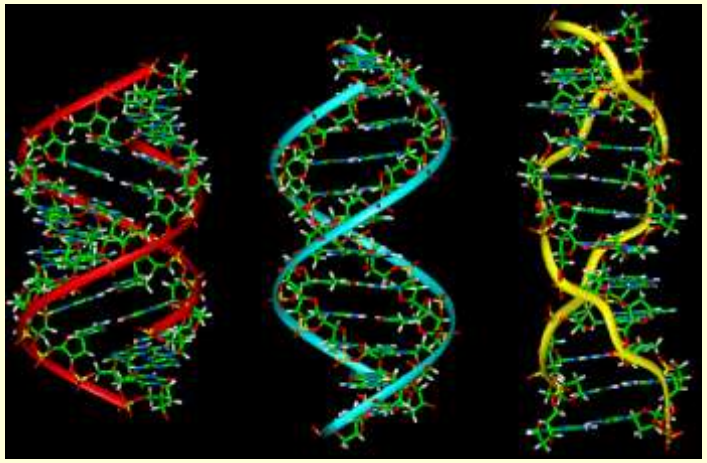

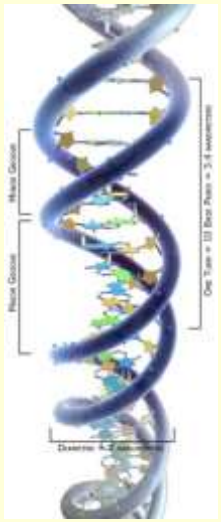

RNA molecules

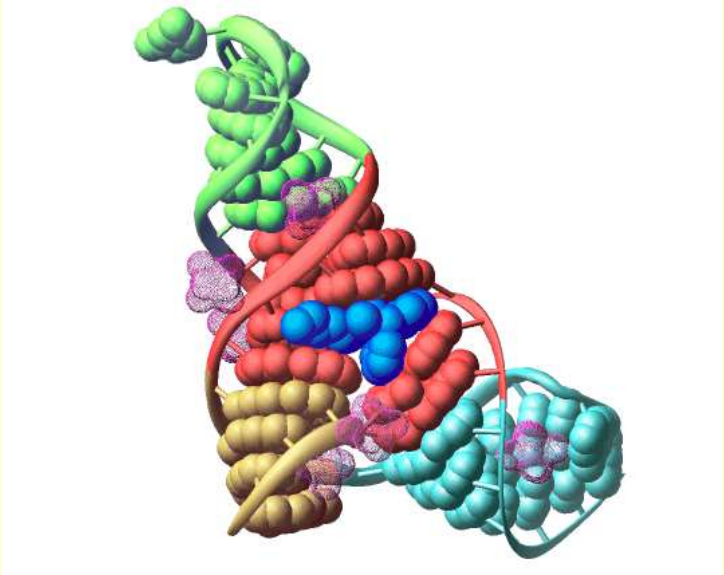

Viral suppressor of RNAi p19

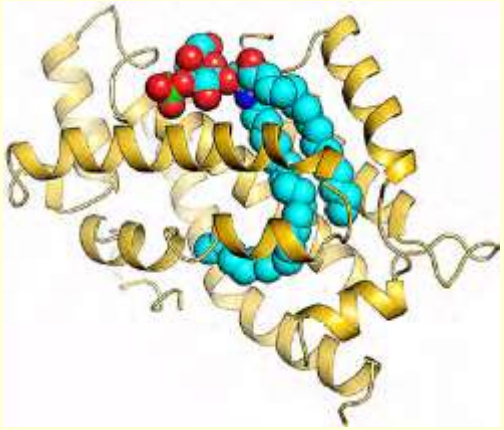

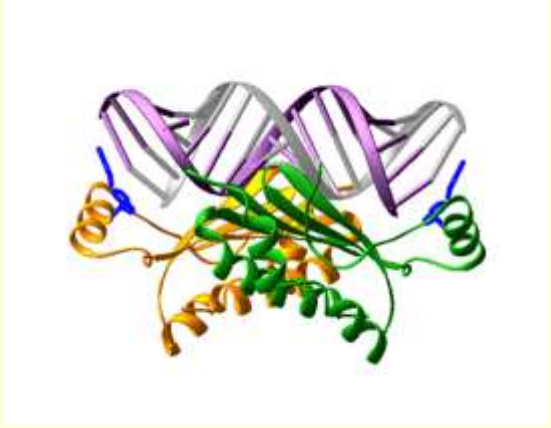

Minute Virus of Mice

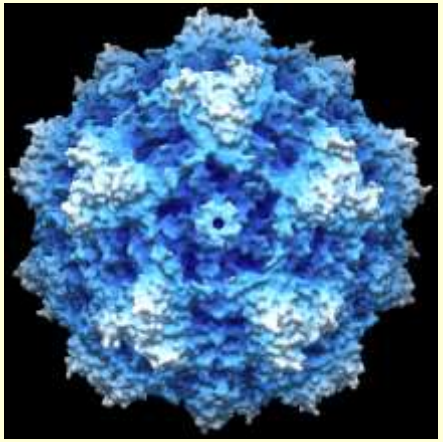

RCSB PDB | Deposit | Search | Visualize | Analyze | Download | Learn | More | MyPDB Login

RCSB PDB PROTEIN DATA BANK

An Information Portal to 127352 Biological Macromolecular Structures

Search by PDB ID, author, macromolecule, sequence, or ligands | Go

Advanced Search | Browse by Annotations

PDB-101 | Worldwide PDB | EMDataBank | NDB Nucleic Acid Database | StructuralBiology Knowledgebase | Worldwide Protein Data Bank Foundation

- Welcome
- Deposit
- Search
- Visualize
- Analyze
- Download
- Learn

A Structural View of Biology

This resource is powered by the Protein Data Bank archive-information about the 3D shapes of proteins, nucleic acids, and complex assemblies that helps students and researchers understand all aspects of biomedicine and agriculture, from protein synthesis to health and disease.

As a member of the wwPDB, the RCSB PDB curates and annotates PDB data.

The RCSB PDB builds upon the data by creating tools and resources for research and education in molecular biology, structural biology, computational biology, and beyond.

A Molecular View of HIV Therapy

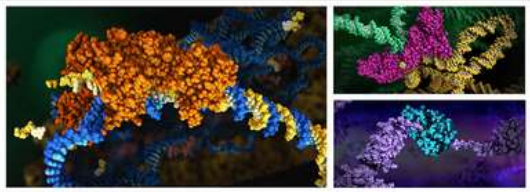

2016 FASEB BioArt Winner

View animation on PDB-101

March Molecule of the Month

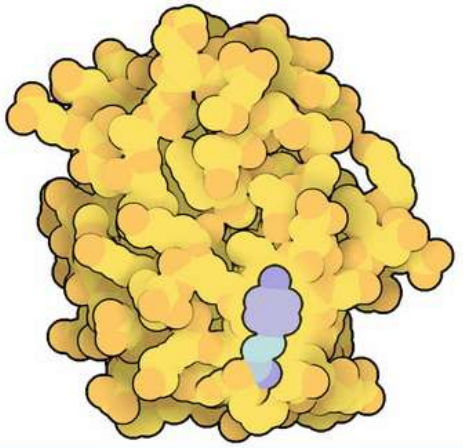

Photoactive Yellow Protein

Latest Entries

As of Tuesday Mar 07

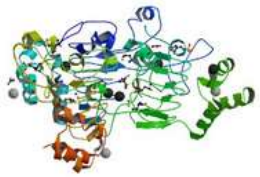

Features & Highlights

View Validation in 3D

Visualizing structure quality metrics in three dimensions » 10/11

Explore Ligand Interactions in 3D

Analyze small molecule interactions with NGL » 10/11

New Images for Transmembrane

News

Publications

Join our Development Team

We are looking for talented Postdoctoral Fellows to join our team at UC San Diego. » 03/07

View Structures and Pathways » 02/28

Enter the 2017 Video Challenge » 02/21

PDB

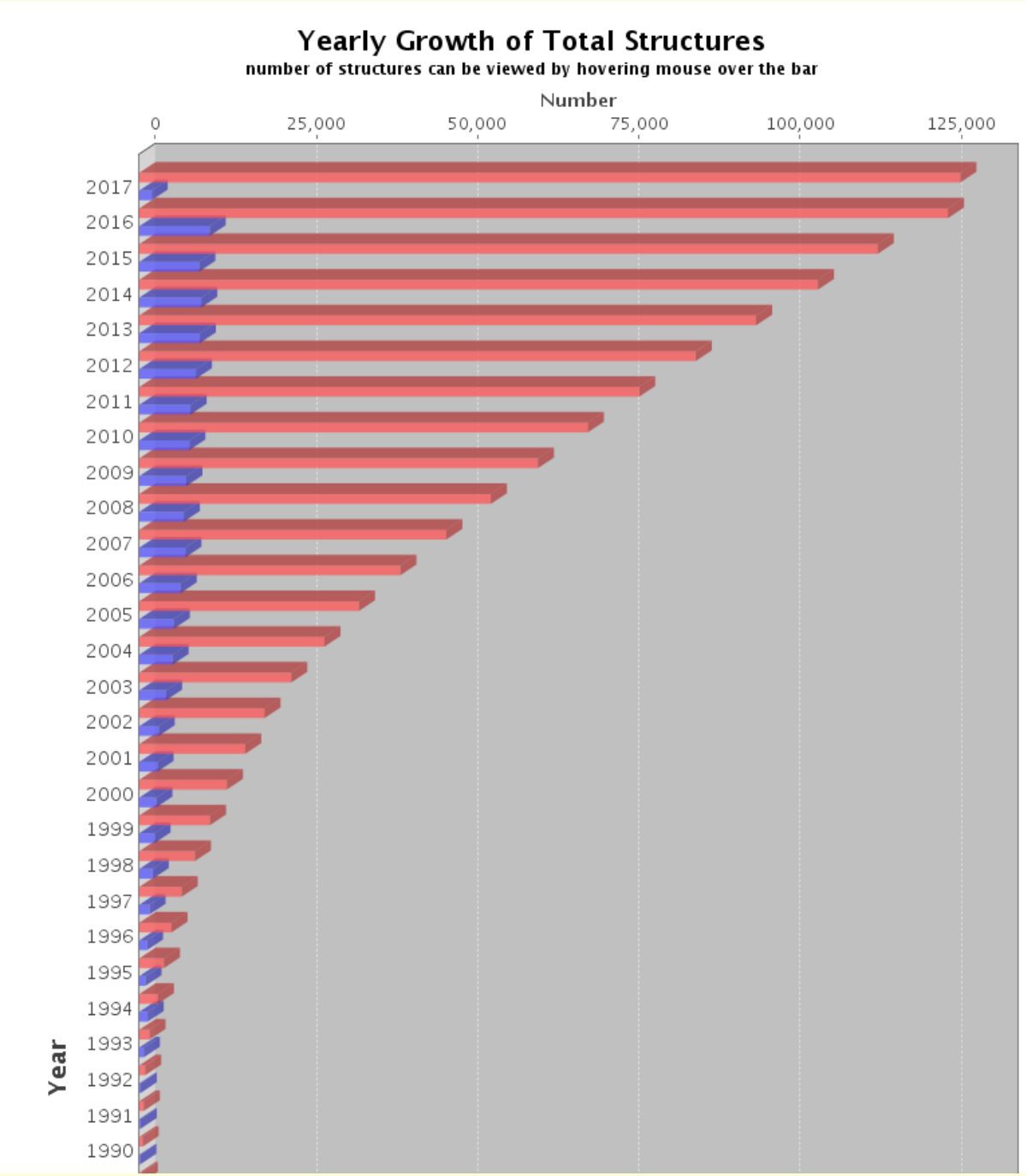
Yearly Growth of Total Structures
number of structures can be viewed by hovering mouse over the bar
Number
0
25,000
50,000
75,000
100,000
125,000
Year
2017
2016
2015
2014
2013
2012
2011
2010
2009
2008
2007
2006
2005
2004
2003
2002
2001
2000
1999
1998
1997
1996
1995
1994
1993
1992
1991
1990

Methods in Structural Biology

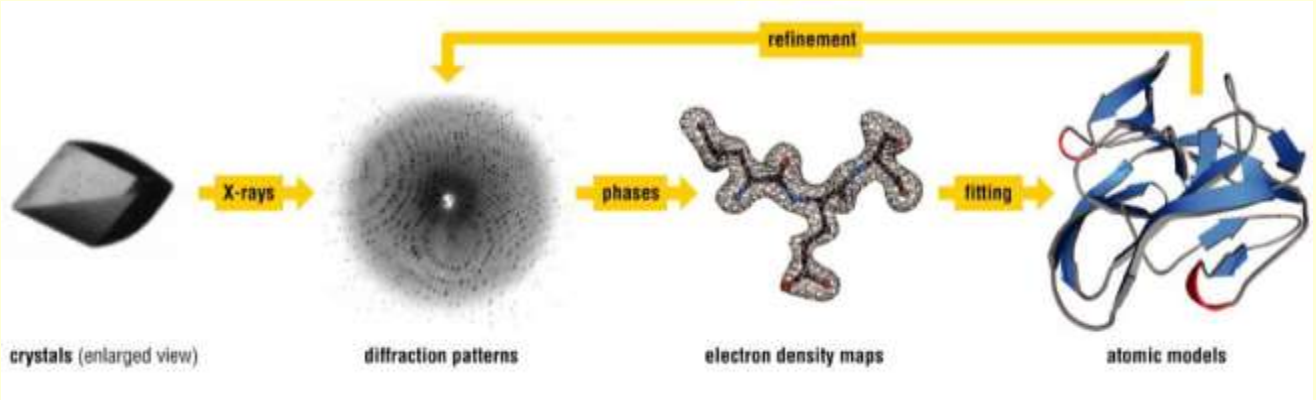

X-ray Crystallography(113958)
- High resolution
- Static snapshot
- Requires crystals

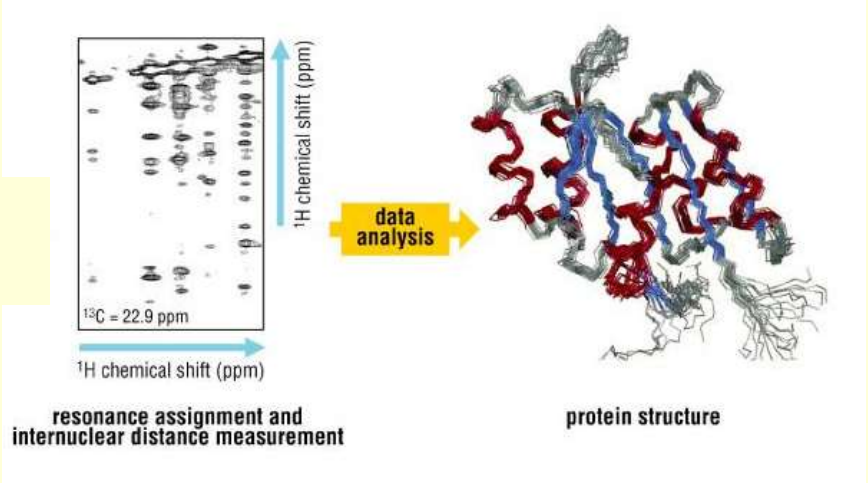

NMR(1427)
- High resolution
- Molecules in solution
- Dynamics
- Size limit (<40 kDa)

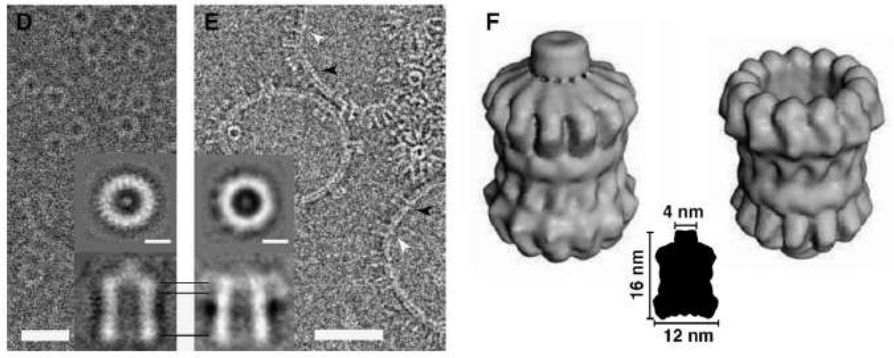

Electron Microscopy(1427)
- Low resolution
- Sample preparation
- Size limit (>400 kDa)

Nobel Prize winners associated with macromolecular crystallography

2012 Chemistry R. J. Lefkowitz and B. K. Kobilka *For studies of G-protein-coupled receptors*

2009 Chemistry V. Ramakrishnan, T. A. Steitz and A. E. Yonath *Studies of the structure and function of the ribosome*

2006 Chemistry R. D. Kornberg *Studies of the molecular basis of eukaryotic transcription*

2003 Chemistry P. Agre and R. MacKinnon *Discoveries concerning channels in cell membranes*

1997 Chemistry P. D. Boyer, J. E. Walker and J. C. Skou *Elucidation of the enzymatic mechanism underlying the synthesis of adenosine triphosphate (ATP) and discovery of an ion-transporting enzyme*

1988 Chemistry J. Deisenhofer, R. Huber and H. Miche *For the determination of the three-dimensional structure of a photosynthetic reaction centre*

1982 Chemistry A. Klug *Development of crystallographic electron microscopy and discovery of the structure of biologically important nucleic acid-protein complexes*

1972 Chemistry C. B. Anfinsen *Folding of protein chains*

1964 Chemistry D. Hodgkin *Structure of many biochemical substances including Vitamin B12*

1962 Physiology or Medicine F. Crick, J. Watson and M. Wilkins *The helical structure of DNA*

1962 Chemistry J. C. Kendrew and M. Perutz *For their studies of the structures of globular proteins*

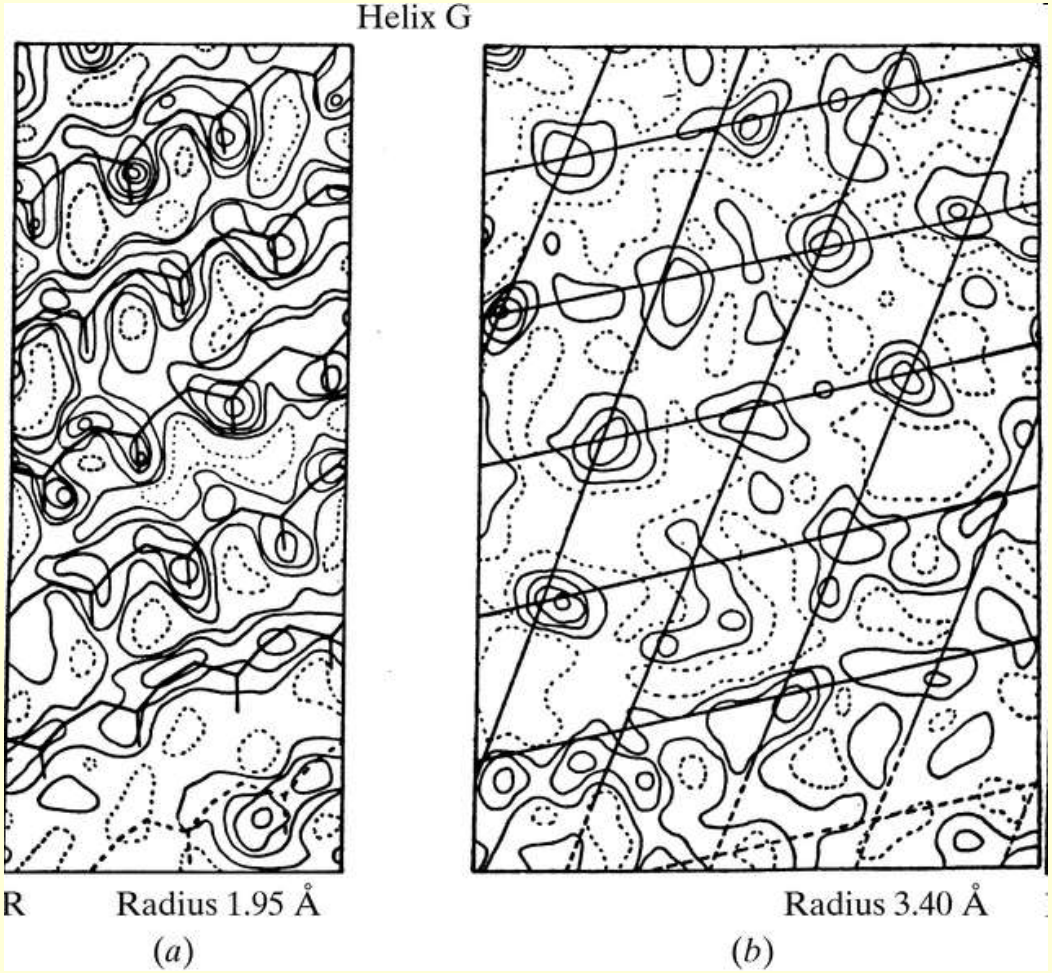

(*a*) The density in a cylindrical mantle of 1.95 Å radius, corresponding to the mean radius of the main-chain atoms in an α-helix. The calculated atomic positions of the α-helix are superimposed and roughly correspond to the density peaks. (*b*) The density at the radius of the β-carbon atoms; the positions of the β-carbon atoms calculated for a right-handed α-helix are marked by the superimposed grid (Kendrew & Watson, unpublished). Reprinted with permission from Perutz (1962). Copyright (1962) Elsevier Publishing Co.

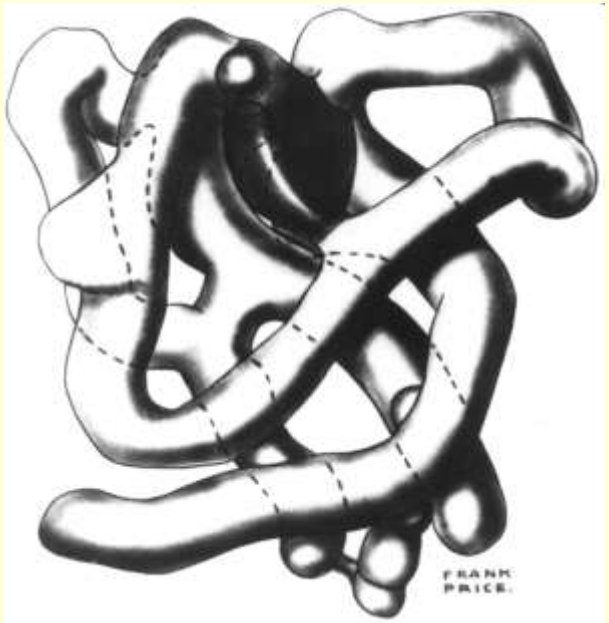

A model of the myoglobin molecule at 6 Å resolution (1959).

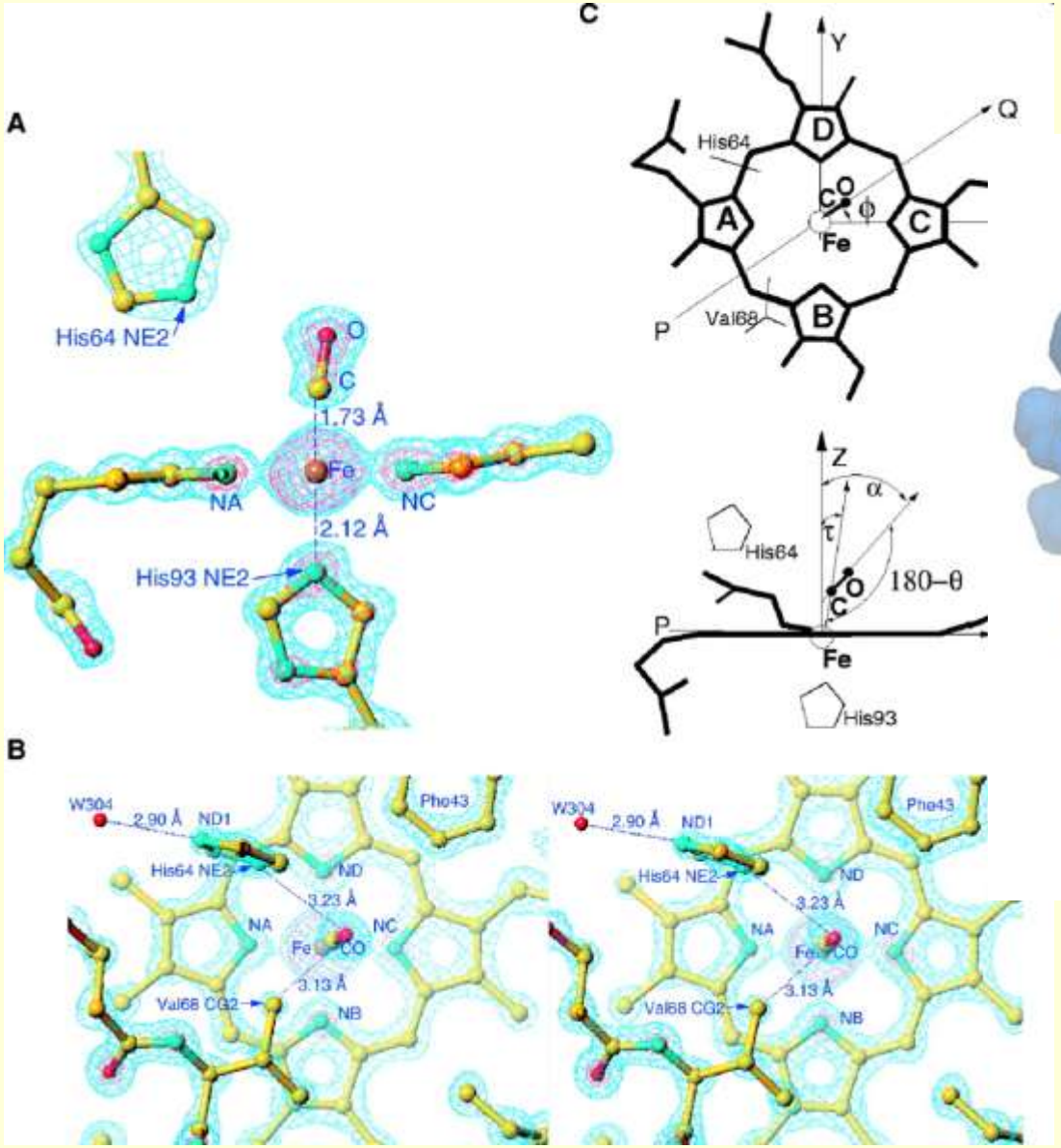

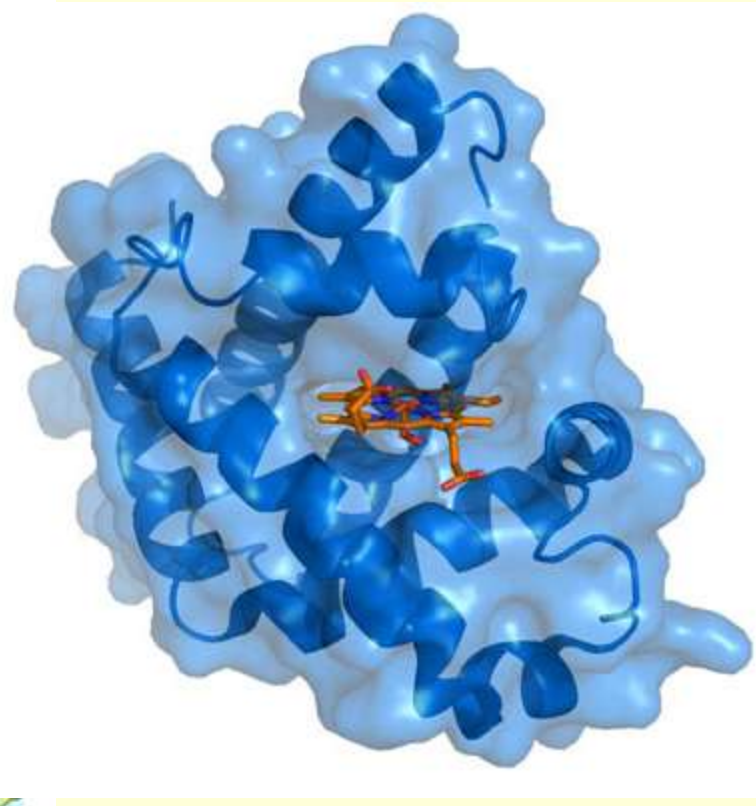

A Steric Mechanism for Inhibition of CO Binding to Heme Proteins

***Kachalova*, G. S., *Popov*, A. N. & Bartunik, H. D.. (1999). Science, 284, 473**

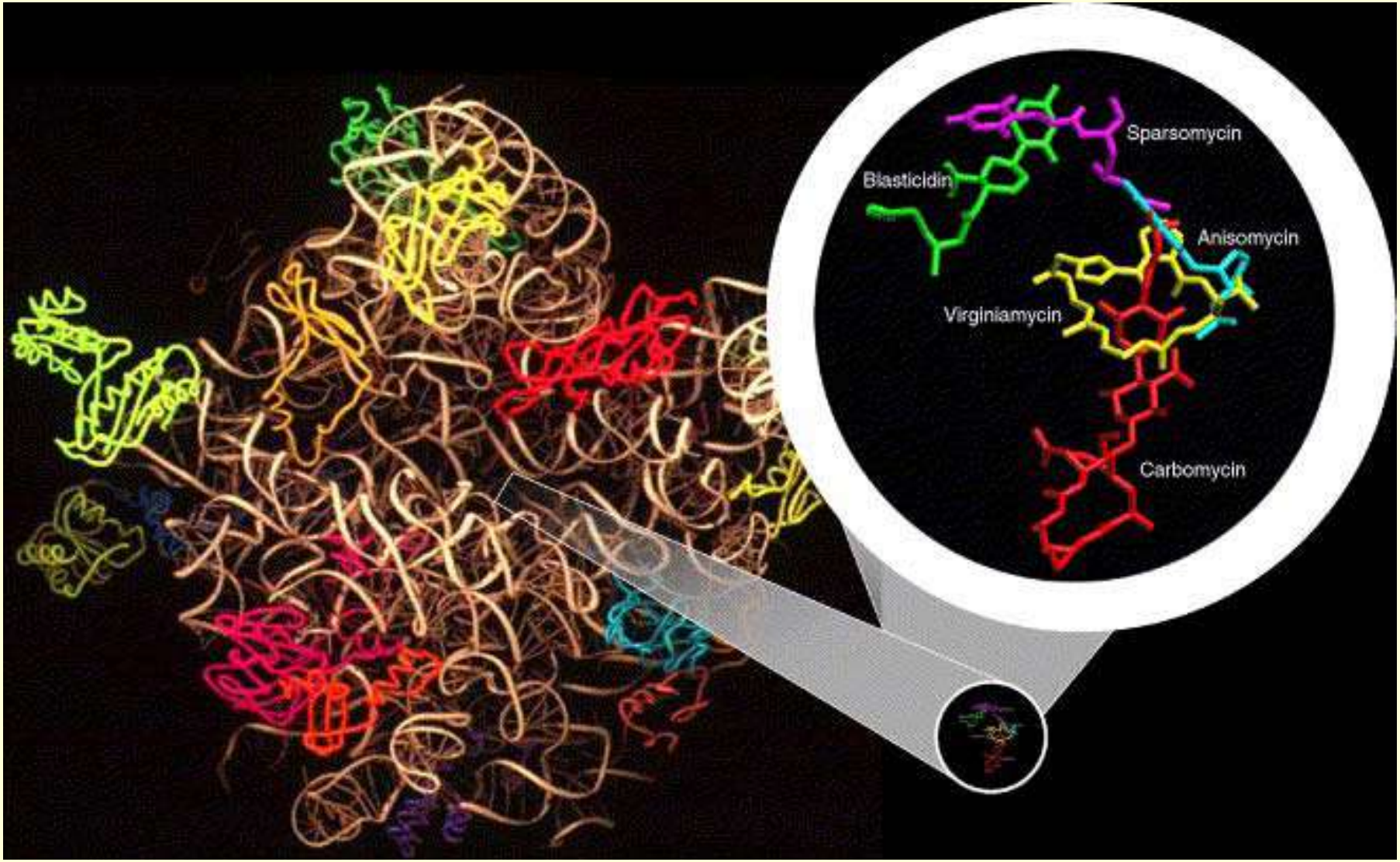

The peptidyl-transferase center in the 50S ribosomal subunit is attacked by a large number of existing antibiotics, now revealed at high resolution in 50S subunit crystal structures (Figure 8) (Franceschi and Duffy, 2006).

Structure in four dimensions:

Primary Structure: Amino-acid sequence.

Secondary Structure: Local regular structure: α-helices and β-sheets.

Tertiary Structure: Packing of secundary structure into one or several compact globular domains

Quarternary Structure: The arrangement of several folded chains together:multimeric proteins

Water in and around protein

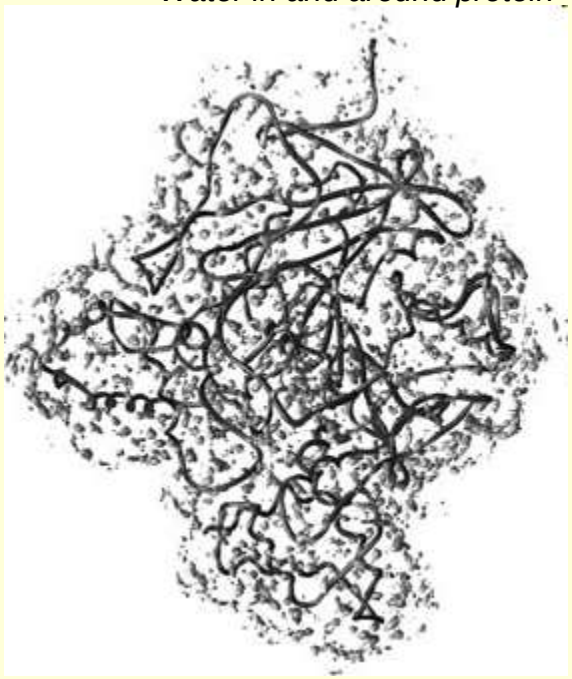

Water density isocontour for the bulk water density. AChE (actylcholine esterase) is the dark gray ribbon, oriented with the amino terminus at the *top* and carboxyl terminus at the lower *left*. In the *middle* is the active site gorge

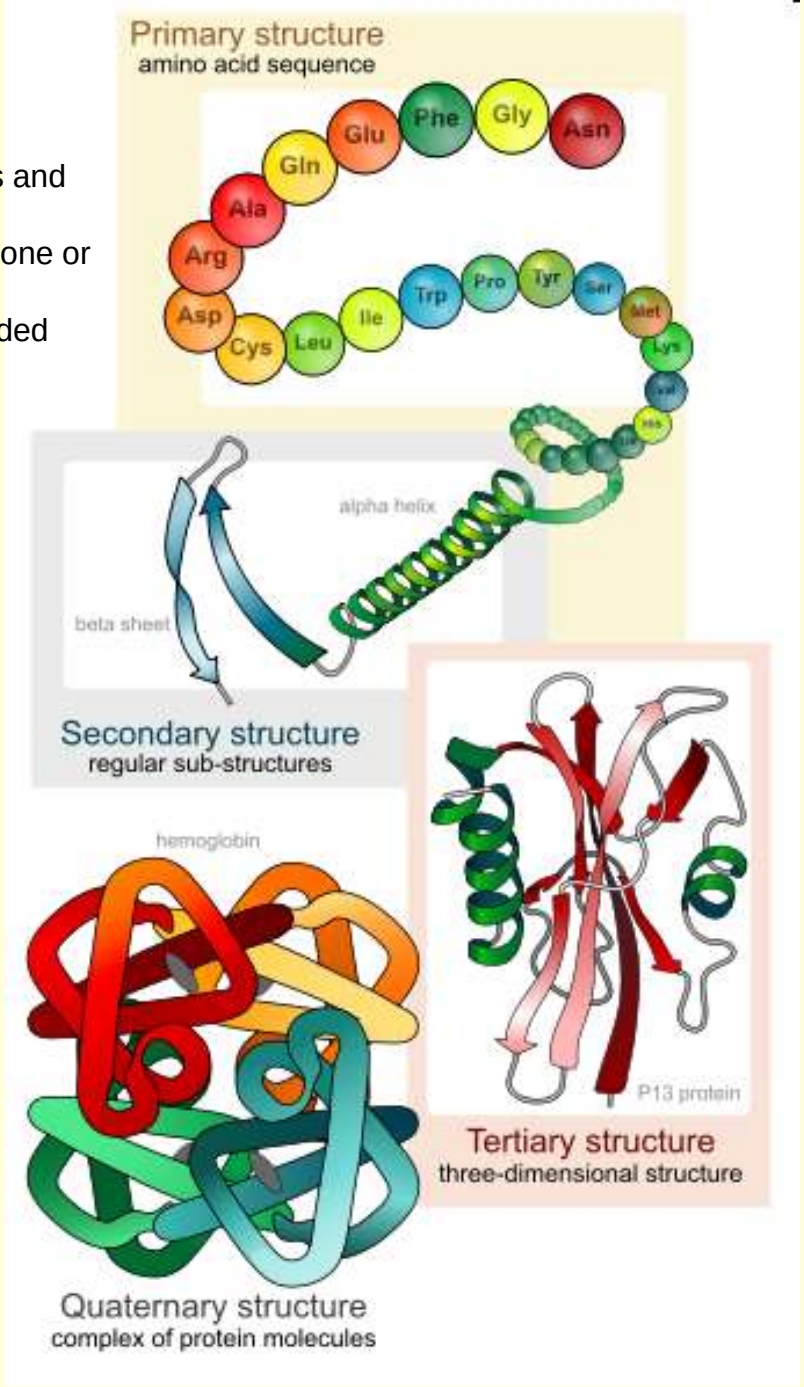

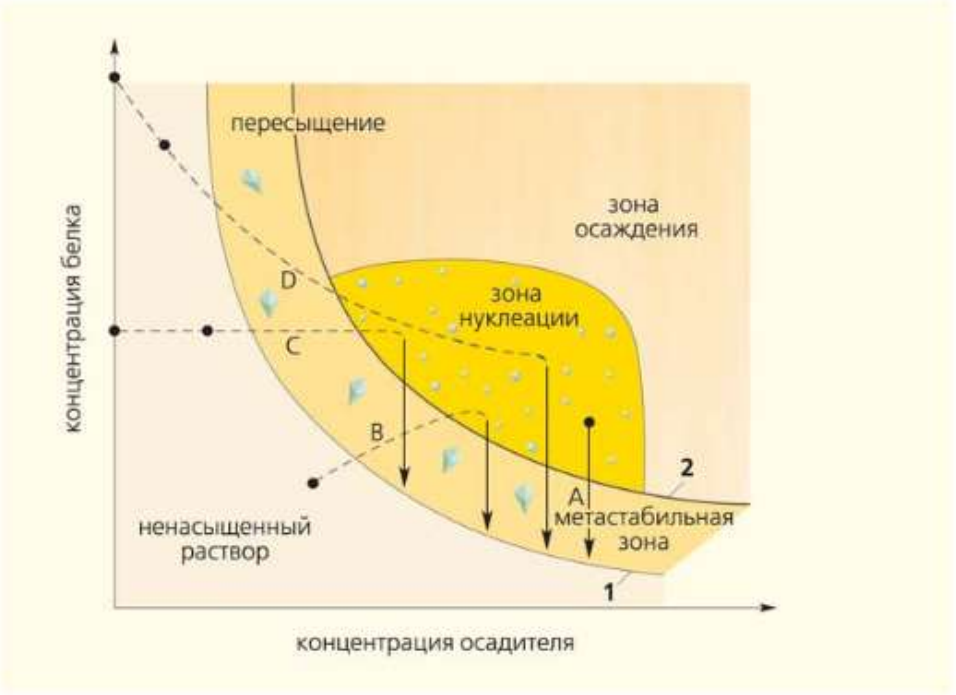

Фазовая диаграмма, показывающая растворимость белка как функцию концентрации осадителя. Приведены кривая растворимости (1) и кривая критического пересыщения (2), над которой белок выпадает в виде аморфного или мелкокристаллического осадка. В зоне нуклеации одновременно происходит образование кристаллических зародышей и рост мелких кристаллов. Оптимальные условия для роста крупных кристаллов — в метастабильной зоне (показано стрелками).

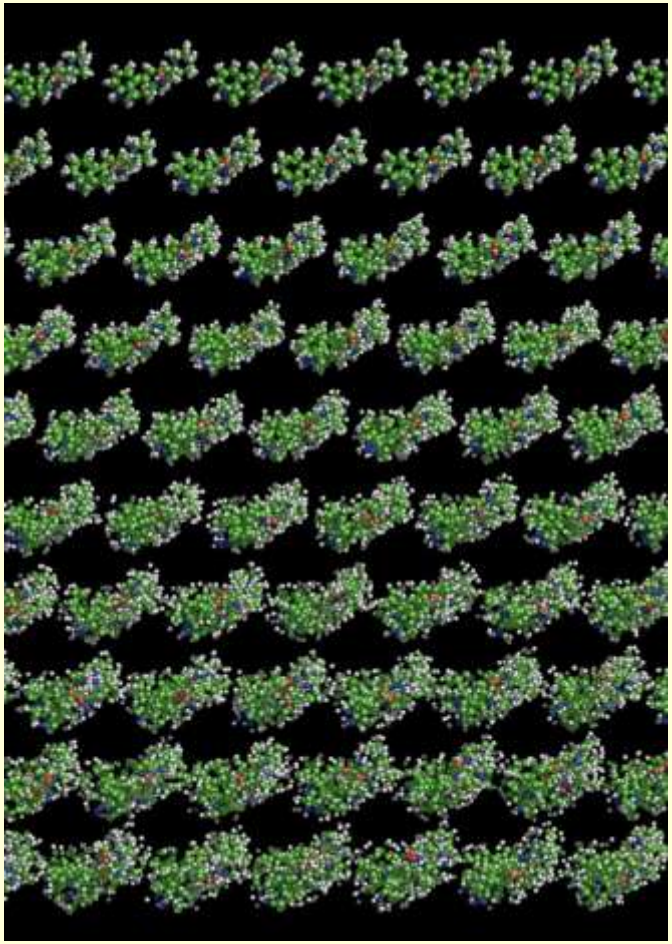

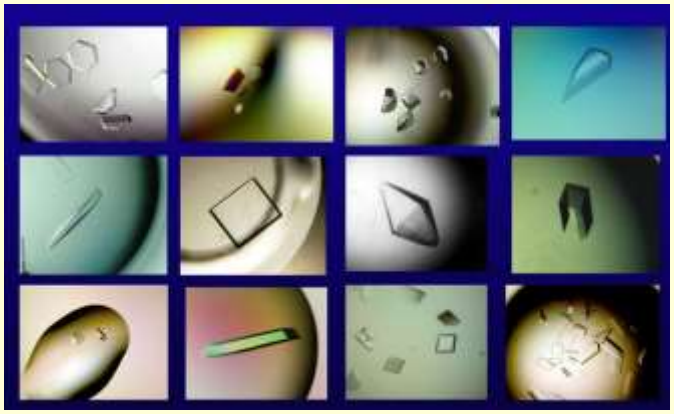

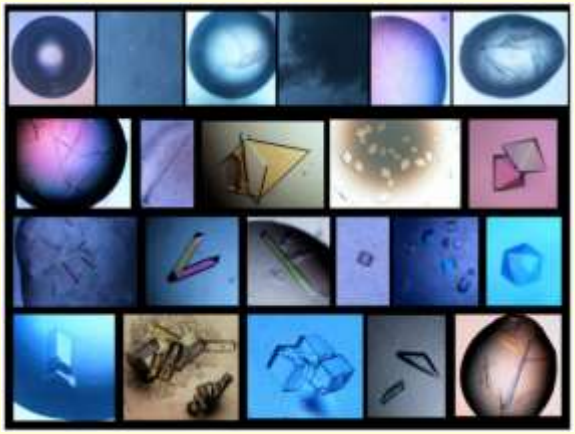

PROSEDURE

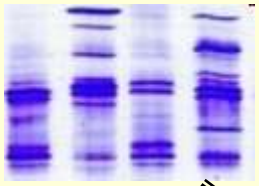

Clone gene
expressing
purification

crystallization

Crystal mounting

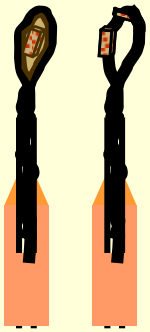

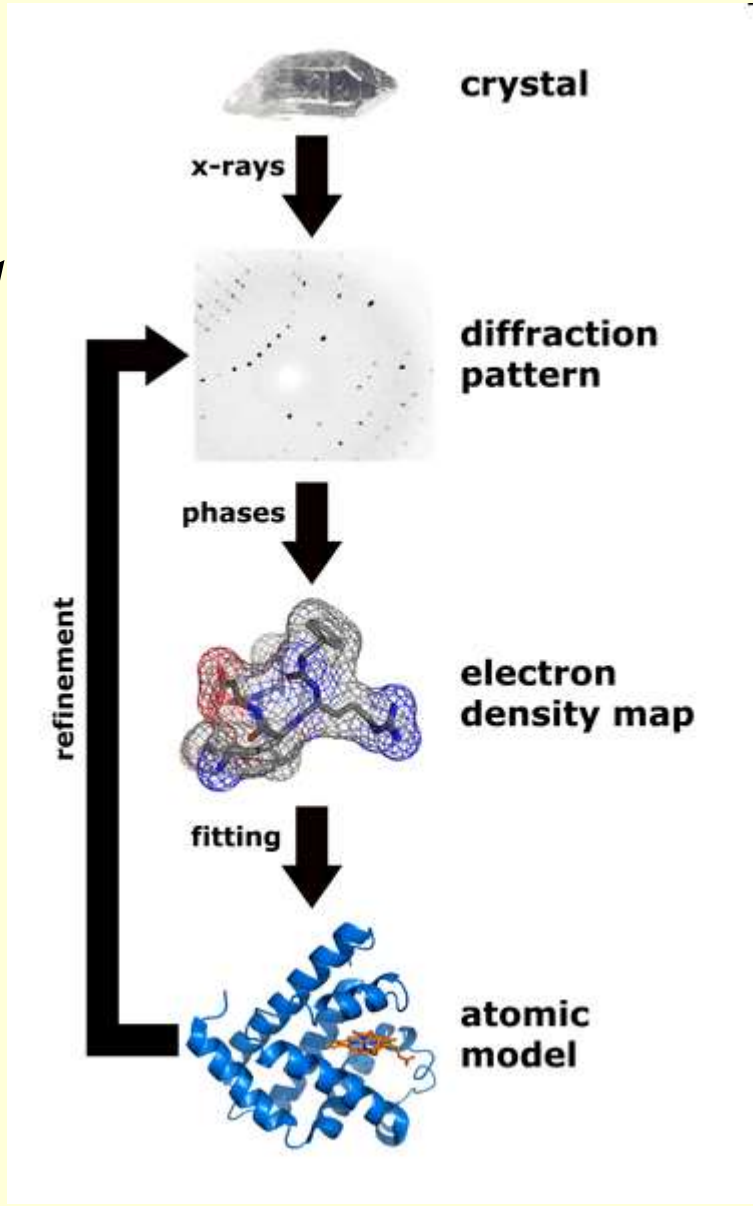

The Crystallization Experiment

Crystal Screen Kit

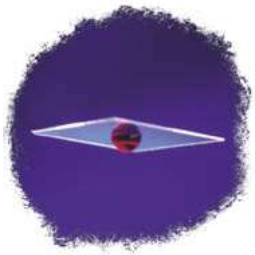

Hanging drop

Growth Techniques

1- Hanging Drop
2- Sitting Drop
3- Sandwich Drop
4- Free interface diffusion (NASA)
5- Batch (Robots)
6- Microbatch - under oil.
7- Mcrodialysis (Buttons)

Micro-bridges
(Sitting drop)

Dialysis Buttons

Virus Crystal
~0.15mm

High-Throughput Nanovolume Crystallization (R. Stevens, TSRI)

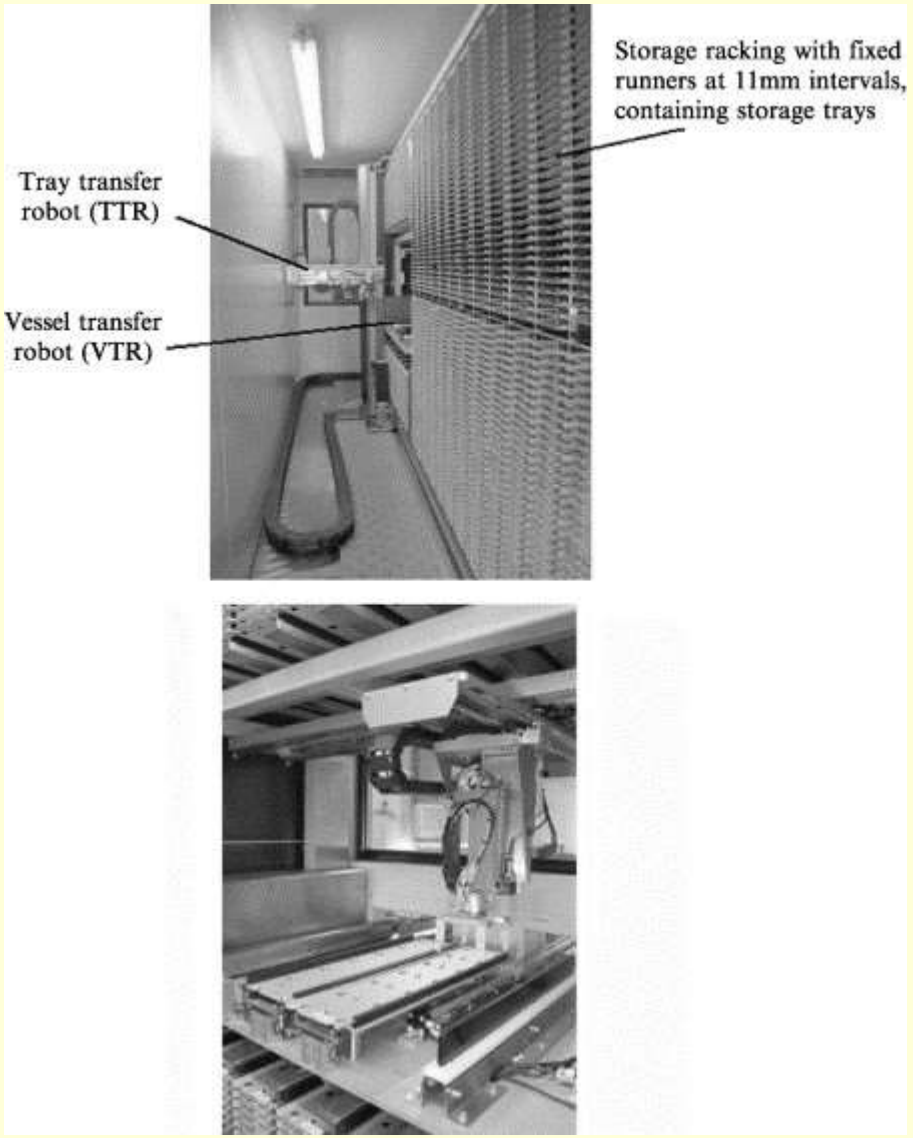

Lipidic cubic phase
Tools and Technologies

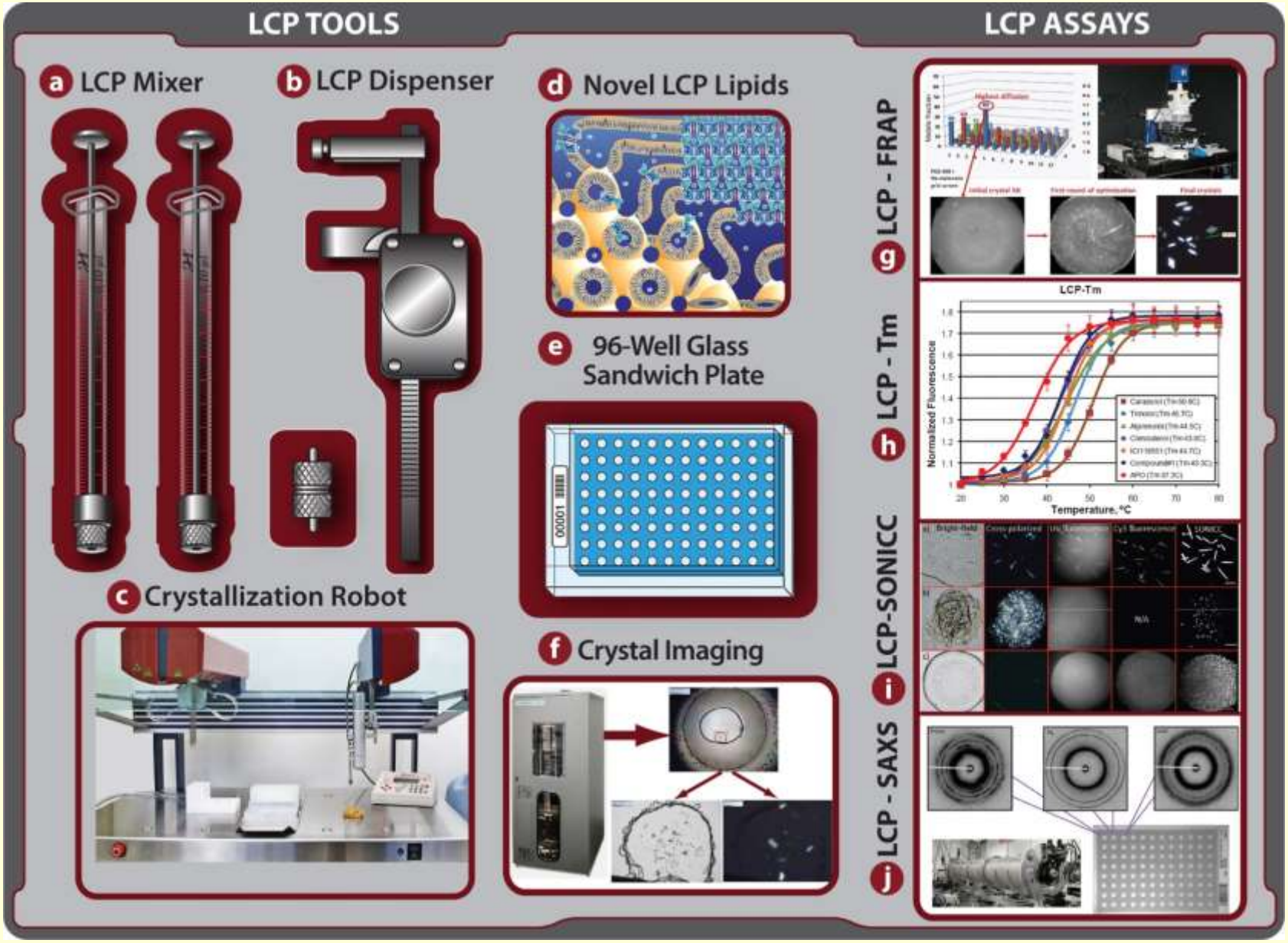

$$F_{(h,k,l)} = \sum_{j=1}^{atoms} f_{(j)} \exp\left[2\pi \cdot i(hx_{(j)} + ky_{(j)} + lz_{(j)})\right]$$

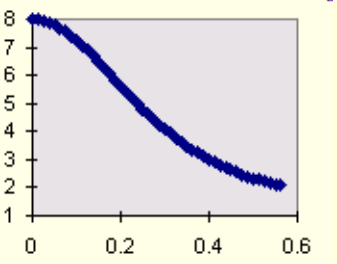

$$f^{o}(\sin\theta/\lambda) = \sum_{i=1}^{4} a_i \cdot e^{-b_i(\sin\theta/\lambda)^2} + c$$

$$\rho_{(x,y,z)} = \frac{1}{V} \sum_{h} \sum_{k} \sum_{l} F_{(h,k,l)} \exp\left[-2\pi \cdot i(hx + ky + lz)\right]$$

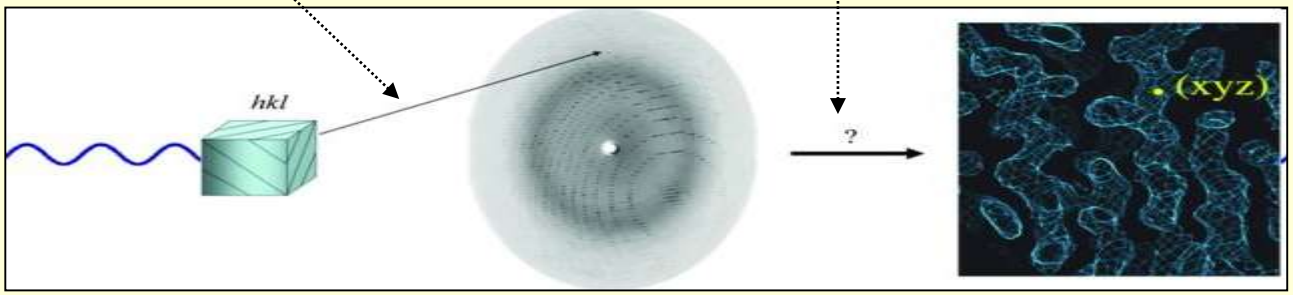

The importance of phases in carrying information. Top, the diffraction pattern, or Fourier transform (FT), of a duck and of a cat. Bottom left, a diffraction pattern derived by combining the amplitudes from the duck diffraction pattern with the phases from the cat diffraction pattern. Bottom right, the image that would give rise to this hybrid diffraction pattern. In the diffraction pattern, different colours show different phases and the brightness of the colour indicates the amplitude. Reproduced courtesy of Kevin Cowtan

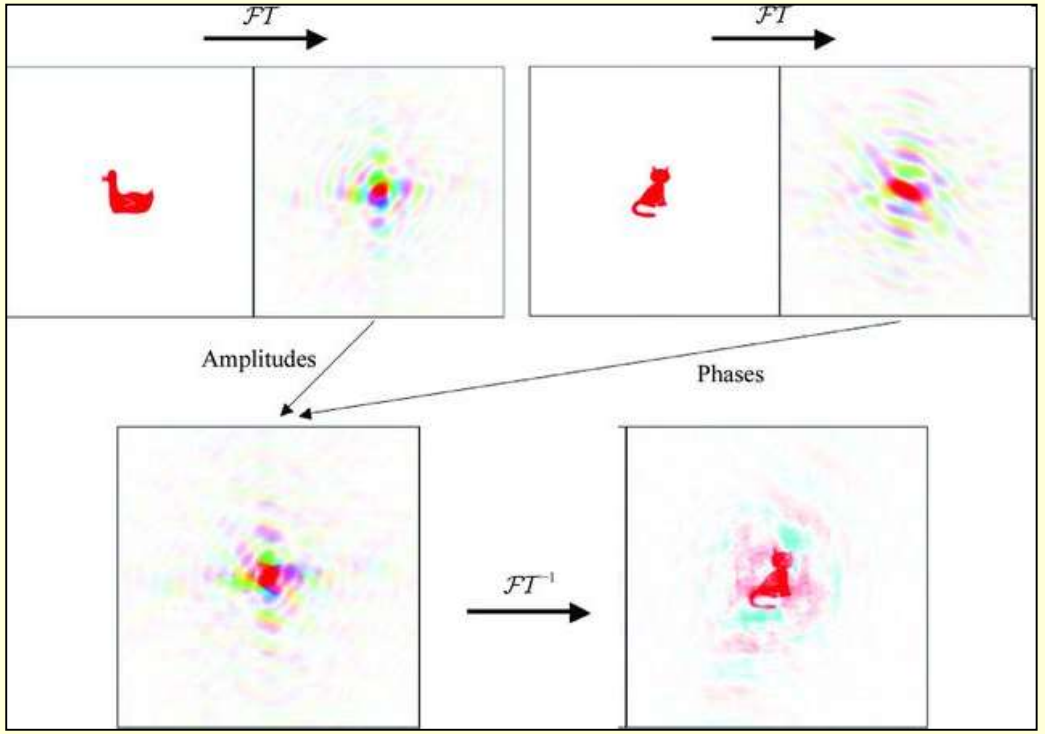

***from G.Taylor, Acta Cryst.* (2010). D66, 325-338**

Isomorphous replacement

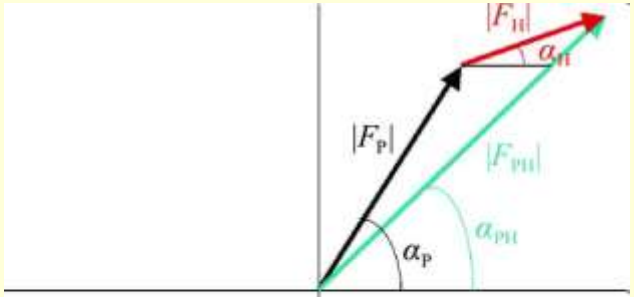

Argand diagram for SIR. |*F*P| is the amplitude of a reflection for the native crystal and |*F*PH| is that for the derivative crystal.

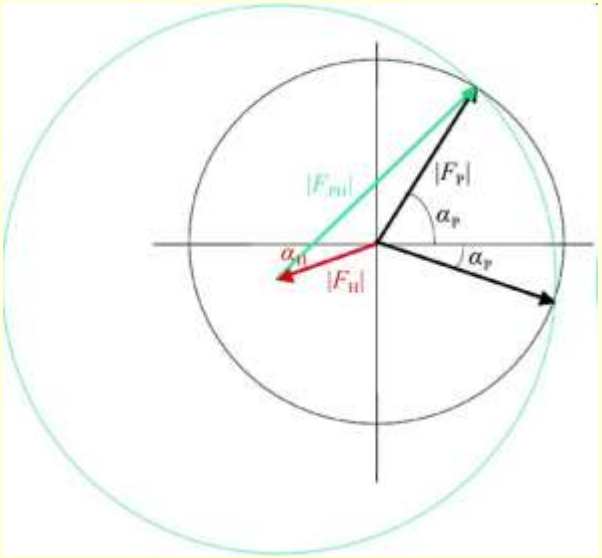

Harker construction for SIR.

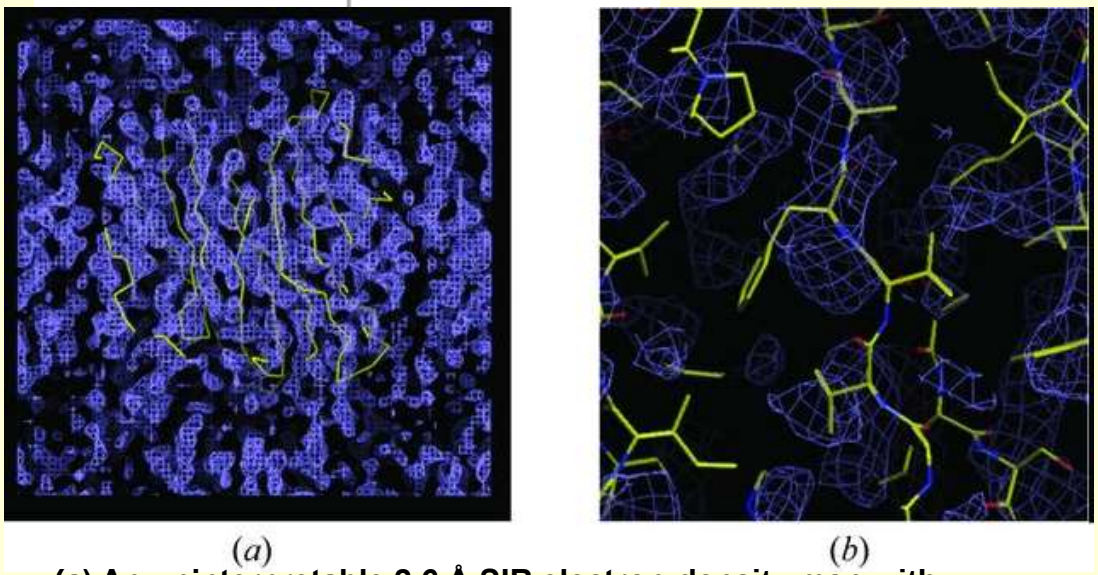

(*a*) An uninterpretable 2.6 Å SIR electron-density map with the final C trace of the structure superimposed. (x) = (1/*V*) *m*|*F*P|exp(*i* best)× exp(-2 *i*h·x). (*b*) A small section of the map with the final structure superimposed.

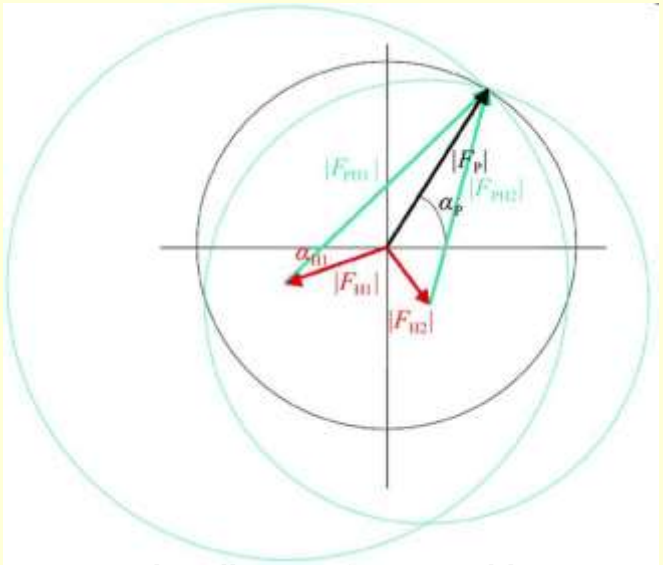

Harker diagram for MIR with two heavy-atom derivatives.

***from G.Taylor, Acta Cryst.* (2010). D66, 325-338**

The process of molecular replacement.

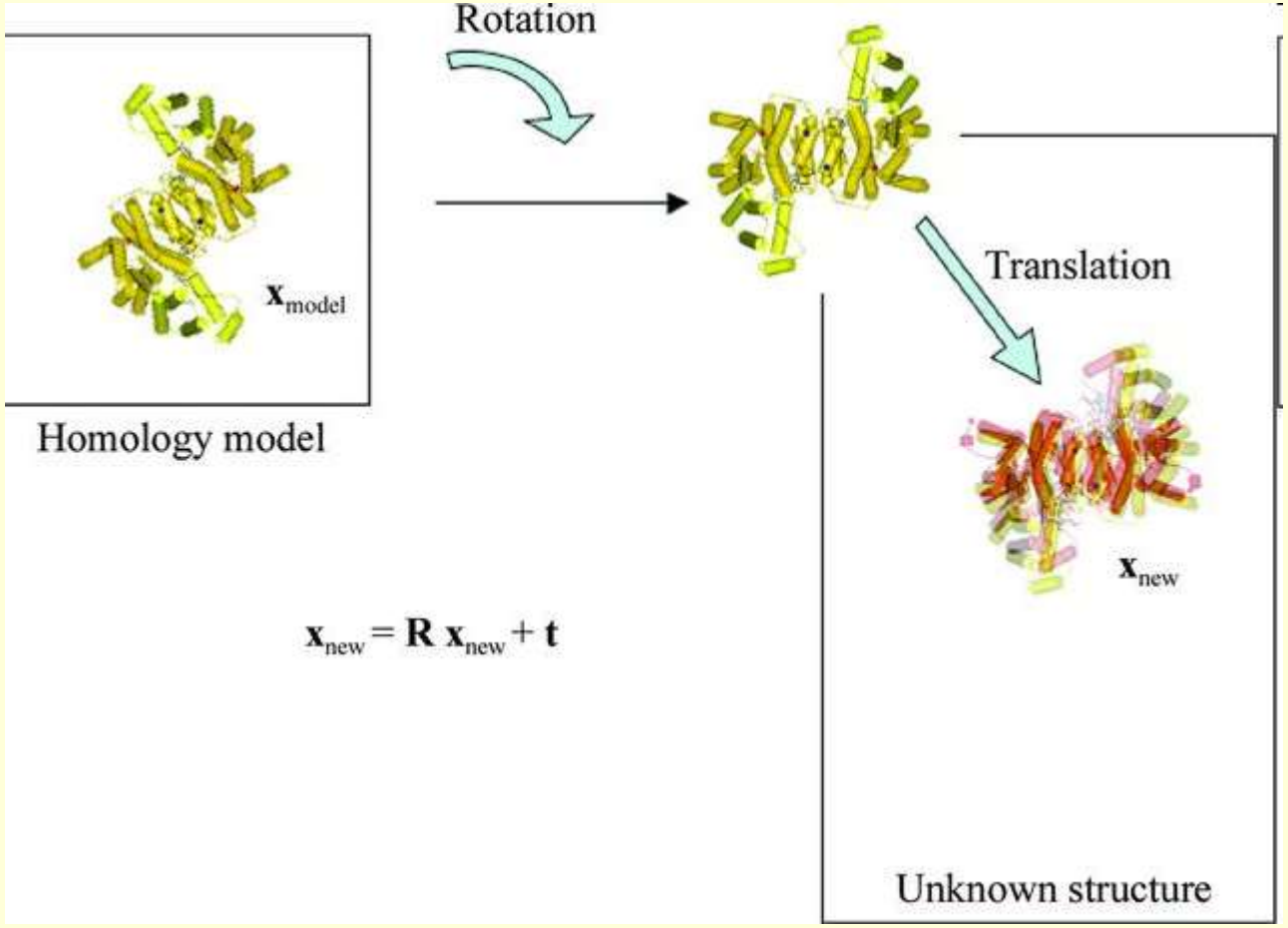

from G.Taylor, Acta Cryst. **(2010). D66, 325-338**

Anomalous scattering

The atomic scattering factor contains three components: a normal scattering term *f*0 that is dependent on the Bragg angle and two terms *f'* and *f''* that are not dependent on scattering angle but are dependent on scattering angle.

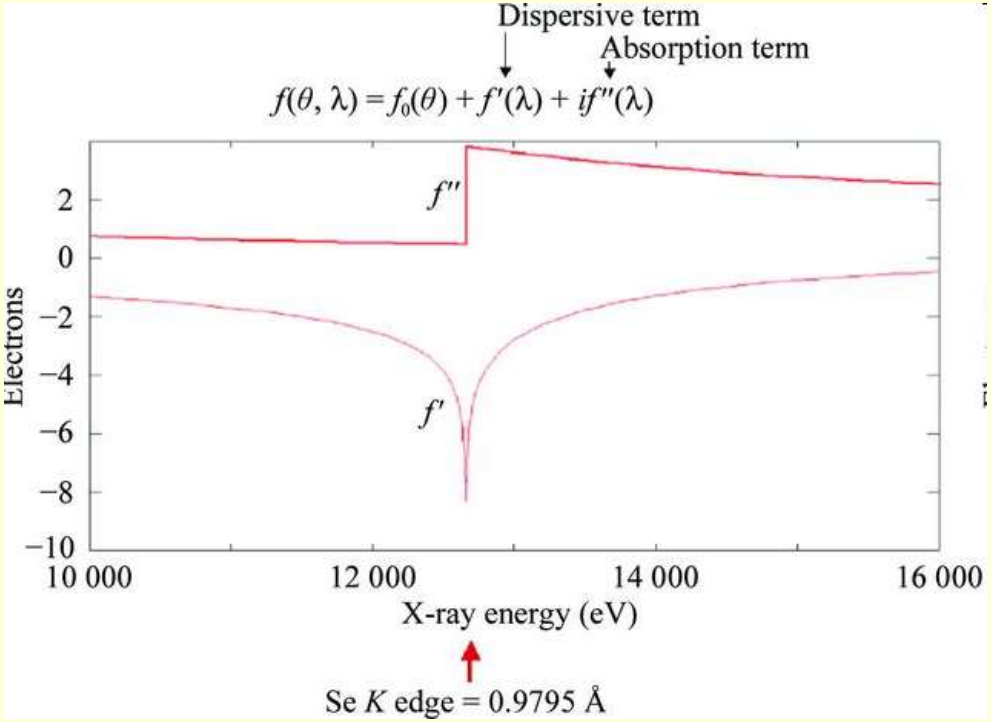

Variation in anomalous scattering signal *versus* incident X-ray energy in the vicinity of the *K* edge of selenium

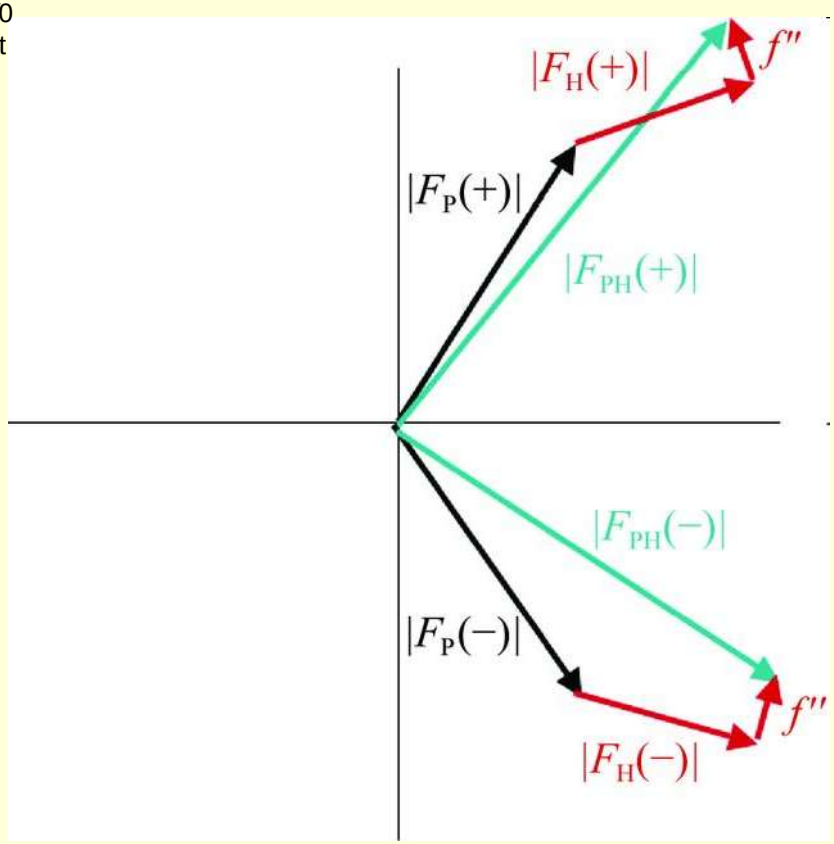

Breakdown of Friedel's law when an anomalous scatterer is present. *f*(,) = *f*0( ) + *f'*( ) + *if''*( ). |*Fhkl*| |*F-h-k-l*| or |*F*PH(+)| |*F*PH(-)|. *F*± = |*F*PH(+)| - |FPH(-)| is the Bijvoet difference.

***from G.Taylor, Acta Cryst.* (2010). D66, 325-338**

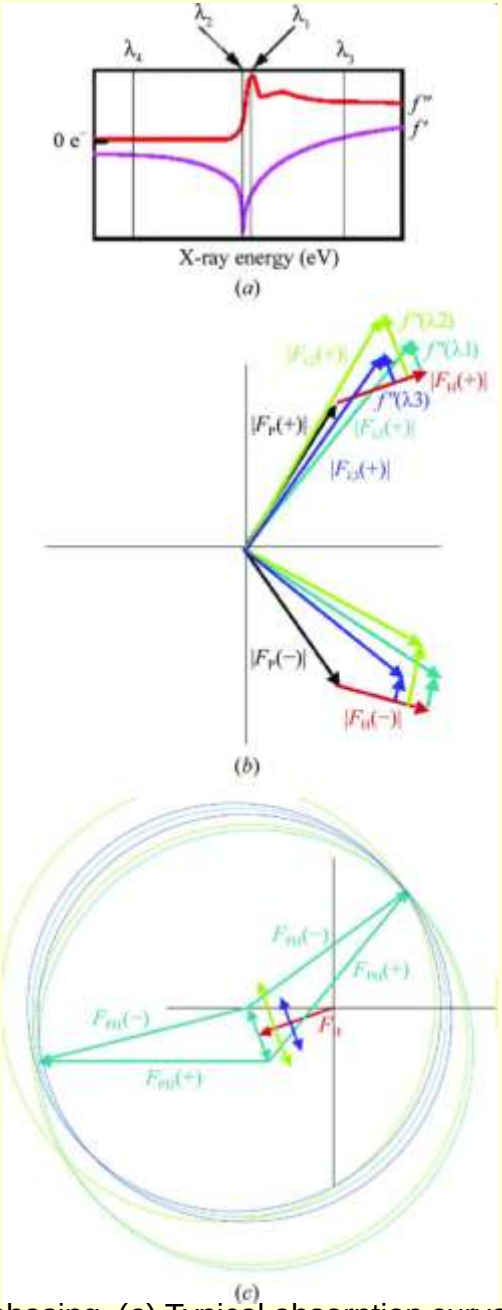

MAD phasing. (*a*) Typical absorption curve for an anomalous scatterer. (*b*) Phase diagram. |*F*P| is not measured, so one of the data sets is chosen as the `native'. (*c*) Harker construction.

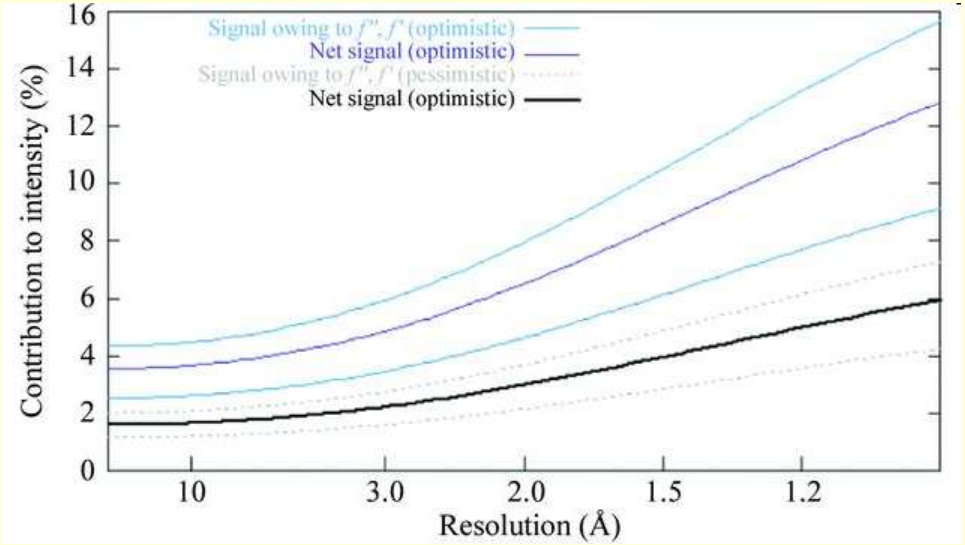

Estimation of signal size. The expected Bijvoet ratio is r.m.s.(*F*±)/r.m.s.(|*F*|) (*N*A/2*N*T)1/2(2*f*''A/*Z*eff). The expected dispersive ratio is r.m.s.(*F*)/r.m.s.(|*F*|) (*N*A/2*N*T)1/2[|*f*'A(*i*) - *f*'A(*j*)|]/*Z*eff, where *N*A is the number of anomalous scatterers, *N*T is the total number of atoms in the structure and *Z*eff is the normal scattering power for all atoms (6.7 e- at 2 = 0)

***from G.Taylor, Acta Cryst.* (2010). D66, 325-338**

Fast iodide-SAD phasing for high throughput membrane protein structure determination

*Igor Melnikov [a] *, Vitaly Polovinkin [bce] *, Kirill Kovalev[ce], Ivan Gushchin[ce], Mikhail Shevtsov[e], Vitaly Shevchenko[cde], Alexey Mishin[e], Alexey Alekseev[ce], Francisco Rodriguez-Valera[f], Valentin Borshchevskiy[e], Vadim Cherezov[eg], Gordon Leonard[a], Valentin Gordeliy[bce] **, Alexander Popov[a] ***

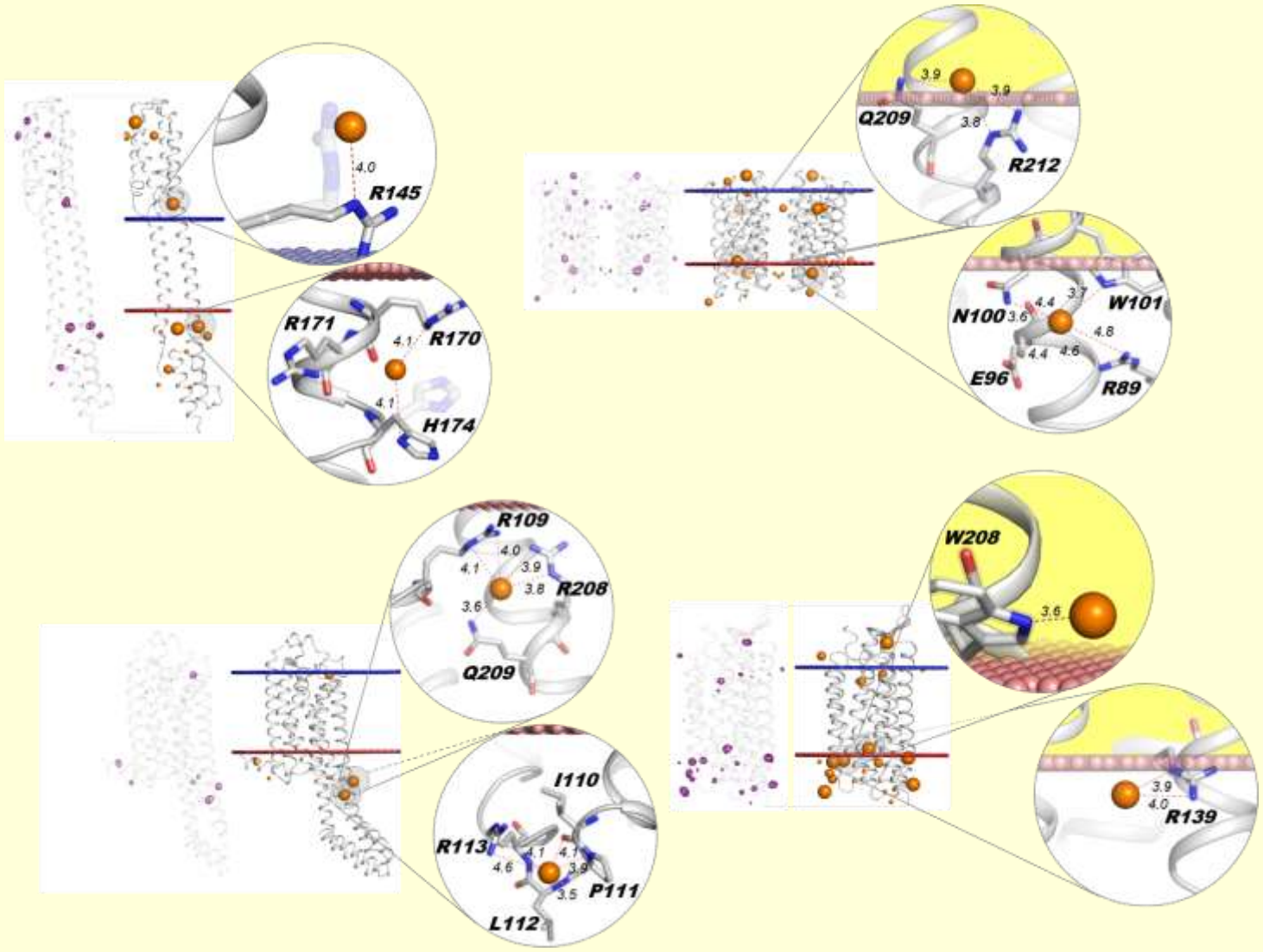

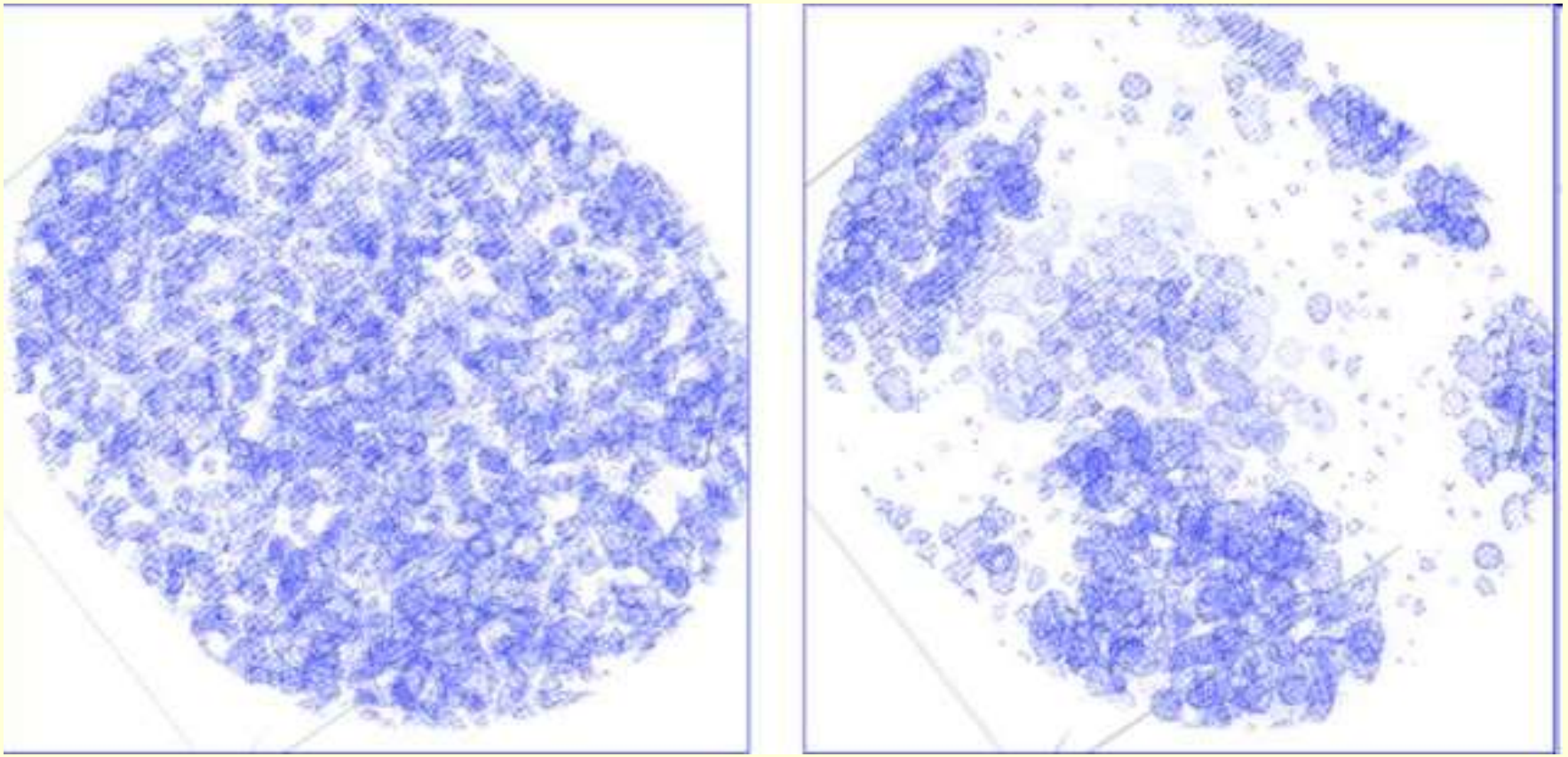

2.1 Å electron-density map for the S-SAD example before and after density modification using *SHELXE*.

***from G.Taylor, Acta Cryst.* (2010). D66, 325-338**

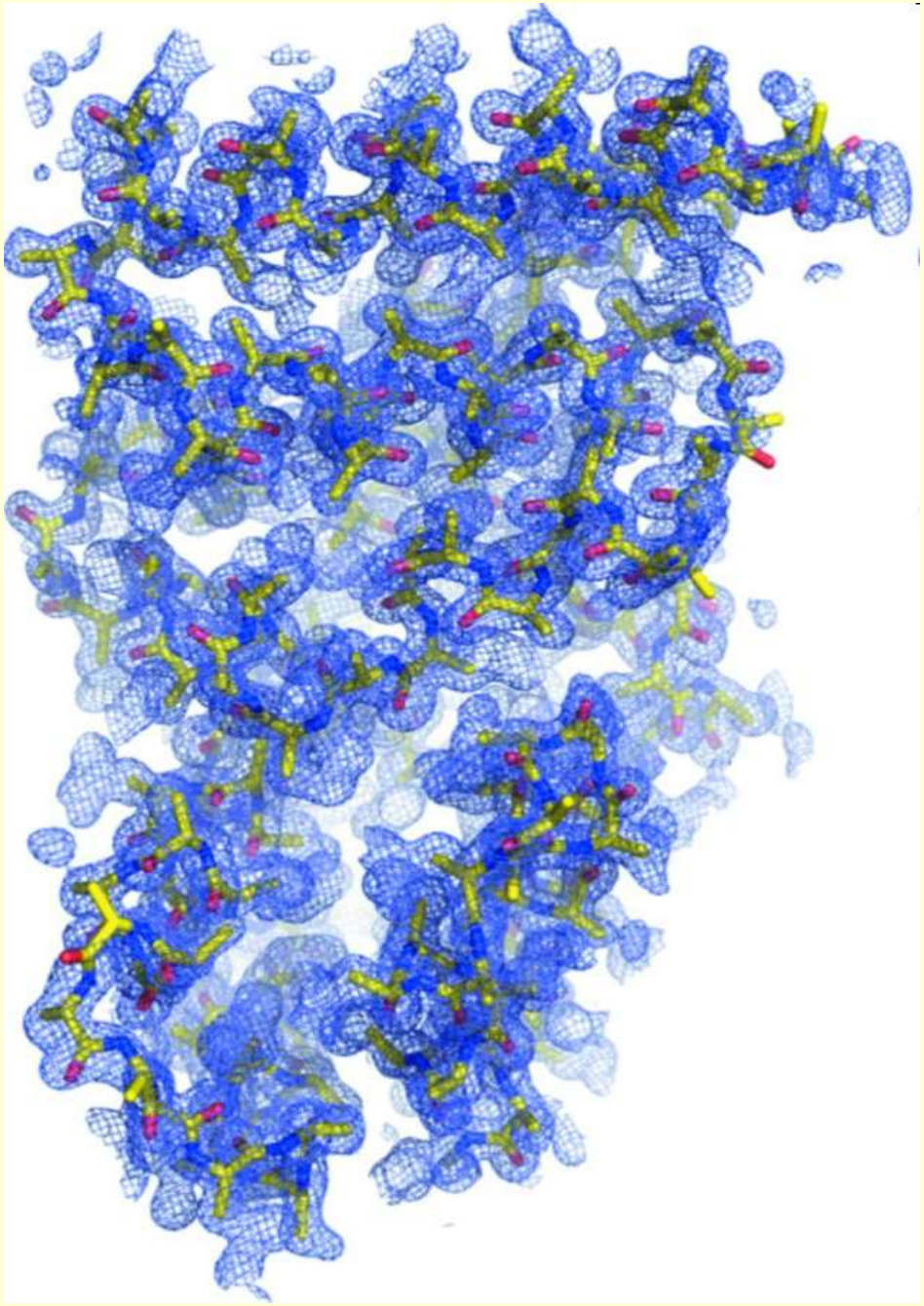

Autotraced polyalanine model produced by *SHELXE* superimposed on the density-modified electron-density map at 1.45 Å resolution.

***from G.Taylor, Acta Cryst.* (2010). D66, 325-338**

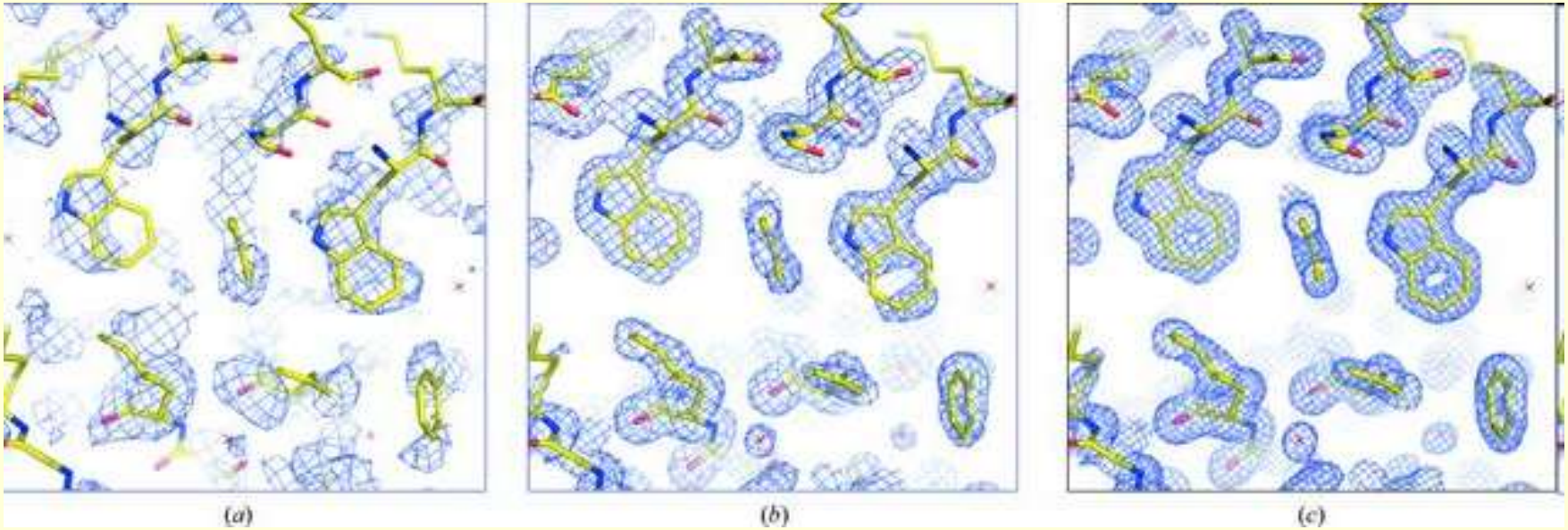

Improving phases for the S-SAD problem. (*a*) 2.1 Å resolution density-modified map. (*b*) 1.45 Å resolution phase-extended map. (*c*) `1.0 Å resolution' free-lunch map

***from G.Taylor, Acta Cryst.* (2010). D66, 325-338**

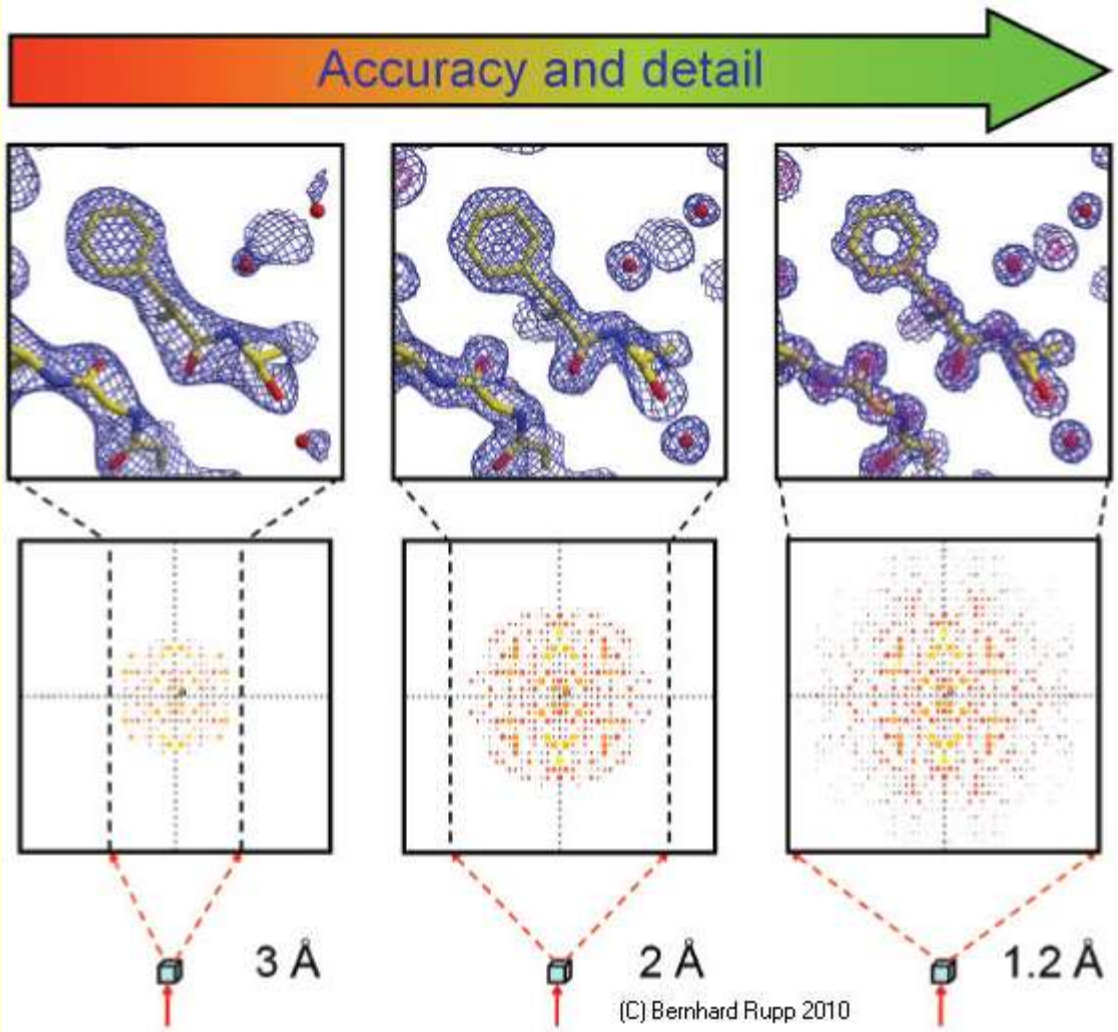

Figure 1-6 Data quality determines structural detail and accuracy. The qualitative relation between the extent of X-ray diffraction, the resulting amount of available diffraction data, and the quality and detail of the electron density reconstruction and protein structure model are evident from this figure: The crystals are labeled with the nominal resolution d_{min} given in Å (Ångström) and determined by the highest diffraction angle (corresponding to the closest sampling distance in the crystal, thus termed d_{min}) at which X-ray reflections are observed. Above each crystal is a sketch of the corresponding diffraction pattern, which contains significantly more data at higher resolution, corresponding to a smaller distance between discernible objects of approximately d_{min}. As a consequence, both the reconstruction of the electron density (blue grid) and the resulting structure model (stick model) are much more detailed and accurate. The non-SI unit Å (10^{-8} cm or 0.1 nm = 10^{-10} m) is frequently used in the crystallographic literature, simply because it is of the same order of magnitude as atomic radii (~0.77 Å for carbon) or bond lengths (~1.54 Å for the C–C single bond).

Resolution and electron density

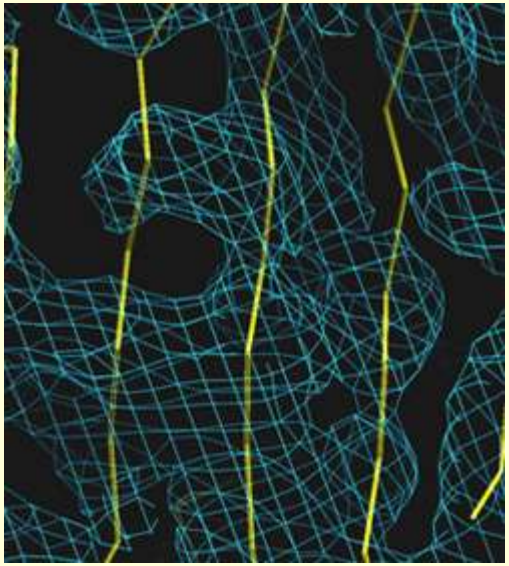

Low resolution ~5 Å
Errors in secondary structure

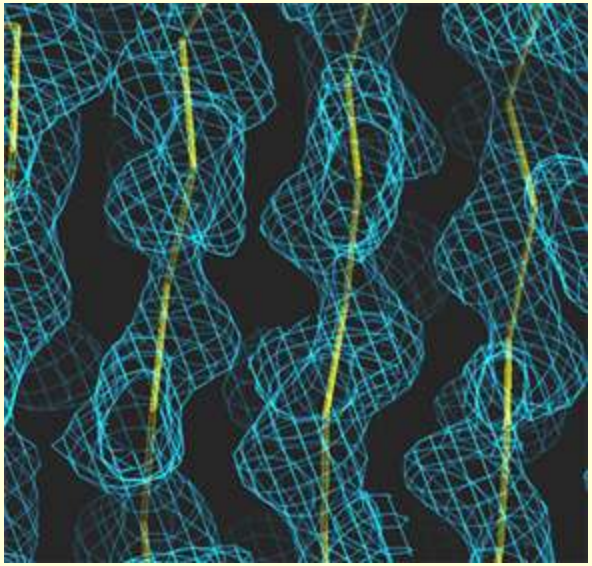

Medium resolution~3 Å
Good secondary structure
Most residues

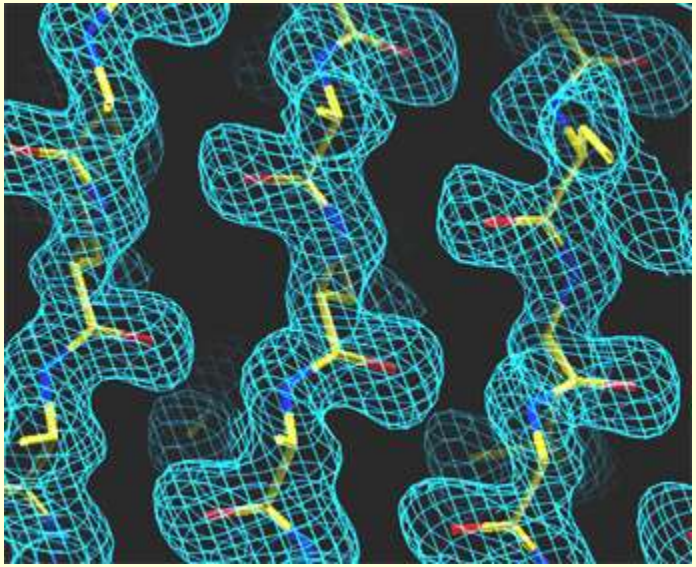

High resolution <2 Å
All residues
Water molecules
High fidelity

Darwin's Formula

$$I(hkl) = I_{beam}\, r_e^2\, \frac{V_{xtal}}{V_{cell}}\, \frac{\lambda^3 L}{\omega V_{cell}}\, P\, A\, |\, F(hkl)\, |^2$$

I(hkl) - photons/spot (fully-recorded)

I_{beam} - incident (photons/s/m^2)

r_e - classical electron radius (2.818×10^{-15} m)

V_{xtal} - volume of crystal (in m^3)

V_{cell} - volume of unit cell (in m^3)

λ - x-ray wavelength (in meters!)

ω - rotation speed (radians/s)

L - Lorentz factor (speed/speed)

P - polarization factor

$(1+\cos^2(2\theta) - Pfac \cdot \cos(2\Phi)\sin^2(2\theta))/2$

A - absorption factor

$\exp(-\mu_{xtal} \cdot l_{path})$

F(hkl) - structure amplitude (electrons)

C. G. Darwin (1914)

Macromolecular crystallography problems

- **Weak diffraction intensity – light atoms**
- **Poor crystal quality – big B-factor**
- **Background intensity > diffraction intensity**

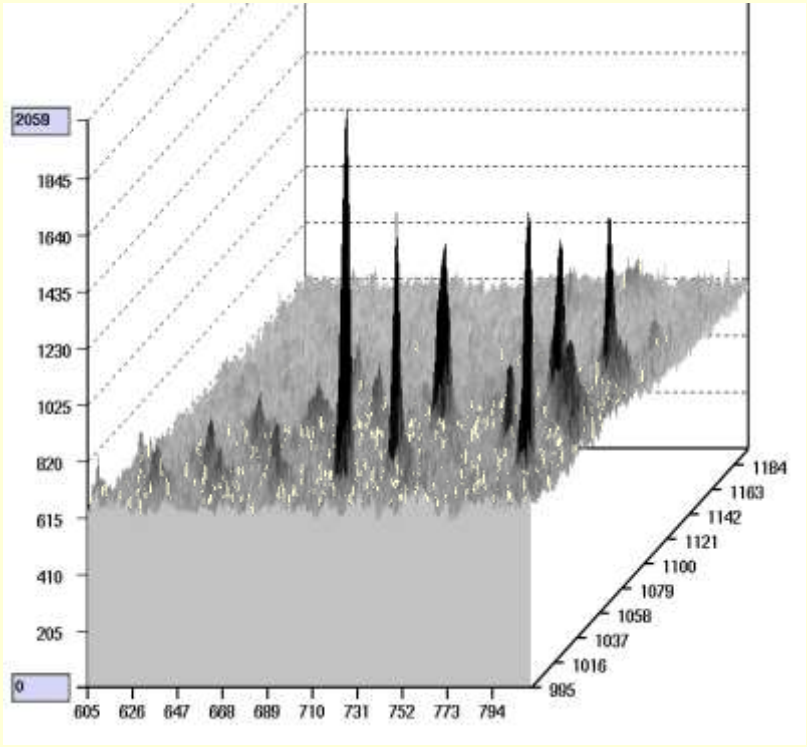

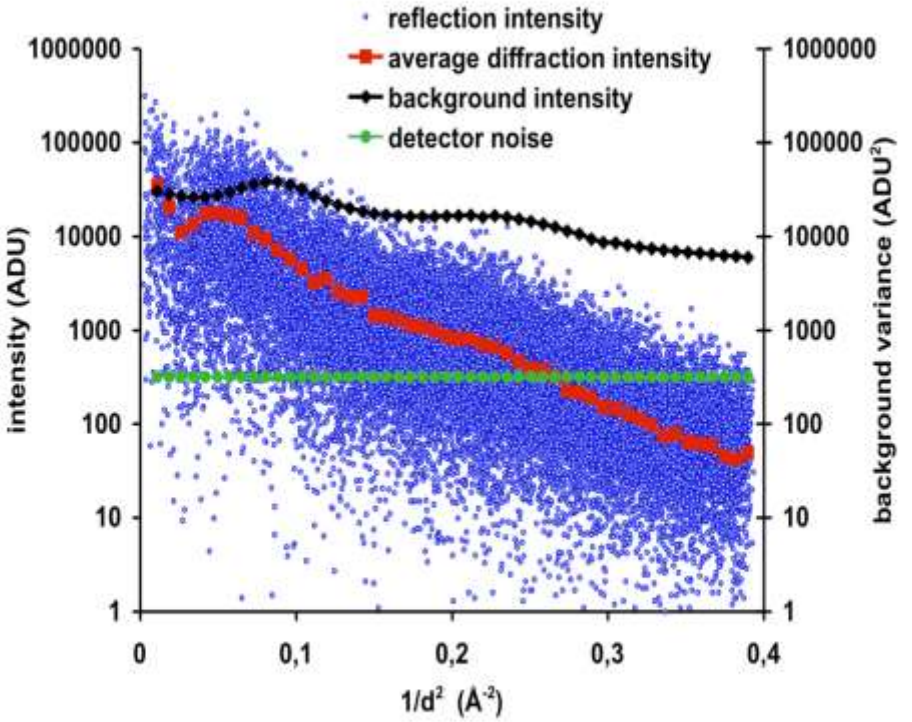

Global damage

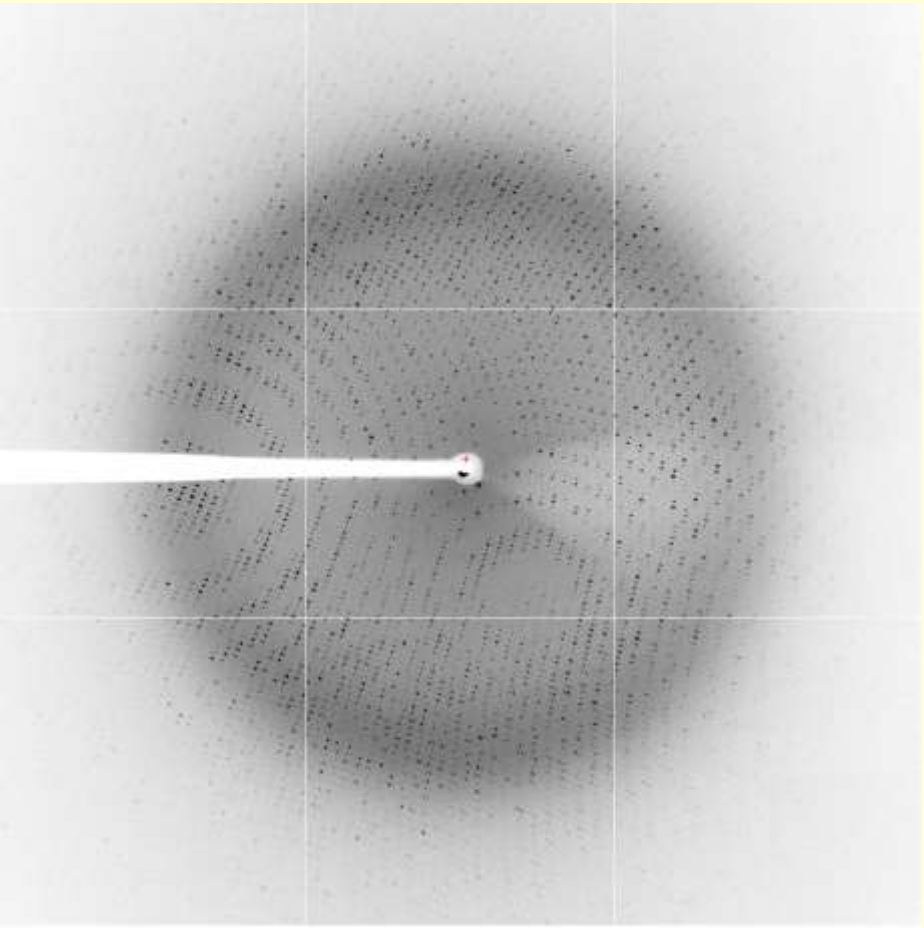

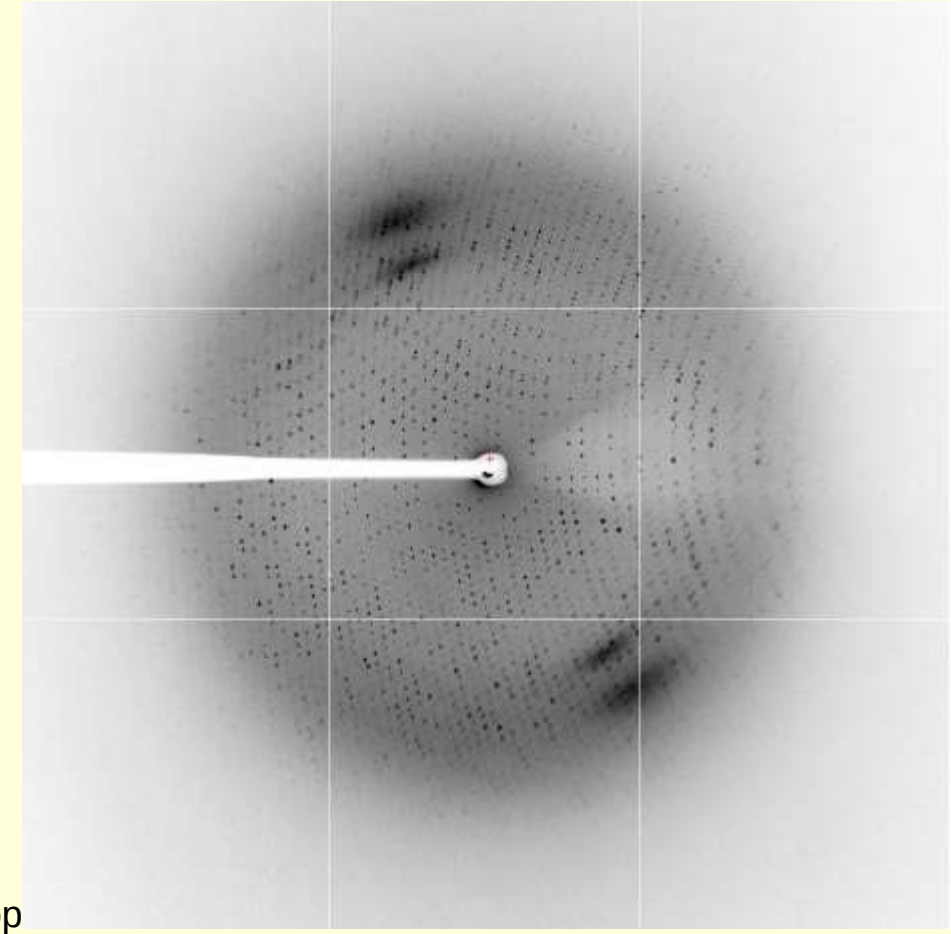

How fast does damage occur? (100K)

0 — KGy — MGy — 10^2 MGy — **Absorbed Dose**

Site-specific damage

1. **Dose of 0.3 MGy - X-ray radiation damage effects are not detectable even at atomic resolution.**
2. **Doses above 2 MGy lead to partial decarboxylation of the most sensitive residues**
3. **Doses above 6 MGy may lead to wrong interpretation of chemistry for some protein residues**

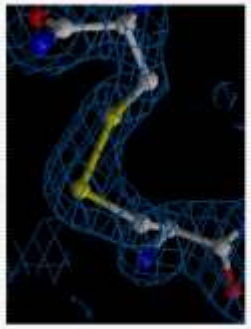

Acetylcholinesterase
Weik *et al.* PNAS, 97 (2), 623-628 (2000)

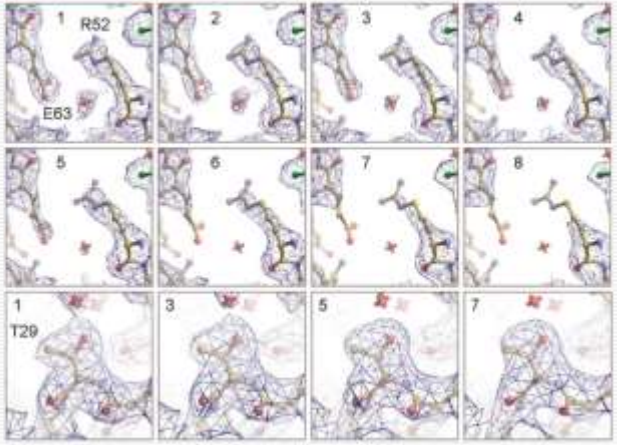

Owen R *et al.*, PNAS, 103 (13), 4912-4917 (2006)

Global damage

- ❑Overall and q-dependent loss of diffraction peak intensity
- ❑Non-specific non-isomorphism
- ❑Changes in unit-cell parameters
- ❑Increase in the mosaicity

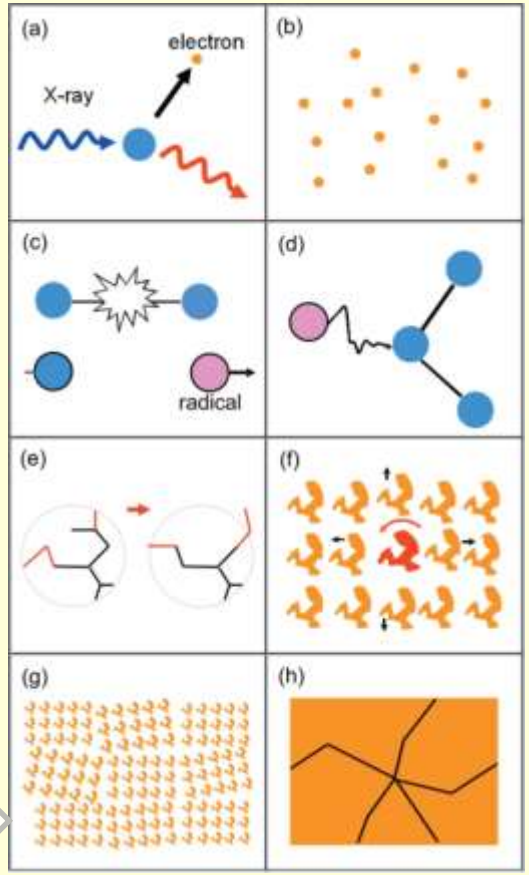

Illustration of some processes involved in the radiation damage cascade.(a) X-ray-induced ejection of a primary photoelectron. (b) Generation of several hundred relatively low-energy (100 eV) electrons. (c) Bond breaking leading to internal stress and radical formation. (d) Radical attack of the protein. (e) Conformation changes of side chains and flexible loops in response to chemical damage. (f) Displacement and reorientation of individual damaged molecules. (g) Deformation and reorientation of local lattice domains. (h) Plastic failure and crystal cracking.
Warkentin et al, 2013, J.Synchrotron Radiation, 20, 7-13

Cryo-crystallography

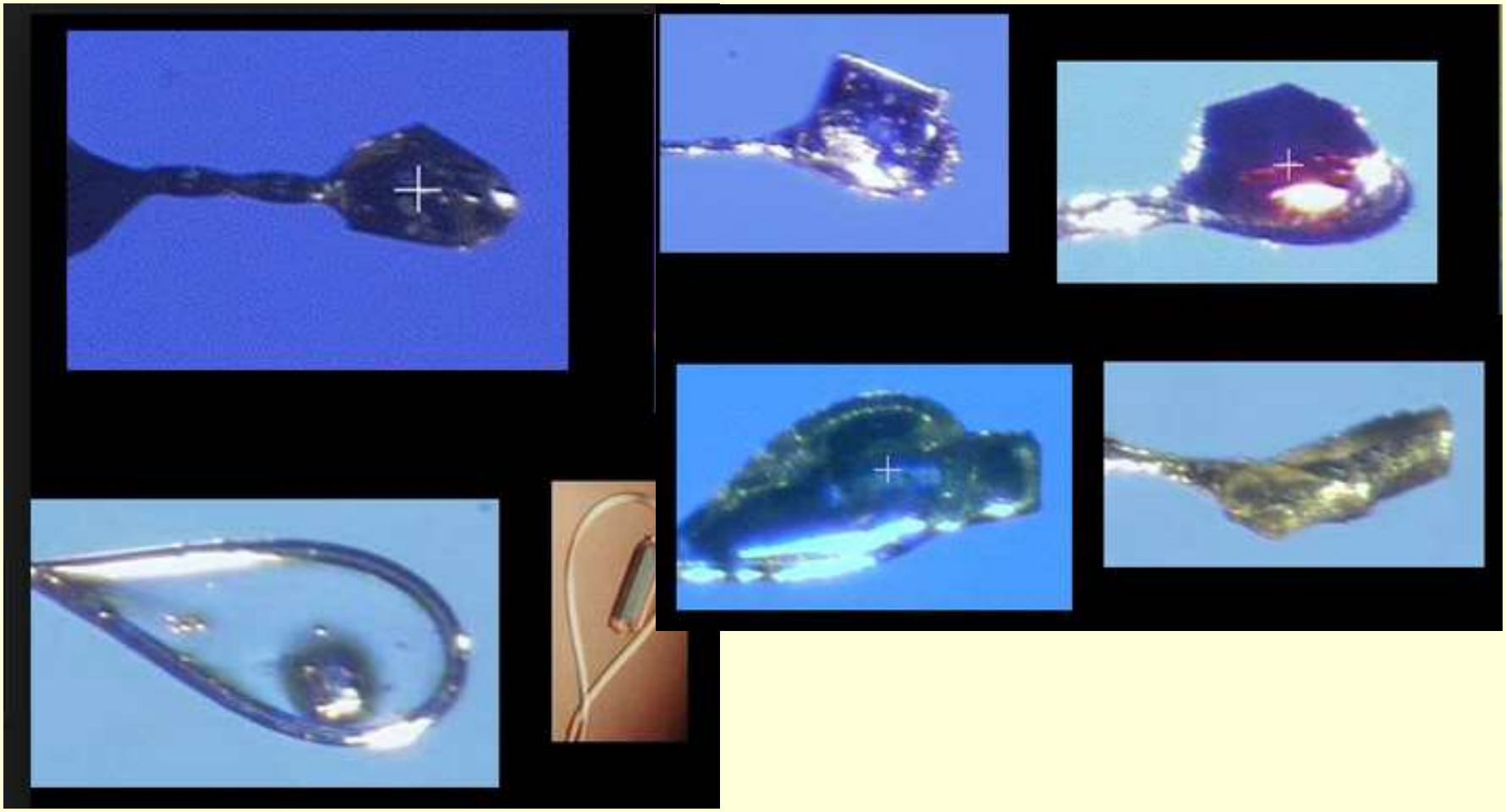

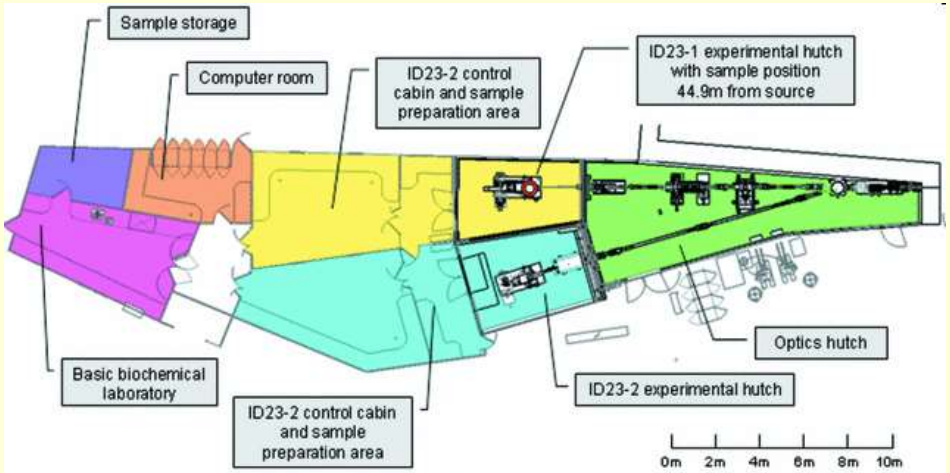
Sample storage
Computer room
ID23-2 control cabin and sample preparation area
ID23-1 experimental hutch with sample position 44.9m from source
Optics hutch
ID23-2 experimental hutch
Basic biochemical laboratory
ID23-2 control cabin and sample preparation area
0m 2m 4m 6m 8m 10m

(*a*)

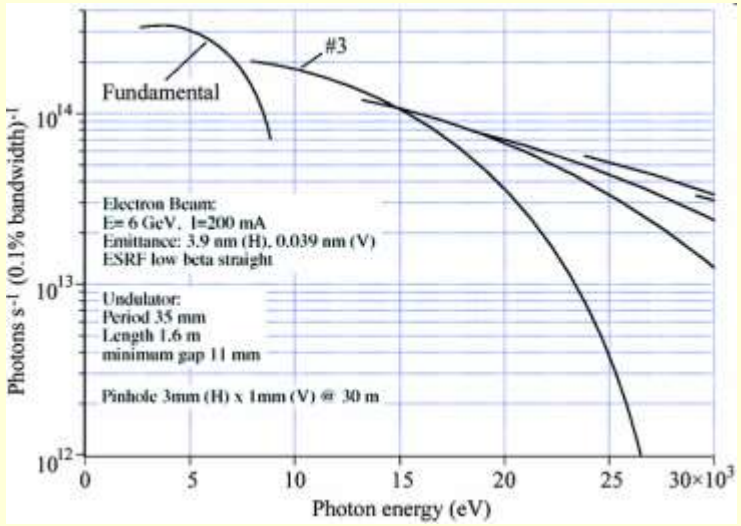
Fundamental
#3
Photons s-1 (0.1% bandwidth)-1
Electron Beam:
E= 6 GeV, I=200 mA
Emittance: 3.9 nm (H), 0.039 nm (V)
ESRF low beta straight
Undulator:
Period 35 mm
Length 1.6 m
minimum gap 11 mm
Pinhole 3mm (H) x 1mm (V) @ 30 m
Photon energy (eV)

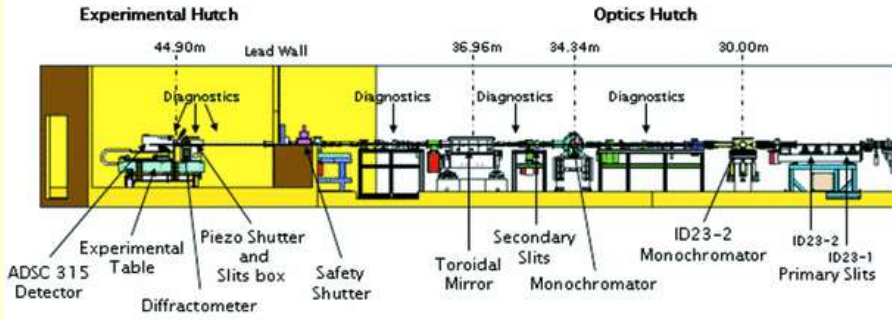
Experimental Hutch
Optics Hutch
44.90m
Lead Wall
36.96m
34.34m
30.00m
Diagnostics
ADSC 315 Detector
Experimental Table
Diffractometer
Piezo Shutter and Slits box
Safety Shutter
Toroidal Mirror
Secondary Slits
Monochromator
ID23-2 Monochromator
ID23-2
ID23-1
Primary Slits

(*b*)

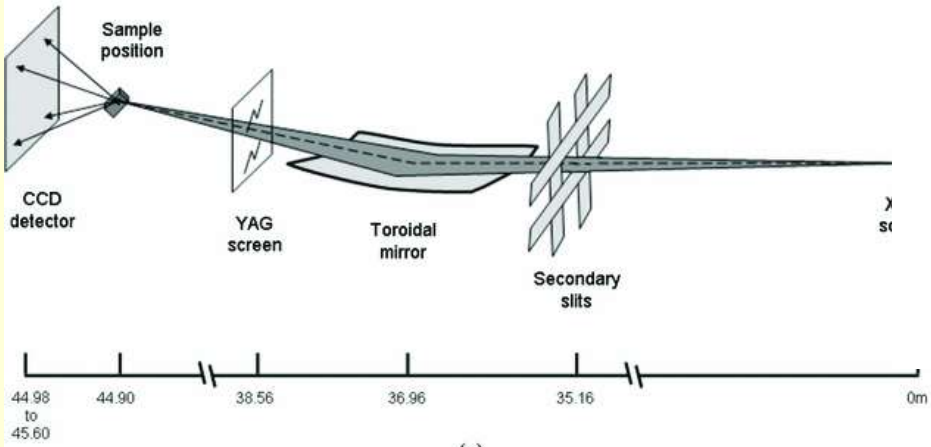
Sample position
CCD detector
YAG screen
Toroidal mirror
Secondary slits
44.98 to 45.60
44.90
38.56
36.96
35.16
0m

(*c*)

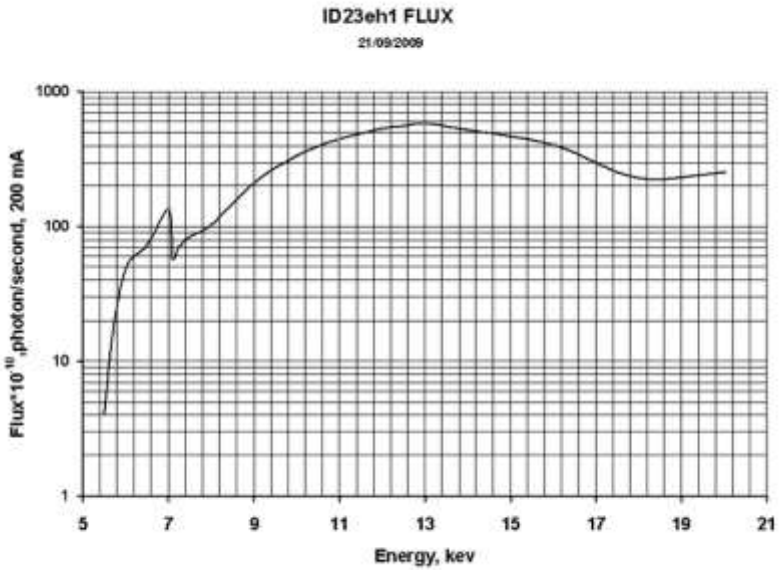
ID23eh1 FLUX
21/09/2009
Flux*10^10 photon/second, 200 mA
Energy, kev

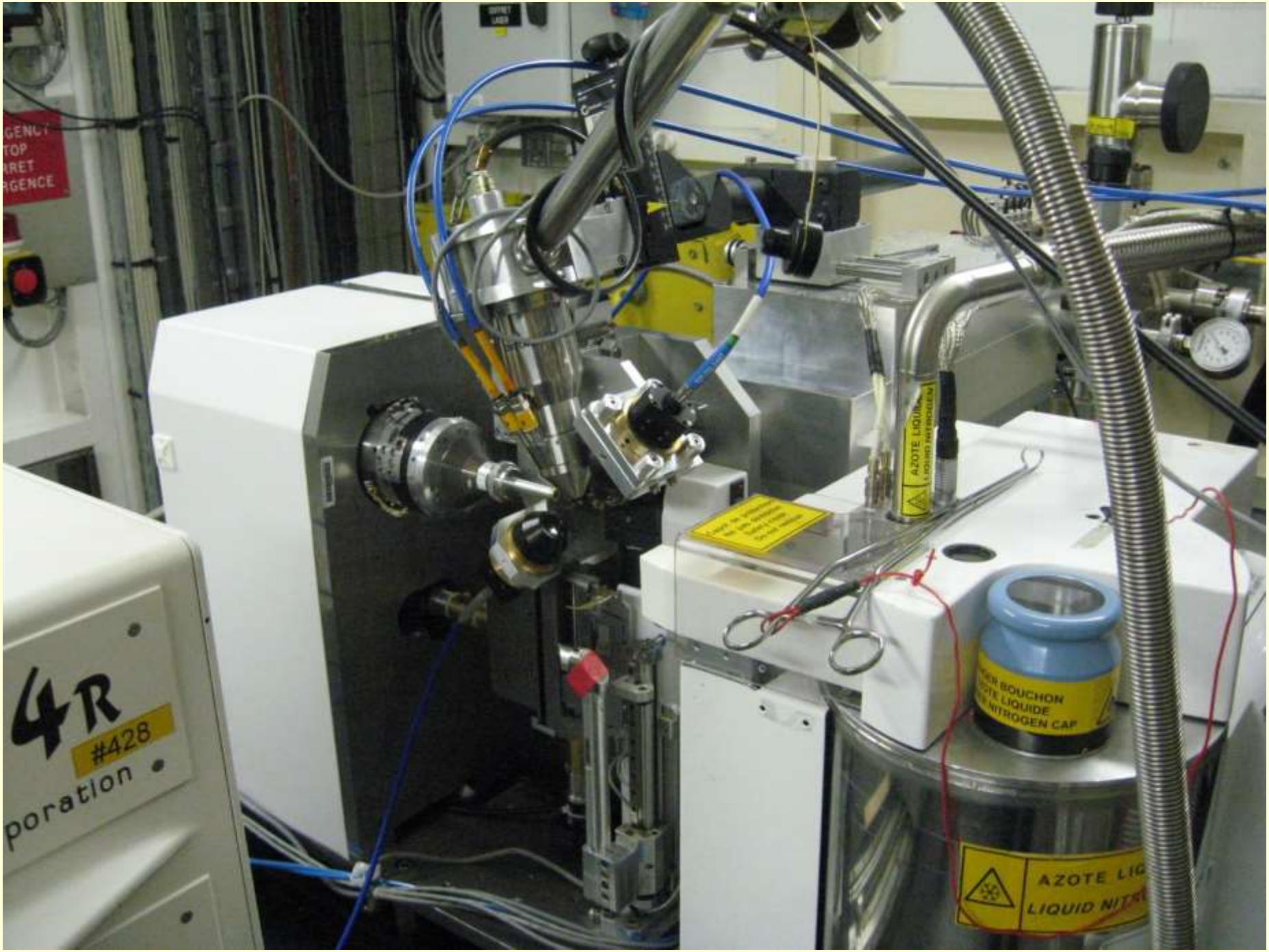
4R
#428
poration
AZOTE LIQUIDE
LIQUID NITROGEN

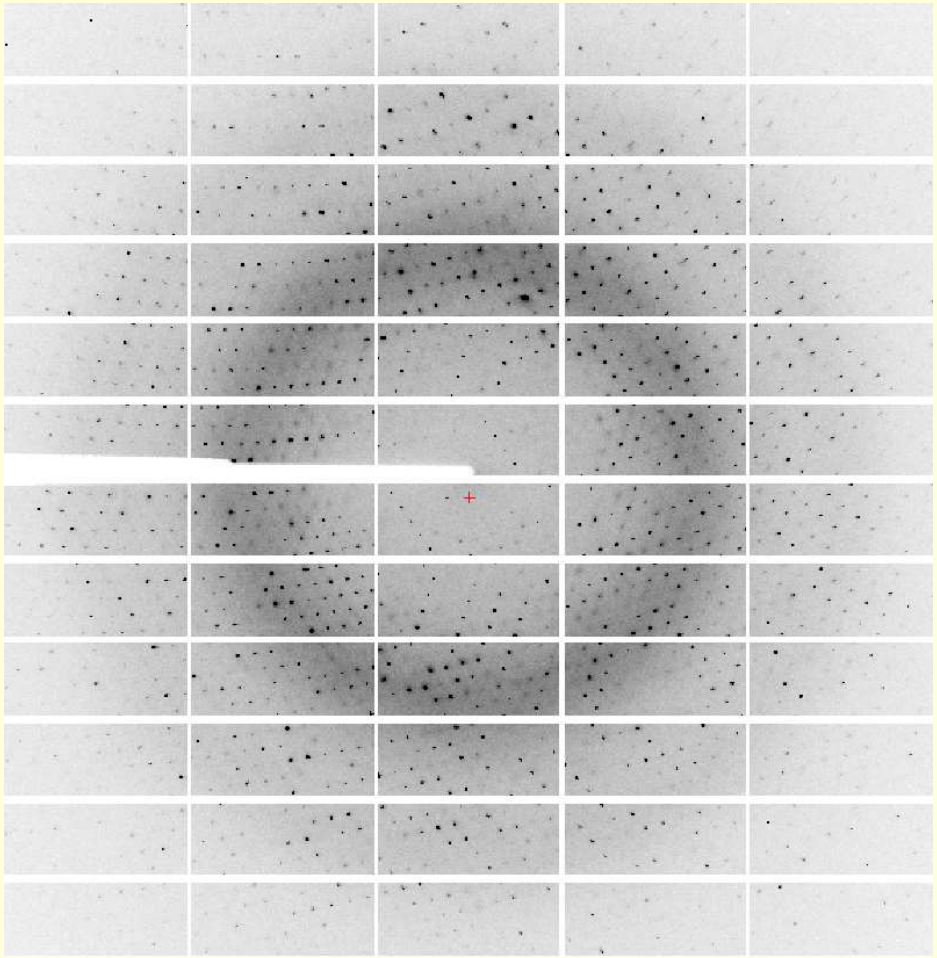

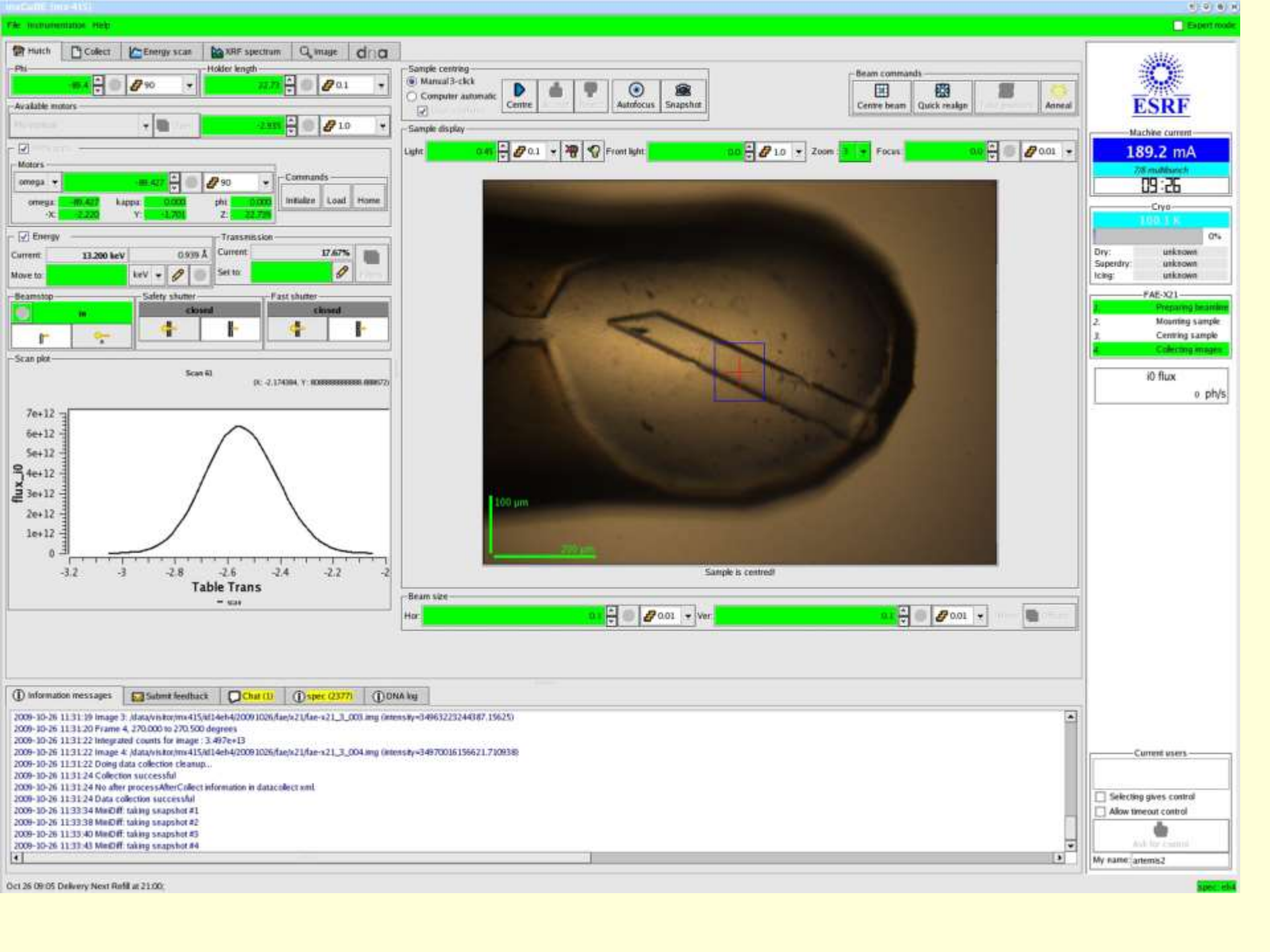
File Instrumentation Help
Expert mode
Hutch
Collect
Energy scan
XRF spectrum
Image
dna
Phi
Holder length
Available motors
Motors
omega
Commands
Initialize
Load
Home
Energy
Current: 13.200 keV
Move to:
Transmission
Current: 17.67%
Set to:
Beamstop
in
Safety shutter
closed
Fast shutter
closed
Scan plot
Scan 61
flux_i0
Table Trans
Sample centring
Manual 3-click
Computer automatic
Centre
Autofocus
Snapshot
Beam commands
Centre beam
Quick realign
Anneal
Sample display
Light:
Front light:
Zoom:
Focus:
100 µm
Sample is centred!
Beam size
Hor:
Ver:
ESRF
Machine current
189.2 mA
78 multibunch
09:26
Cryo
100.1 K
Dry: unknown
Superdry: unknown
Icing: unknown
FAE-X21
1. Preparing beamline
2. Mounting sample
3. Centring sample
4. Collecting images
i0 flux
0 ph/s
Information messages
Submit feedback
Chat (1)
spec (2377)
DNA log
2009-10-26 11:31:19 Image 3: /data/visitor/mx415/id14eh4/20091026/fae/x21/fae-x21_3_003.img (intensity=3496322324387.15625)
2009-10-26 11:31:20 Frame 4, 270.000 to 270.500 degrees
2009-10-26 11:31:22 Integrated counts for image : 3.497e+13
2009-10-26 11:31:22 Image 4: /data/visitor/mx415/id14eh4/20091026/fae/x21/fae-x21_3_004.img (intensity=3497001615662 1.710938)
2009-10-26 11:31:22 Doing data collection cleanup...
2009-10-26 11:31:24 Collection successful
2009-10-26 11:31:24 No after processAfterCollect information in datacollect.xml
2009-10-26 11:31:24 Data collection successful
2009-10-26 11:33:34 MiniDiff: taking snapshot #1
2009-10-26 11:33:38 MiniDiff: taking snapshot #2
2009-10-26 11:33:40 MiniDiff: taking snapshot #3
2009-10-26 11:33:43 MiniDiff: taking snapshot #4
Current users
Selecting gives control
Allow timeout control
My name: artemis2
Oct 26 09:05 Delivery Next Refill at 21:00:

Transport and ship in LN2

- Dry shipper
- Foam insulation
- Pour off LN2
- Fedex, Airborne
- Checked luggage
- Get the paperwork

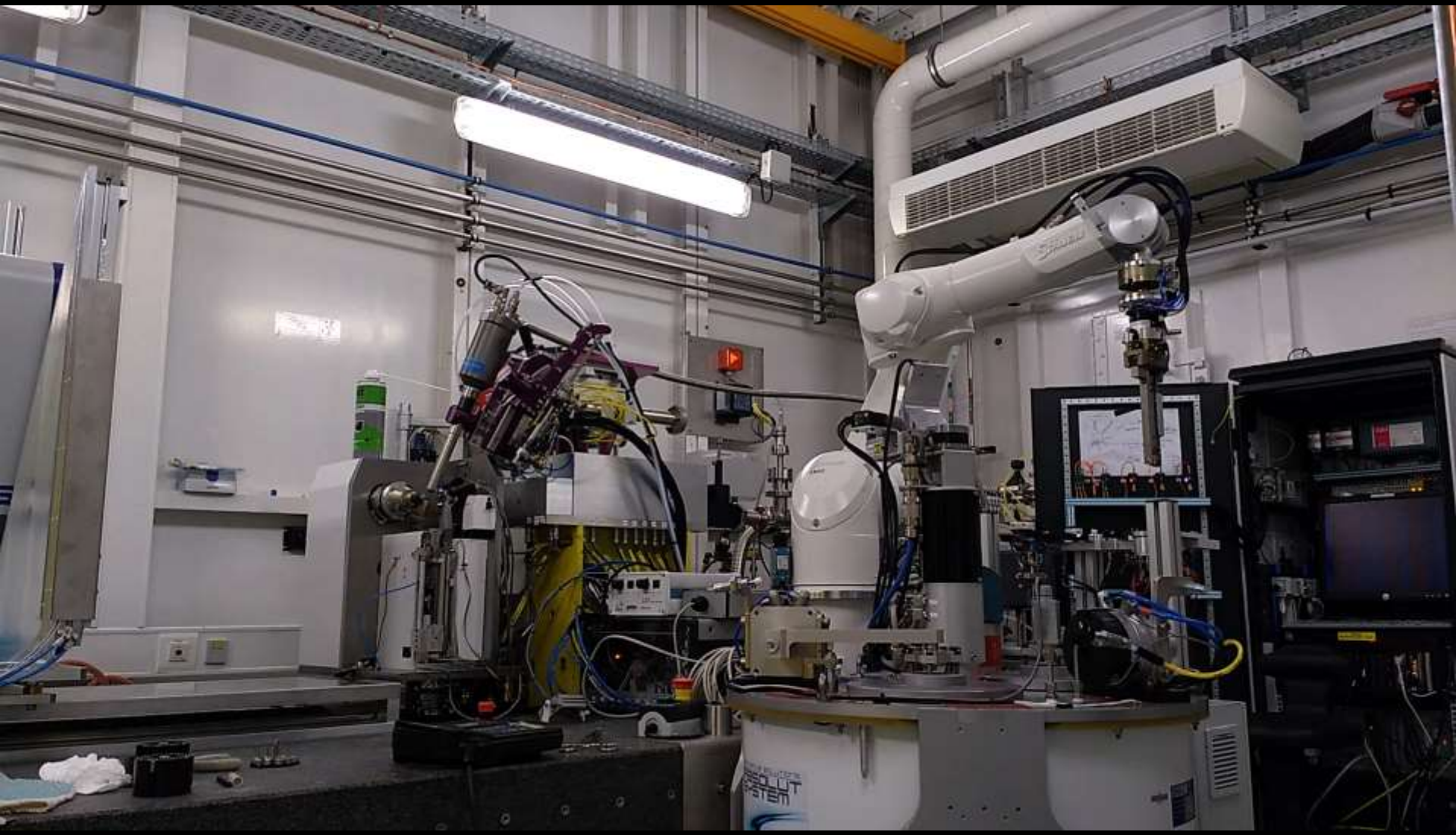

Micro-crystallography

• Thermolysin, Space Group $P6_122$; B-factor=11.5 Å^2

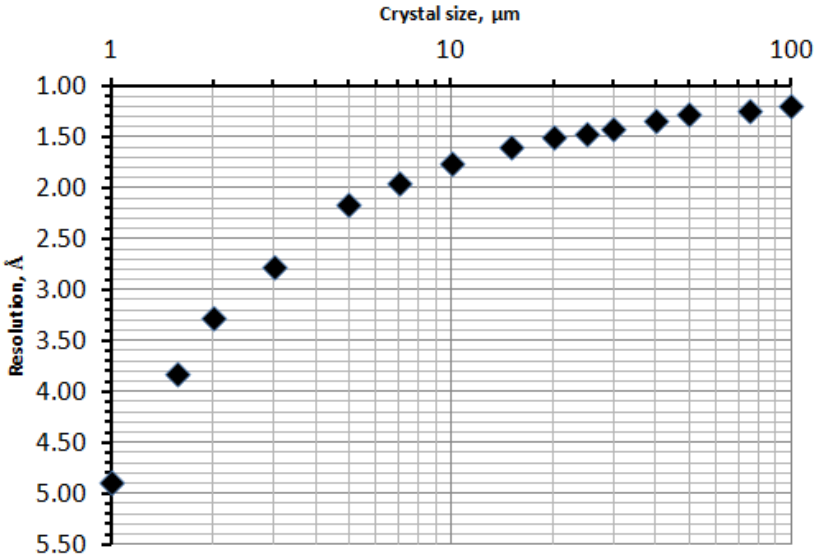

Complete data set resolution *vs.* crystal size

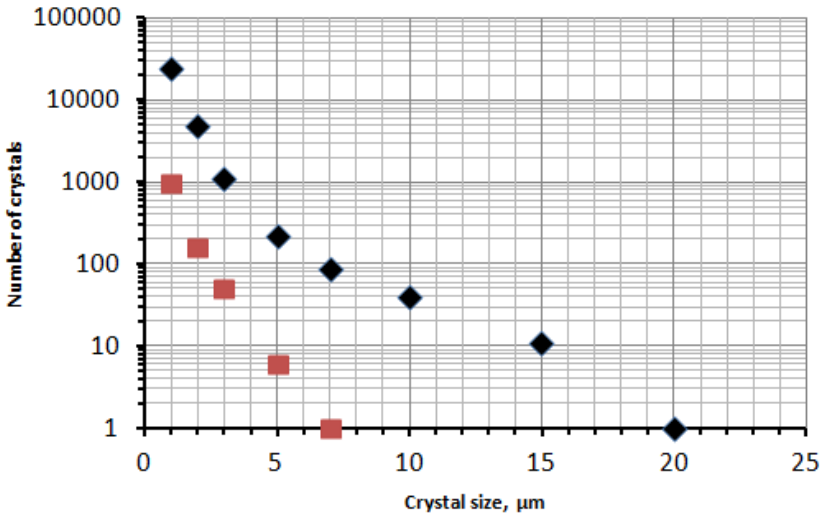

Number of cryocooled crystals of a given size required to achieve dataset resolutions of 1.5 Å (black) and 2.0 Å (blue).

• For a crystal 1x1x1 µm^3 in dimensions partial data sets *from about 1000 crystals* would be needed to achieve a final data set resolution of d_{min} = 2.0 Å .

Серийная кристаллография

Суть метода заключается в измерении частичных наборов данных, используя большое количества кристаллов, с последующим шкалированием и объединением этих данных для получении полного набора.

Мотивация

Преодоление эффектов радиационного повреждения

Сбор дифракционных данных используя кристаллы микронных размеров

Fully automatic multi-crystal position recognition, enhanced characterisation and data collection

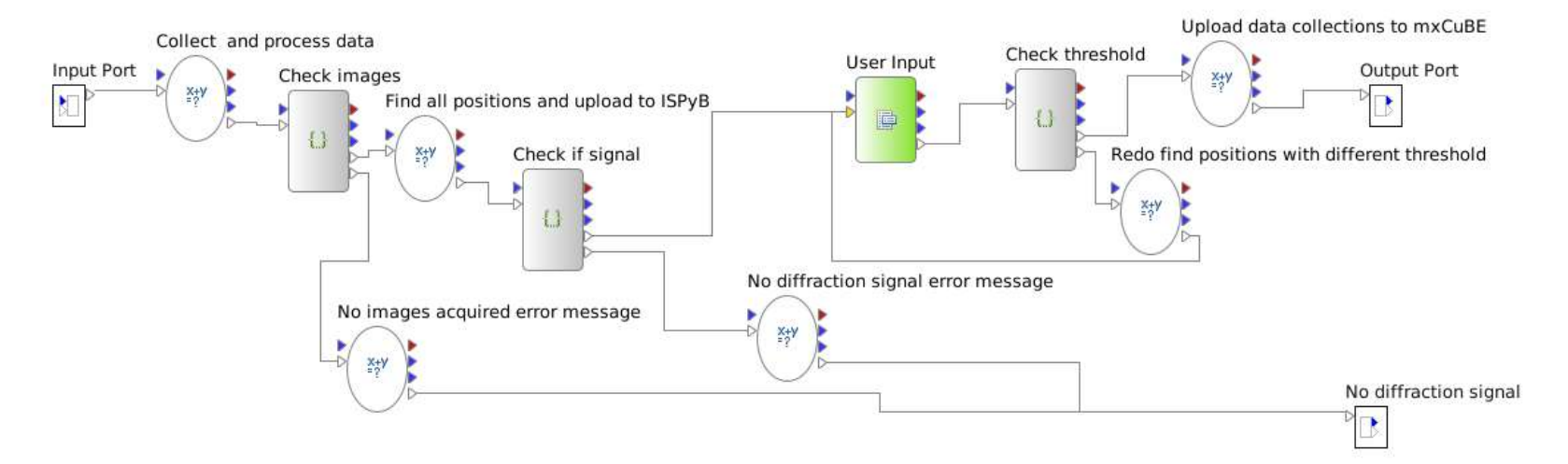

Fast Two-dimension mesh scan

Recognition of crystals using diffraction images

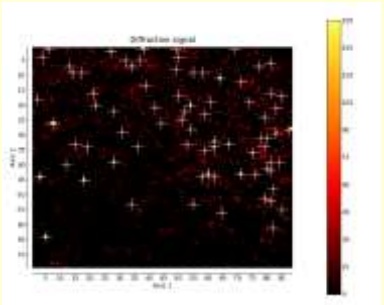

Data collection

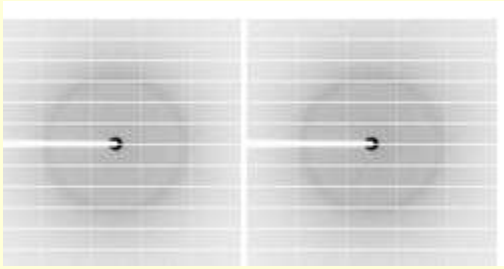

Thaumatin

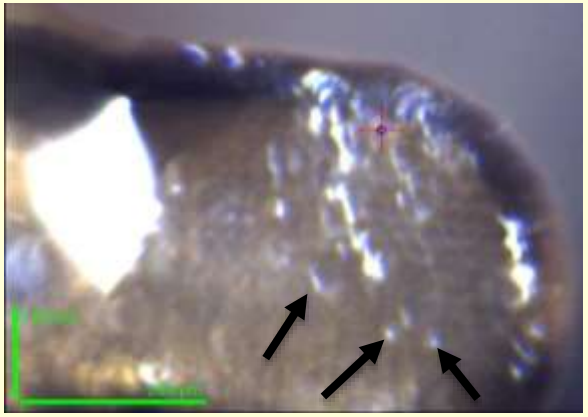

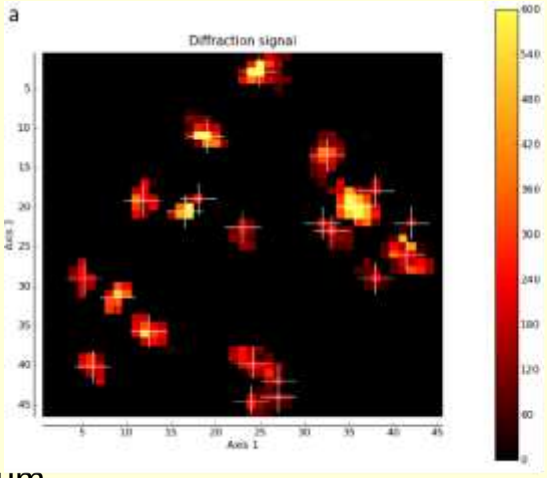

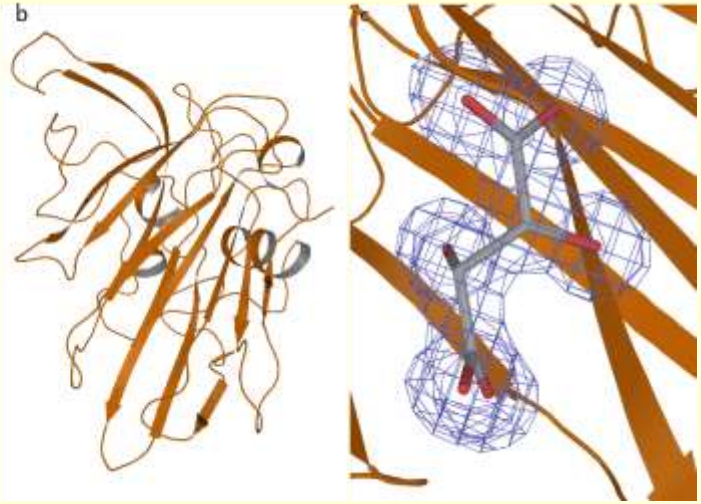

Micromesh with crystals, size about 20um

Results:

- All data sets could be processed
- all were usable for merging
- Resolution: 1.3 A
- Completenness: 99.8%
- I/SigmaI: 13.13
- Rmeas: 14.8%

Result of mesh scan: 22 hits,
10 deg oscillation per spot were collected

Bacteriorhodopsin

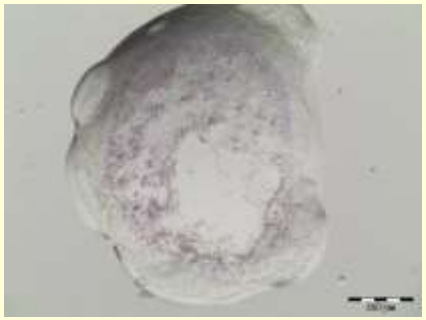

Bacteriorhodopsin crystals,
size about 5um

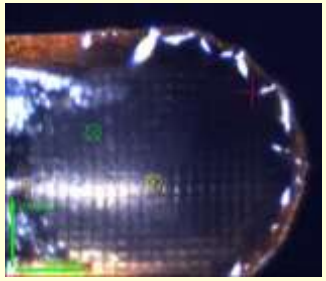

Micromesh used
for data collection

Result of mesh scan: 59 hits,
10 deg oscillation per spot were collected

Results:

- 14 data sets could be processed
  - Resolution: 3 A
  - Completenness: 91.2%

Bacteriorhodopsin crystals
size 10–20um

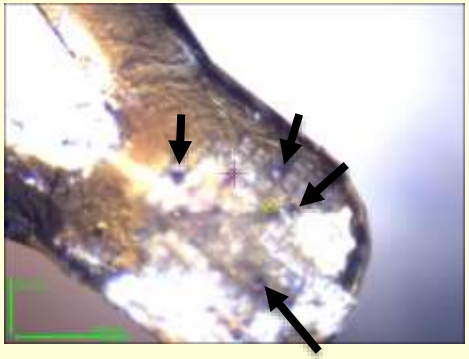

Results:

- All data sets could be processed
- 6 were usable for merging
  - Resolution: 2.4 A
  - Completenness: 95.3

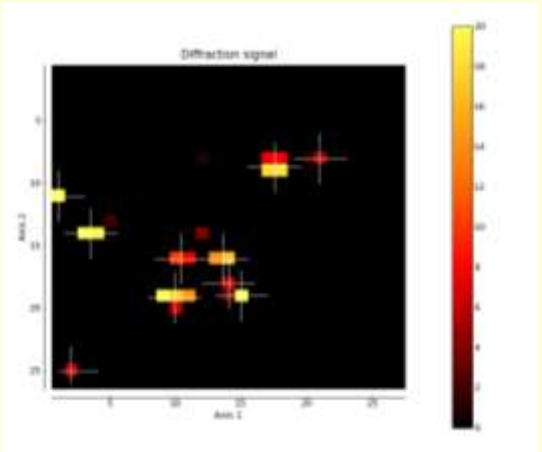

Result of mesh scan: 10 hits,
10 deg oscillation per spot were collected

PETRA III @ DESY

2.3 km – 6 GeV – 100 mA – 280 M€

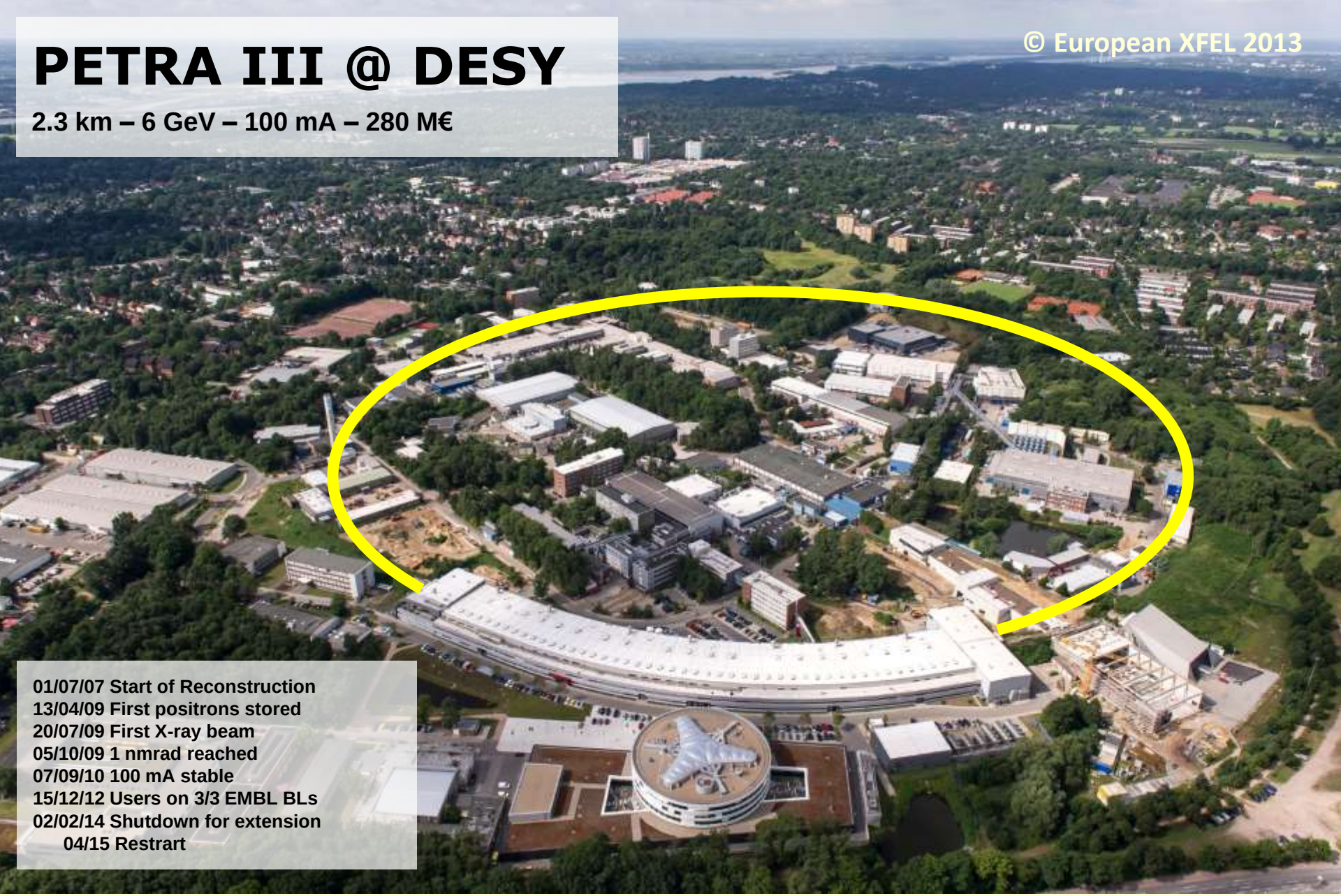

01/07/07 Start of Reconstruction
13/04/09 First positrons stored
20/07/09 First X-ray beam
05/10/09 1 nmrad reached
07/09/10 100 mA stable
15/12/12 Users on 3/3 EMBL BLs
02/02/14 Shutdown for extension
04/15 Restrart

Cathepsin B

Redecke, L., ... Chapman, H. (2012): Natively Inhibited Trypanosoma brucei Cathepsin B Structure Determined by Using an X-ray Laser. Science 339:227 [4HWY:2.1 Å]

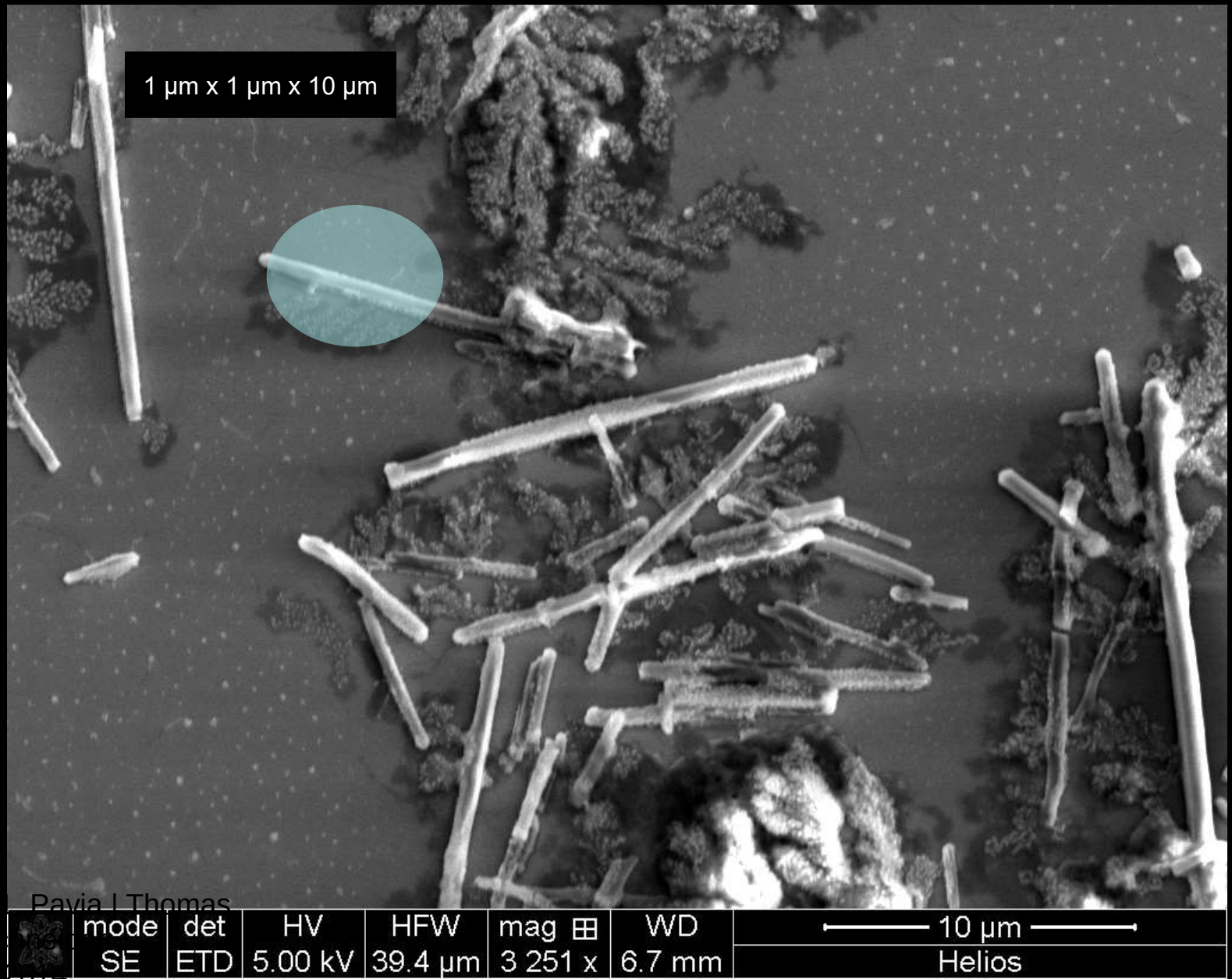

Cathepsin B suspension in a cryo loop

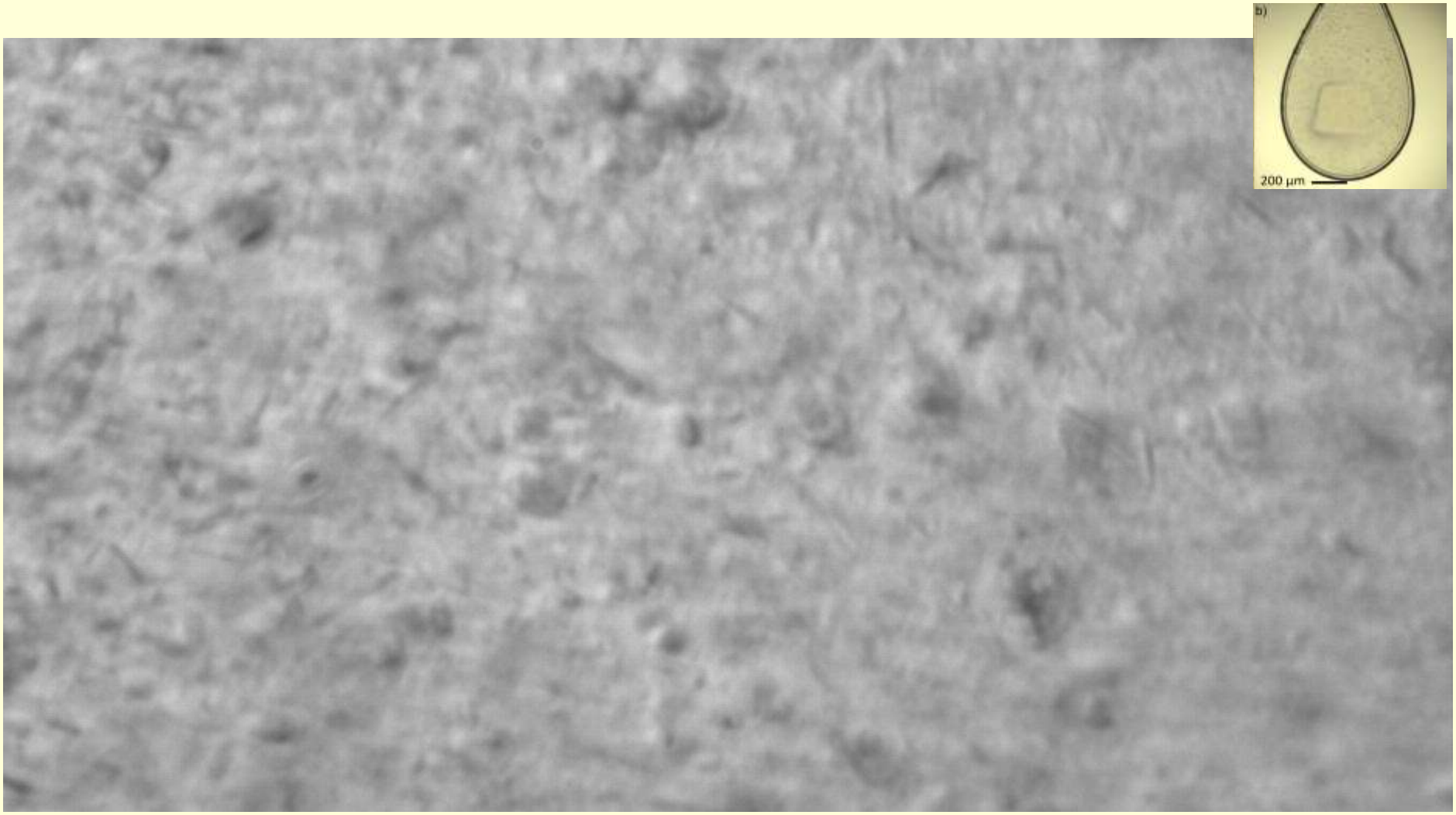

Cathepsin B – diffraction exposure dose 34 MGy

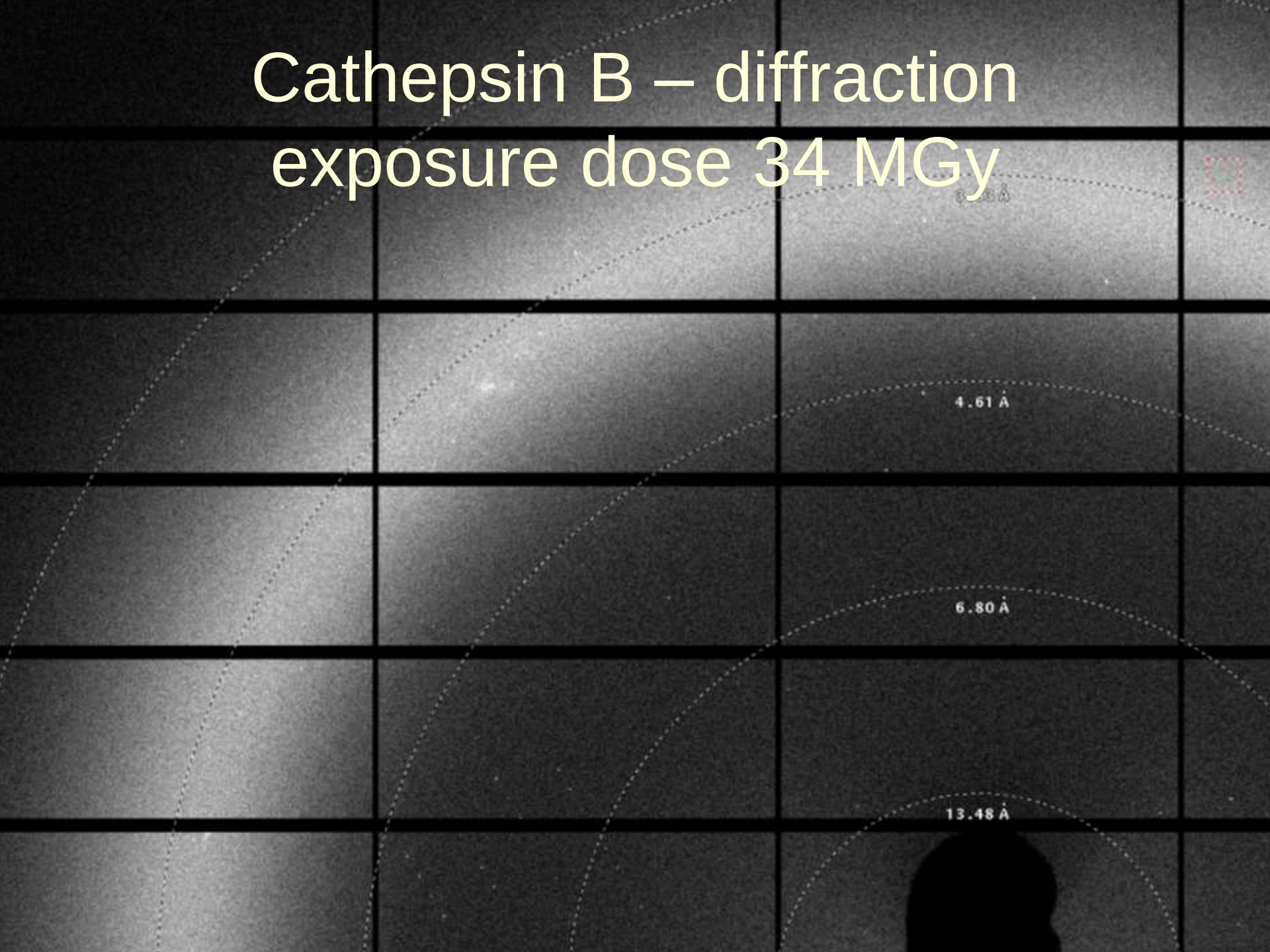

Fast rastering by rotation exposures

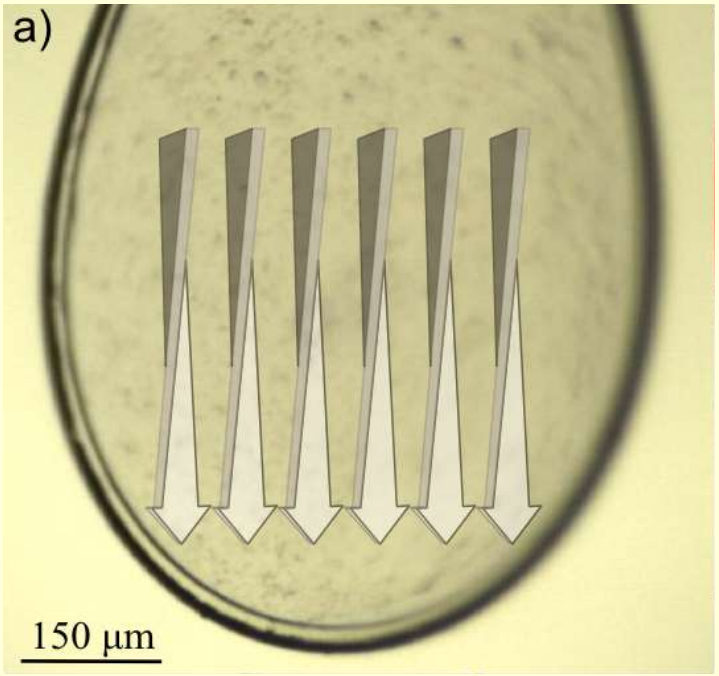

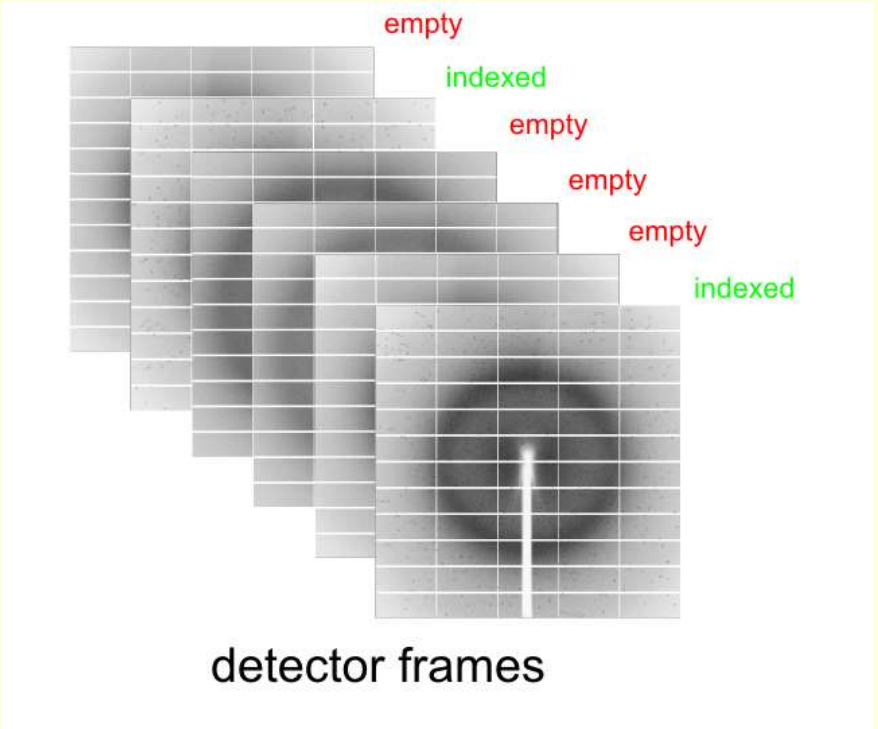

Series of frames acquired shutter-less during continuous motion of sample mount
In such a way that each crystal passes through the beam while rotating by 1-2° and receiving its life-dose exposure

- Rotation method - angular integration (*vs Monte-Carlo in SFX*)

Cathepsin B data collection and processing

22800 frames recorded

2200 frames indexed (CRYSTFEL, White et al. 2012)

600 frames passing successfully integrated/scaled (XDS, Kabsch 2010)

80 crystals contributed to the final data set

SFX + continuity = SSX

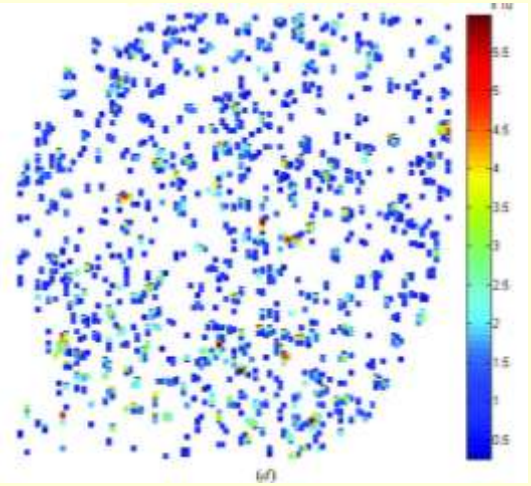

initial hits

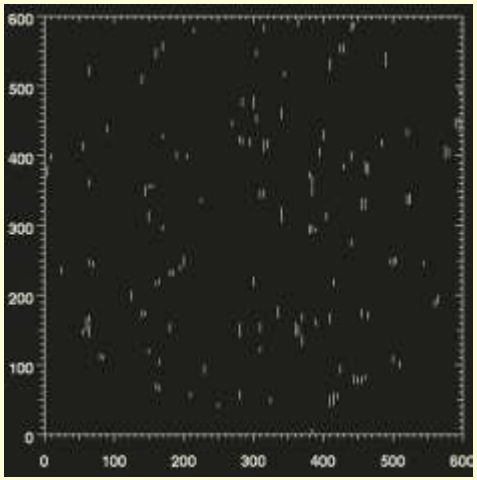

final data

$P4_122$ a=123.5 Å, c=54.3 Å
Resolution= [88.1-3.0 Å]
Completeness= 99.8%
Multiplicity= 12.3
$CC_{1/2}$= 0.99 (0.79 high-res)
<I/SigI>= 3.7 (8.9 low, 1.0 high)

Mol. Replacement + refinement
Rwork,free = 22.9, 26.1

X-ray free-electron lasers

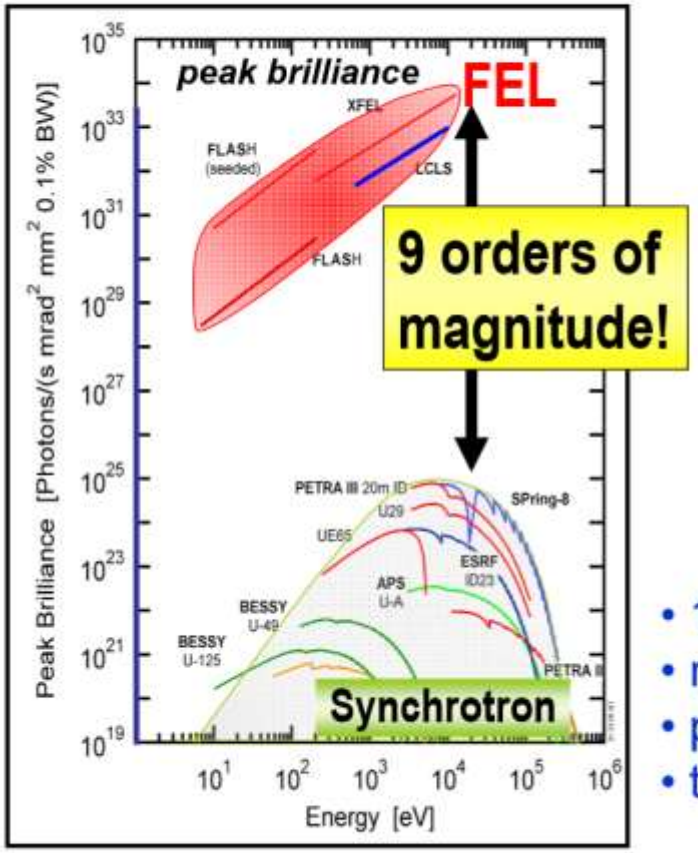

- FLASH: 2005
- Fermi: 2009
- LCLS: 2009
- SACLA: 2011
- Fermi 2011
- XFEL: 2017
- PSI, LCLSII, KVI, Shanghai,…

- $10^{12\text{-}13}$ photons ~ 3-500 fs pulses
- repetition rate: 120 Hz
- photon energy: 300 eV-10 keV
- transversally fully coherent

Potential for biomolecular imaging with femtosecond X-ray pulses

NATURE | VOL 406 | 17 AUGUST 2000 | www.nature.com

Richard Neutze*, Remco Wouts*, David van der Spoel*, Edgar Weckert†‡ & Janos Hajdu*

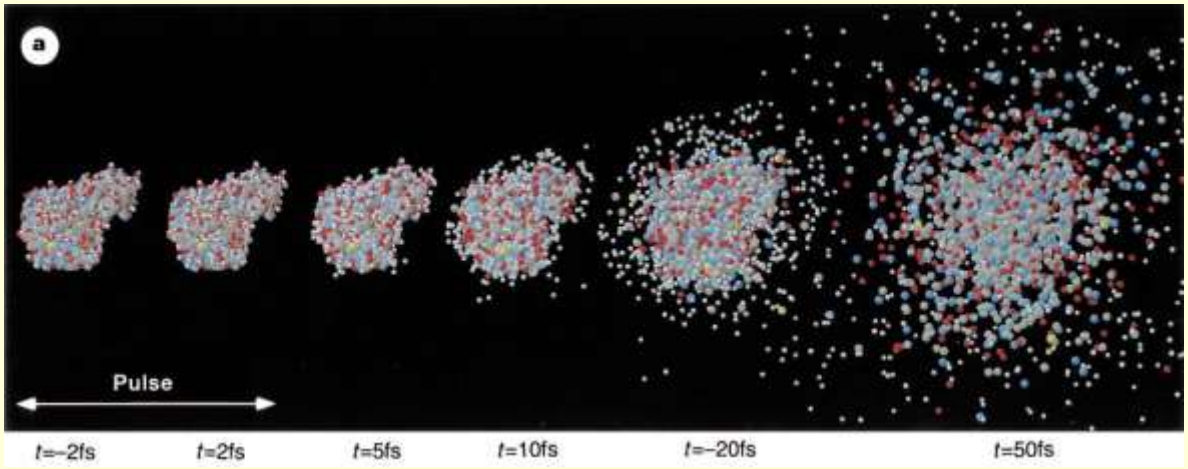

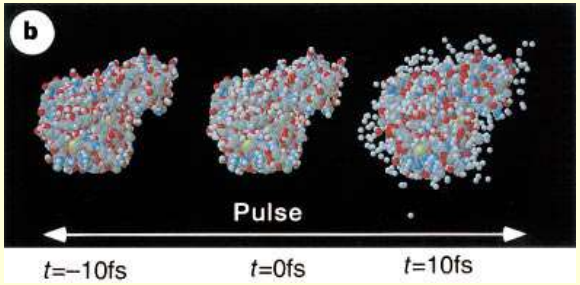

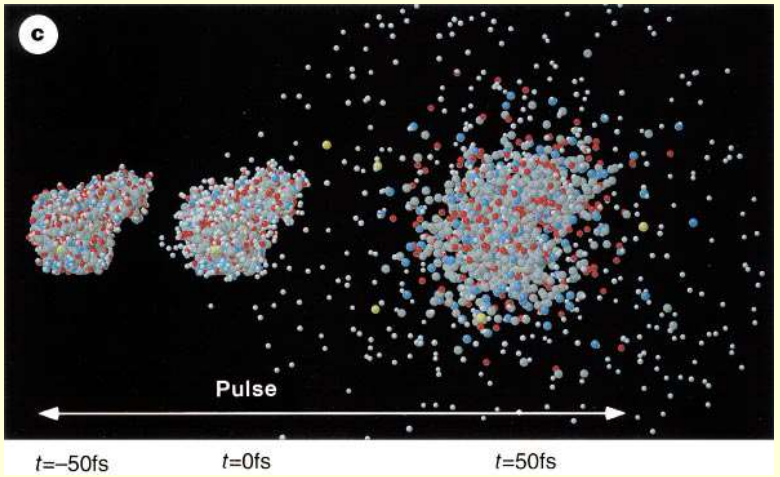

Figure 2 Explosion of T4 lysozyme (white, H; grey, C; blue, N; red, O; yellow, S) induced by radiation damage. The integrated X-ray intensity was 3×10^{12} (12 keV) photons per 100-nm diameter spot (3.8×10^6 photons per Å^2) in all cases. **a**, A protein exposed to an X-ray pulse with an FWHM of 2 fs, and disintegration followed in time. Atomic positions in the first two structures (before and after the pulse) are practically identical at this pulse length because of an inertial delay in the explosion. $R_{nucl} = 3\%$, $R_{elec} = 11\%$ **b**, Lysozyme exposed to the same number of photons as in **a**, but the FWHM of the pulse was 10 fs. Images show the structure at the beginning, in the middle and near the end of the X-ray pulse. $R_{nucl} = 7\%$, $R_{elec} = 12\%$ **c**, Behaviour of the protein during an X-ray pulse with an FWHM of 50 fs. $R_{nucl} = 26\%$, $R_{elec} = 30\%$.

LETTER | 3 FEBRUARY 2011 | VOL 470 | NATURE | 73

doi:10.1038/nature09750

Femtosecond X-ray protein nanocrystallography

Henry N. Chapman[1,2], Petra Fromme[3], Anton Barty[1], Thomas A. White[1], Richard A. Kirian[4], Andrew Aquila[1], Mark S. Hunter[3], Joachim Schulz[1], Daniel P. DePonte[1], Uwe Weierstall[4], R. Bruce Doak[4], Filipe R. N. C. Maia[5], Andrew V. Martin[1], Ilme Schlichting[6,7], Lukas Lomb[7], Nicola Coppola[1]†, Robert L. Shoeman[7], Sascha W. Epp[6,8], Robert Hartmann[9], Daniel Rolles[6,7], Artem Rudenko[6,8], Lutz Foucar[6,7], Nils Kimmel[10], Georg Weidenspointner[11,10], Peter Holl[9], Mengning Liang[1], Miriam Barthelmess[12], Carl Caleman[1], Sébastien Boutet[13], Michael J. Bogan[14], Jacek Krzywinski[13], Christoph Bostedt[13], Saša Bajt[12], Lars Gumprecht[1], Benedikt Rudek[6,8], Benjamin Erk[6,8], Carlo Schmidt[6,8], André Hömke[6,8], Christian Reich[9], Daniel Pietschner[10], Lothar Strüder[6,10], Günter Hauser[10], Hubert Gorke[15], Joachim Ullrich[6,8], Sven Herrmann[10], Gerhard Schaller[10], Florian Schopper[10], Heike Soltau[9], Kai-Uwe Kühnel[8], Marc Messerschmidt[13], John D. Bozek[13], Stefan P. Hau-Riege[16], Matthias Frank[16], Christina Y. Hampton[14], Raymond G. Sierra[14], Dmitri Starodub[14], Garth J. Williams[13], Janos Hajdu[5], Nicusor Timneanu[5], M. Marvin Seibert[5]†, Jakob Andreasson[5], Andrea Rocker[5], Olof Jönsson[5], Martin Svenda[5], Stephan Stern[1], Karol Nass[2], Robert Andritschke[10], Claus-Dieter Schröter[8], Faton Krasniqi[6,7], Mario Bott[7], Kevin E. Schmidt[4], Xiaoyu Wang[4], Ingo Grotjohann[3], James M. Holton[17], Thomas R. M. Barends[7], Richard Neutze[18], Stefano Marchesini[17], Raimund Fromme[3], Sebastian Schorb[19], Daniela Rupp[19], Marcus Adolph[19], Tais Gorkhover[19], Inger Andersson[20], Helmut Hirsemann[12], Guillaume Potdevin[12], Heinz Graafsma[12], Björn Nilsson[12] & John C. H. Spence[4]

X-ray crystallography provides the vast majority of macromolecular structures, but the success of the method relies on growing crystals of sufficient size. In conventional measurements, the necessary increase in X-ray dose to record data from crystals that are too small leads to extensive damage before a diffraction signal can be recorded[1–3]. It is particularly challenging to obtain large, well-diffracting crystals of membrane proteins, for which fewer than 300 unique structures have been determined despite their importance in all living cells. Here we present a method for structure determination where single-crystal X-ray diffraction 'snapshots' are collected from a fully hydrated stream of nanocrystals using femtosecond pulses from a hard-X-ray free-electron laser, the Linac Coherent Light Source[4]. We prove this concept with nanocrystals of photosystem I, one of the largest membrane protein complexes[5]. More than 3,000,000 diffraction patterns were collected in this study, and a three-dimensional data set was assembled from individual photosystem I nanocrystals (~200 nm to 2 μm in size). We mitigate the problem of radiation damage in crystallography by using pulses briefer than the timescale of most damage processes[6]. This offers a new approach to structure determination of macromolecules that do not yield crystals of sufficient size for studies using conventional radiation sources or are particularly sensitive to radiation damage.

Serial femtosecond crystallography

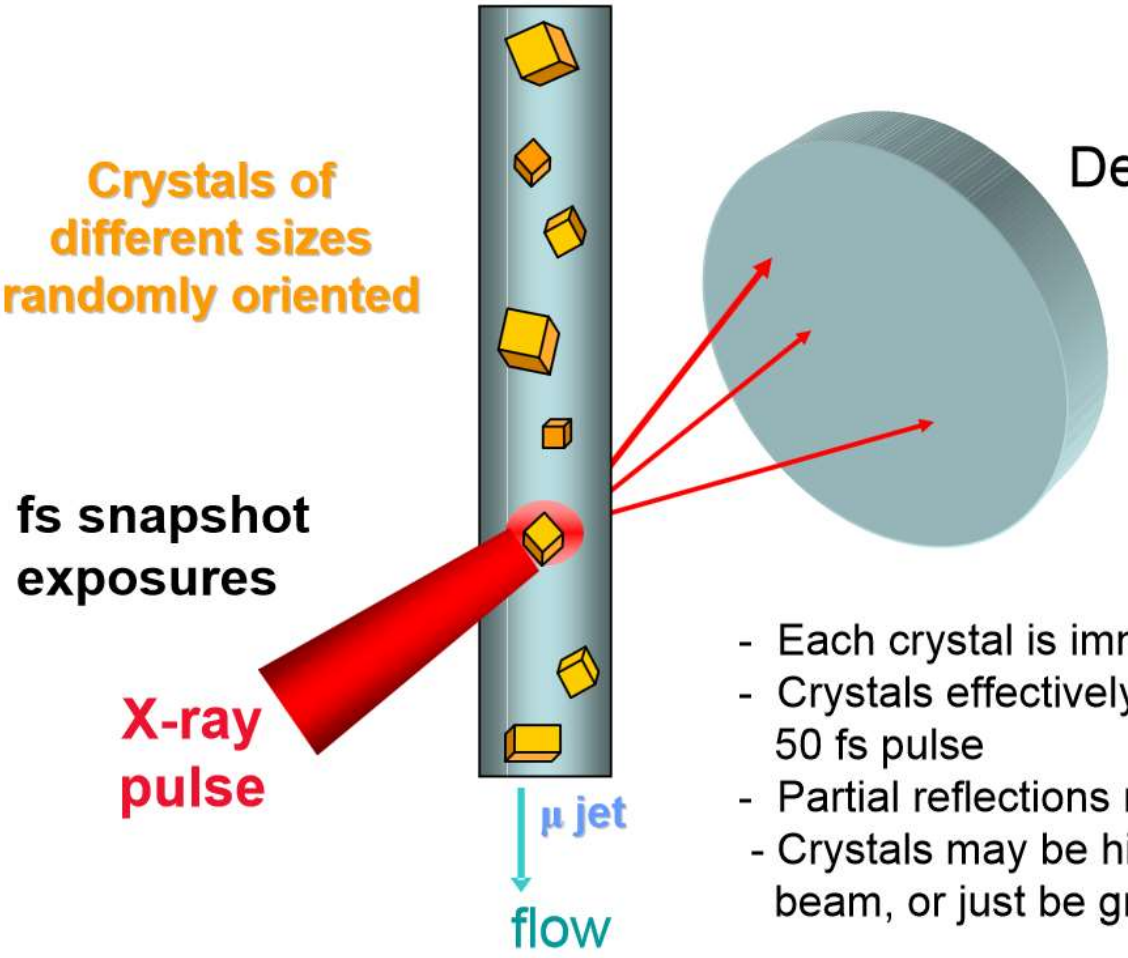

- Each crystal is immediately destroyed
- Crystals effectively stand still during a 50 fs pulse
- Partial reflections not fully integrated
- Crystals may be hit by center of the beam, or just be grazed by it

Figure 5. Gas-dynamic virtual nozzle (upper) and breakup of a Rayleigh droplet beam (lower). In the upper figure, a cone of liquid is seen at A being focused as it speeds up under the influence of a coaxial high pressure gas jet running between the outer glass capillary tube B (inner diameter 40 μm) and the inner hollow fiber-optic line C carrying the buffer and protein mixture. The stream emerges into vacuum where it will break up into droplets as shown below. The x-ray beam may be positioned in either the continuous-flow or droplet region, along which temperature falls, producing micrometer-sized balls of ice.

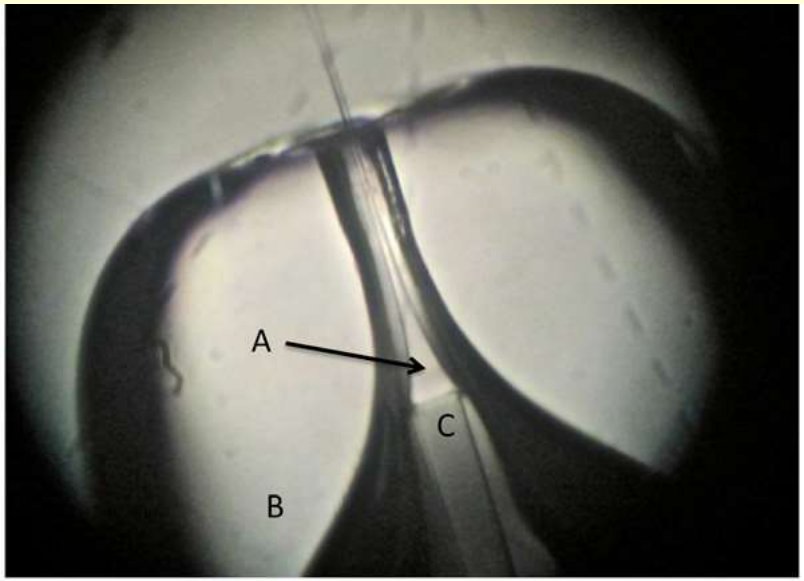

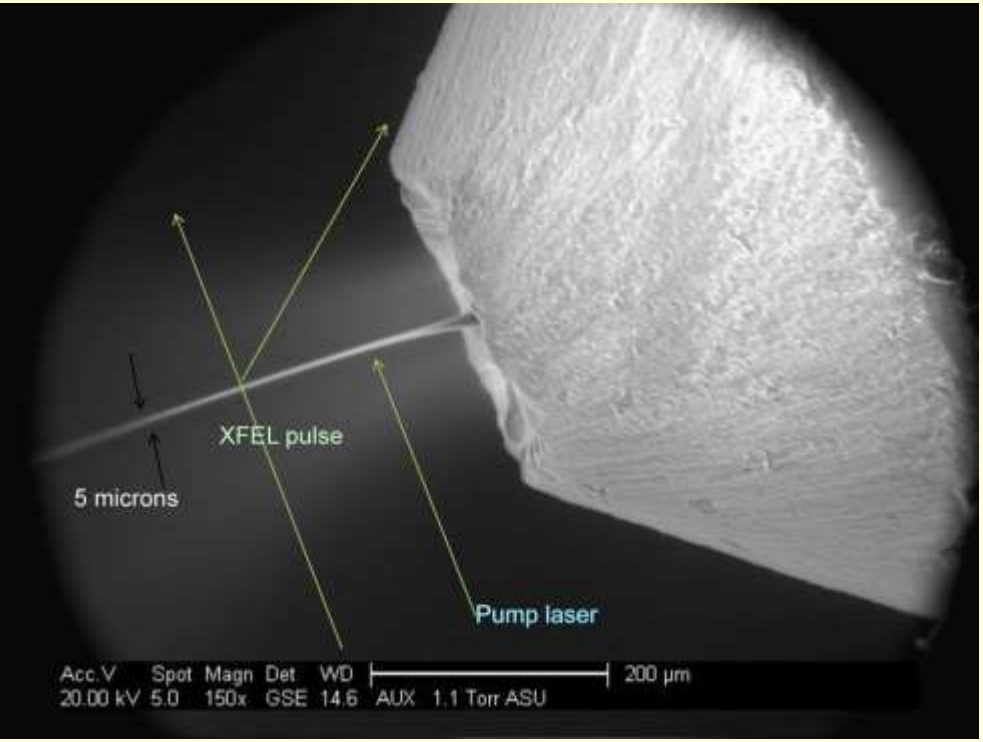

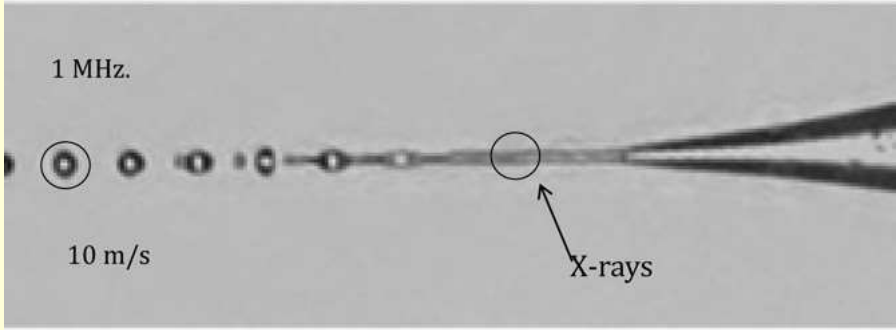

Figure 4. Liquid jet nozzle seen operating inside an environmental SEM (submicrometer droplets cannot be resolved in an optical microscope). The hollow fiber-optic carrying the fluid terminates just to inside (to the right) of the ground cone on this glass capillary tube. From this is seen a bright diverging stream of gas, which is focusing the liquid stream. The positions of the XFEL and pump laser beams are shown. The droplets freeze over a distance of about 1 cm as they cool by evaporation into vacuum, travelling at about 10 m s^{-1}. A flow rate of 10 μl min^{-1} is common.

Data analysis

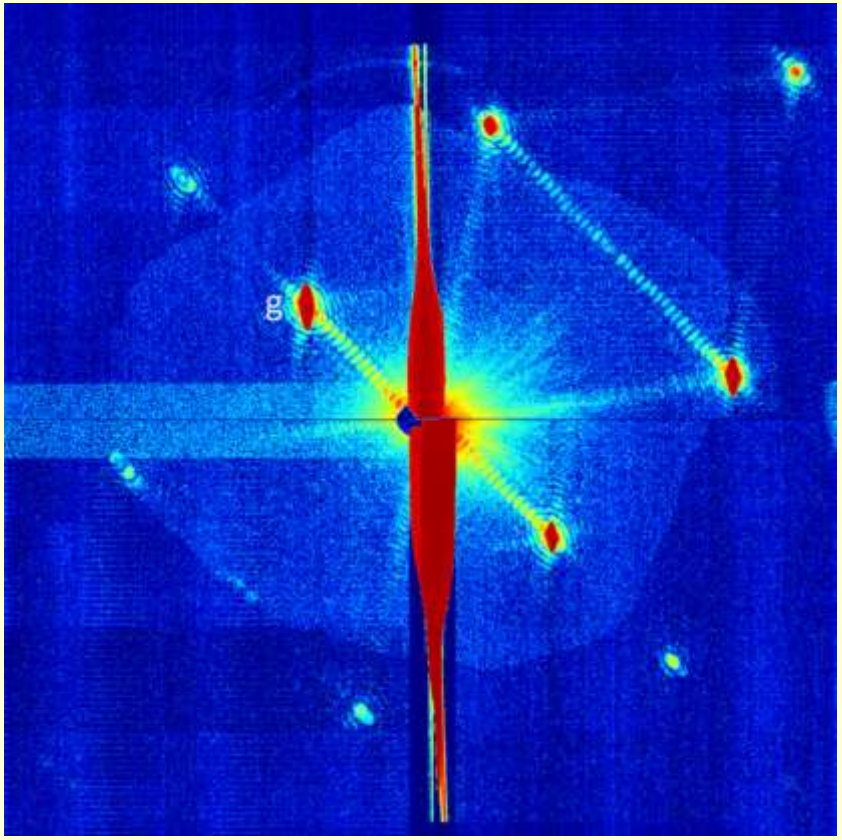

Figure 6. Shape transforms. Single 40 fs XFEL diffraction pattern from a single nanocrystal of Photosystem I recorded in the liquid jet at 2 keV on a rear detector. The thick streak running up the page through the center results from diffraction by the continuous column of liquid. From the number of subsidiary minima we can determine that this nanocrytal consisted of just 17 unit cells between facets along direction g. Reproduced with permission from Chapman *et al* (2011). Copyright 2011 Nature Publishing Group.

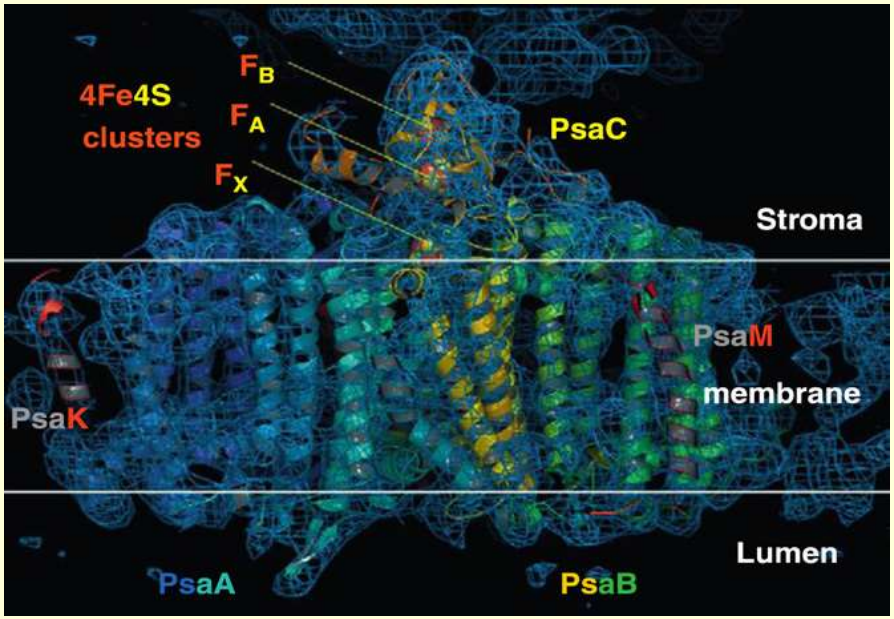

Figure 7. Charge-density map at 0.8 nm resolution, for Photosytem I (PSI) complex (1 MDa, two trimers per unit cell) reconstructed from tens of thousands of 2 keV XFEL snapshots, taken from size-varying nanocrystals in random orientations at 100 K. The cell membrane is indicated, with the Stroma side outermost toward the light. The crystals are hexagonal ($P6_3$, $a = b = 28.8$ nm, $c = 16.7$ nm) with 78% water content. Some of the 12 proteins making up this complex of 72 000 non-hydrogen atoms are labelled. This complex, together with Photosystem II, in all green plants is responsible for all the oxygen we breath (by splitting water in sunlight) and for CO_2 degradation. Reproduced with permission from Kirian *et al* (2011a). Copyright 2011 International Union of Crystallography.

20 JULY 2012 VOL 337 SCIENCE

High-Resolution Protein Structure Determination by Serial Femtosecond Crystallography

Sébastien Boutet,[1*] Lukas Lomb,[2,3] Garth J. Williams,[1] Thomas R. M. Barends,[2,3] Andrew Aquila,[4] R. Bruce Doak,[5] Uwe Weierstall,[5] Daniel P. DePonte,[4] Jan Steinbrener,[2,3] Robert L. Shoeman,[2,3] Marc Messerschmidt,[1] Anton Barty,[4] Thomas A. White,[4] Stephan Kassemeyer,[2,3] Richard A. Kirian,[5] M. Marvin Seibert,[1] Paul A. Montanez,[1] Chris Kenney,[6] Ryan Herbst,[6] Philip Hart,[6] Jack Pines,[6] Gunther Haller,[6] Sol M. Gruner,[7,8] Hugh T. Philipp,[7] Mark W. Tate,[7] Marianne Hromalik,[9] Lucas J. Koerner,[10] Niels van Bakel,[11] John Morse,[12] Wilfred Ghonsalves,[1] David Arnlund,[13] Michael J. Bogan,[14] Carl Caleman,[4] Raimund Fromme,[15] Christina Y. Hampton,[14] Mark S. Hunter,[15] Linda C. Johansson,[13] Gergely Katona,[13] Christopher Kupitz,[15] Mengning Liang,[4] Andrew V. Martin,[4] Karol Nass,[16] Lars Redecke,[17,18] Francesco Stellato,[4] Nicusor Timneanu,[19] Dingjie Wang,[5] Nadia A. Zatsepin,[5] Donald Schafer,[1] James Defever,[1] Richard Neutze,[13] Petra Fromme,[15] John C. H. Spence,[5] Henry N. Chapman,[4,16] Ilme Schlichting[2,3]

Structure determination of proteins and other macromolecules has historically required the growth of high-quality crystals sufficiently large to diffract x-rays efficiently while withstanding radiation damage. We applied serial femtosecond crystallography (SFX) using an x-ray free-electron laser (XFEL) to obtain high-resolution structural information from microcrystals (less than 1 micrometer by 1 micrometer by 3 micrometers) of the well-characterized model protein lysozyme. The agreement with synchrotron data demonstrates the immediate relevance of SFX for analyzing the structure of the large group of difficult-to-crystallize molecules.

Figure 8. Single-shot 40 fs XFEL diffraction pattern from a single lysozyme nanocrystal recorded at 9.4 keV in the liquid jet at RT, extending to 0.18 nm resolution. The dose of 33 MGy is similar to the Henderson 'safe dose' for frozen samples, but 30 times higher than the tolerable dose for RT synchrotron data collection. Reproduced with permission from Boutet *et al* (2012). Copyright 2012 American Association for the Advancement of Science.

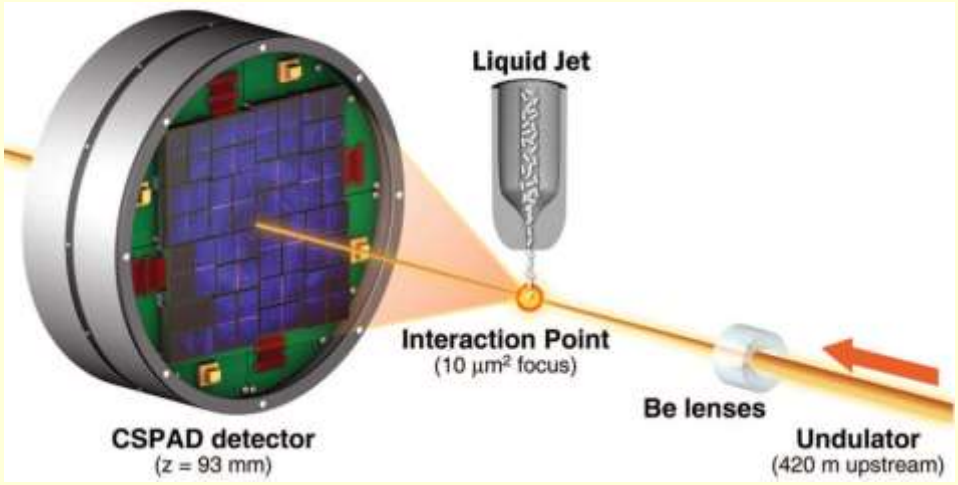

Experimental geometry for SFX at the CXI instrument. Single-pulse diffraction patterns from single crystals flowing in a liquid jet are recorded on a CSPAD at the 120-Hz repetition rate of LCLS. Each pulse was focused at the interaction point by using 9.4-keV x-rays.

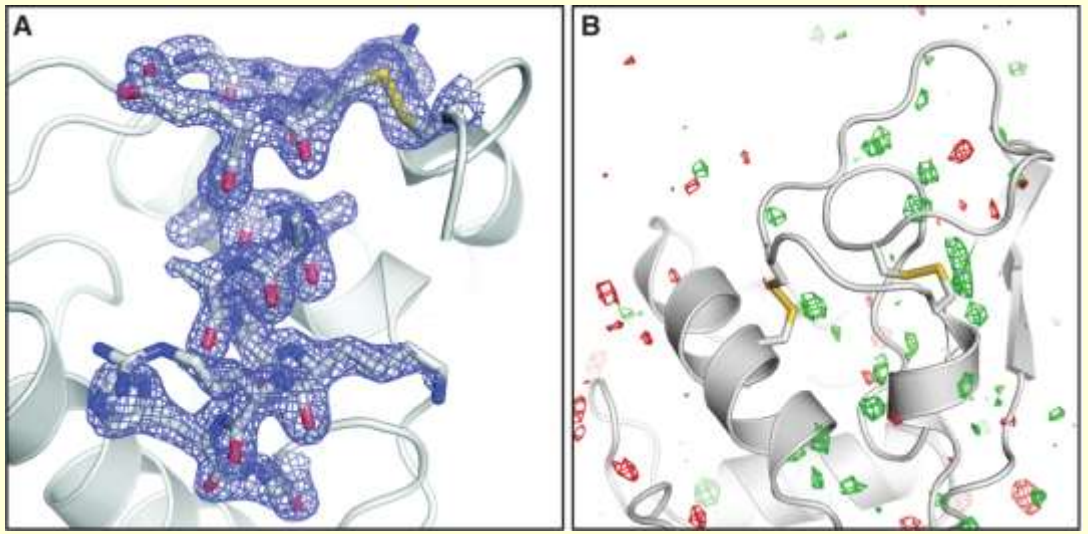

Fig. 2. (**A**) Final, refined $2mF_{obs} - DF_{calc}$ (1.5σ) electron density map (*17*) of lysozyme at 1.9 Å resolution calculated from 40-fs pulse data. (**B**) F_{obs}(40 fs) − F_{obs} (synchrotron) difference Fourier map, contoured at +3 σ (green) and −3 σ (red). No interpretable features are apparent. The synchrotron data set was collected with a radiation dose of 24 kGy.

High resolution femtosecond diffraction of micron-sized lysozyme crystals

Lysozyme crystals
1-2 μm Ø

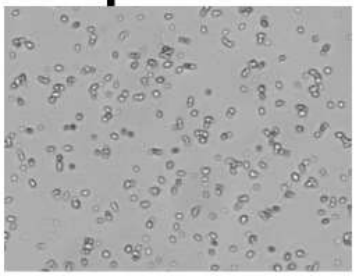

40 fs pulse*, 3 mJ/pulse
10 μm^2 focus
Transmission 15%
0.6 mJ/sample
33 MGy/pulse
9.4 keV , λ =1.32 A
Resolution 1.9 Å

*electron bunch length

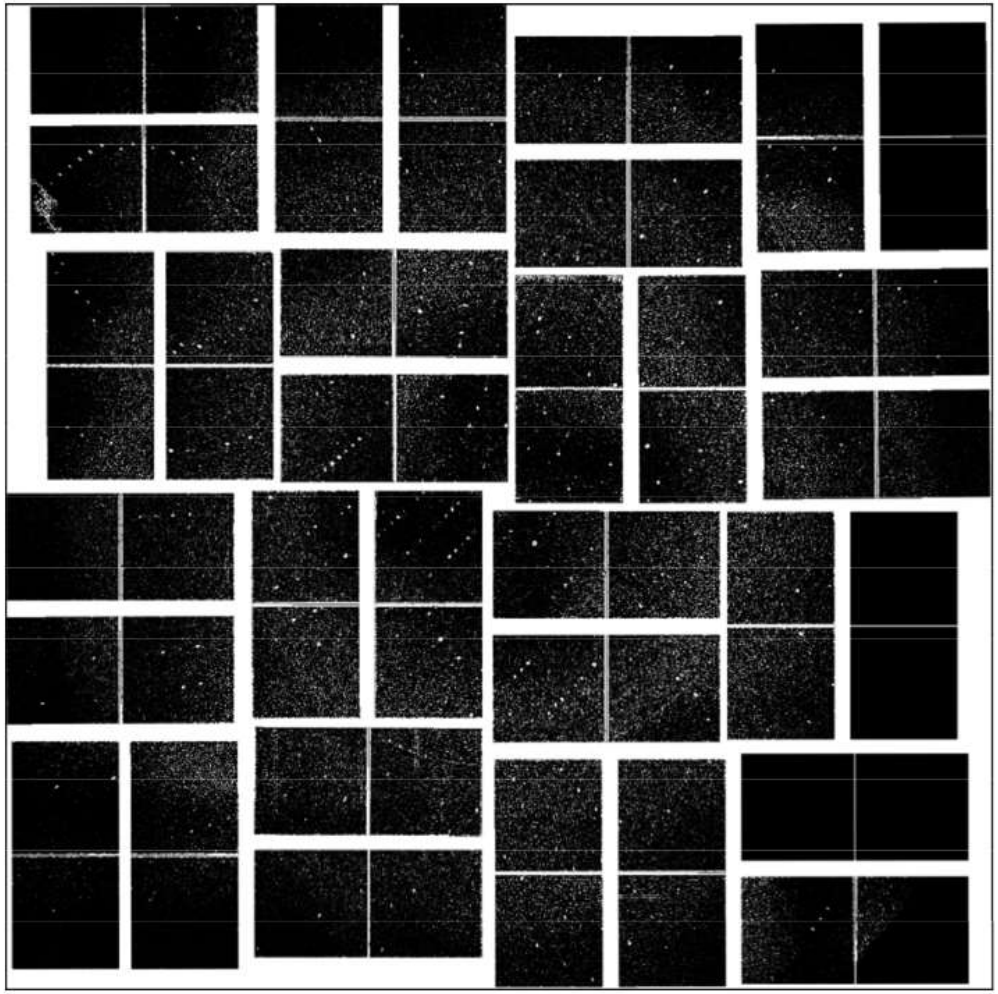

Comparison of FEL and synchrotron data

	40 fs	5 fs	Synchrot.
Dose / crystal	33 MGy	3 MGy	0.02 MGy
Dose rate [Gy / s]	8.3 x 10^{20}	5.8 x 10^{20}	9.6 x 10^{2}
Number of DP	~1.5 x 10^{6}	~2 x 10^{6}	100
Hits	66442	40115	100
Indexed DP	12247	10575	100
B-factor [Å^2]	28.3	28.5	19.4
R/R_{free} [%]	19.2 / 22.09	18.5 / 22.7	16.8 / 20.0

Resolution limit: 1.9 Å

R-factor *vs* resolution

40 fs LCLS data

(1 µm lysozyme crystals)

and

SLS synchrotron data

(200 µm lysozyme crystal, room temperature)

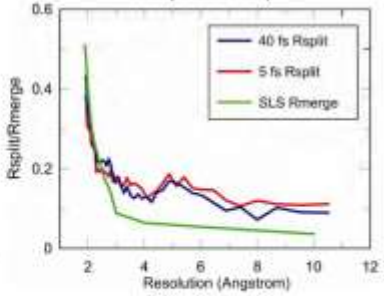

Boutet et al Science **337**:362 (2012)

Serial femtosecond crystallography yields undamaged high resolution structures

No difference density Fobs (synchrotron (SLS) – Fobs (LCLS))

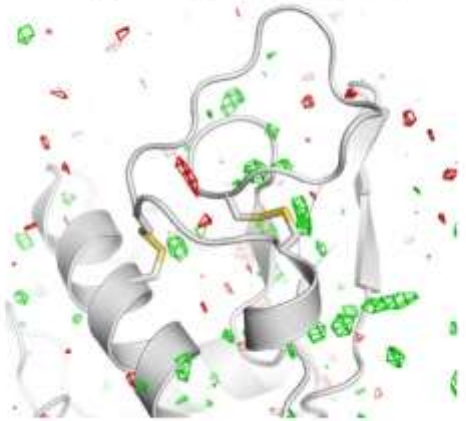

Boutet et al Science **337**:362 (2012)

FEL derived intensities provide high resolution structures

Molecular replacement-phased density, 1.9 Å resolution

-Resolution better than 2 Å because S-atoms in disulfides can be resolved separately, S-S distance is 2 Å

-Good definition of side chains

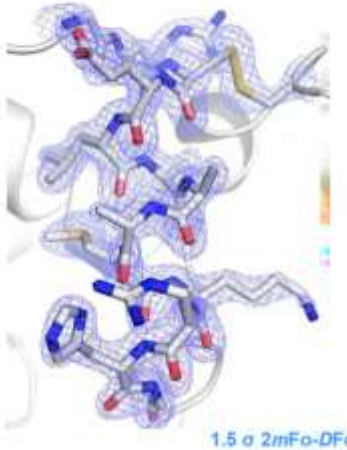

FEL derived intensities are good enough to see small differences

Molecular replacement with turkey lysozyme (Valine where there should be histidine)

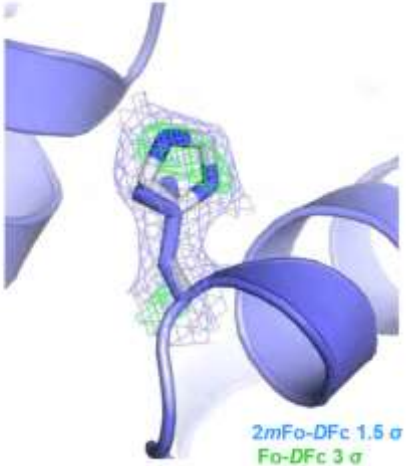

Applications of serial femtosecond crystallography

- Analysis of (sub)micron crystals, including membrane proteins in sponge (Nature Meth. **9**: 263 (2012)) or lipidic cubic phase (Science **342**: 1521 (2013))
- SAXS and WAXS measurements
- Time-resolved pump-probe studies on light-sensitive systems

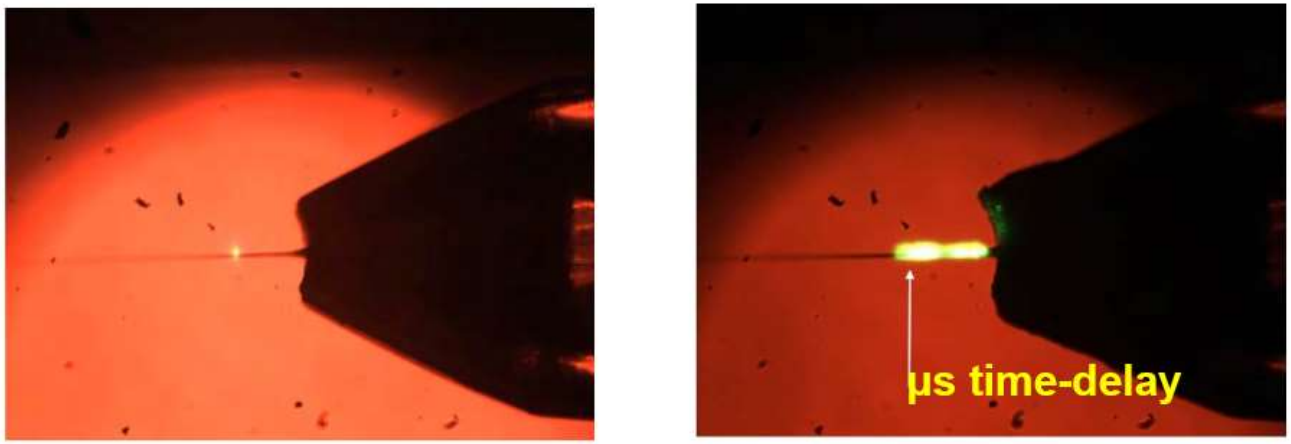

Placement of pump laser beam determines time delay

Aquila *et al* Optics Express **20**:2706 (2012)

European XFEL and PETRAIII in Hamburg

XFEL SPB/SFX beamline
Focus size 0.1 -1 µm
Photons/pulse 1 – 8 x 10^{12}
Pulse length few – 100 fs

PETRAIII P14 beamline
Focus size: 4-5 µm
Photons/second 7 10^{12}

Altarelli & Mancuso (2014)

ESRF UPGRADE PROGRAMME PHASE II 2015 -2022

The Phase II of ESRF UP will:

- Make the ESRF synchrotron light source more than 30 times brighter than ever before,
- Increase the coherence of the X-ray beams to levels approaching those of lasers,
- Boost instrumentation capacities,
- Enable new technologies in magnet, radiofrequency and vacuum systems,
- Reduce the energy consumption of the storage ring by 30%,
- Optimise returns on previous investments by a 90% re-use of existing infrastructure.

Table 1: Main beam and bare lattice parameters

Parameter	*Existing Lattice*	New Lattice
Energy, *E* [GeV]	*6.03*	6.03
Circumference, *C* [m]	*844*	844
Beam current [mA]	*200*	200
Horizontal Emittance [pm ·rad]	*4000*	160
Vertical Emittance [pm ·rad]	*5*	3.2
Bunch length, σ_z [ps]	*13*	11
Energy spread, σ_δ	*1.06 10^{-3}*	1.06 10^{-3}
Tune, ν_x, ν_y, ν_z	*36.44 , 13.39, 0.0054*	75.60 , 25.60 , 0.0034
Momentum compaction	*17.6 10^{-5}*	8.7 10^{-5}
Damping time, τ_x, τ_y, τ_z [ms]	*7 , 7 , 3.5*	7 , 11 , 7.9
Natural chromaticity, $\xi x0$, $\xi y0$	*-130 , -58*	-97, -79
Energy loss per turn, U0 [MeV]	*4.9*	3.05
RF voltage, *VRF* [MV]	*9*	6
RF frequency, *fRF* [MHz]	*352*	352
Harmonic number	*992*	992
Beta at ID center, βx , βy [m]	*37.6 , 3.0 (high β)* *0.35 , 3.0 (low β)*	3.35 , 2.79
Beam size at ID center, σx , σy [µm]	*413 , 3.9 (high β)* *50 , 3.9 (low β)*	23.5 , 3.7
Beam div. at ID center, $\sigma x'$, $\sigma y'$ [µrad]	*10 , 1.3 (high β)* *107, 1.3 (low β)*	6.9 , 1.3
Beta, beam size and div. at BM	βx= 1,1.6 βy= 42,32 [m] σx =85,113 σy= 13,11 [µm] σx'=114,99 σy'=0.5,0.4 [µrad]	βx= 0.68 βy= 4.02 [m] σx =13.1 σy= 3.5 [µm] σx'=15.4 σy'= 0.9 [µrad]

Phase I
180 million € during the period 2009 to 2015

- The constuction of 19 new generation experimental stations to explore the nanoworld
- The creation of a new ultra-stable experimental hall of 8000 m²
- The improvement and refurbishment of most of the cutting-edge scientific equipment and accelerator infrastructure

Phase II
150 million € during the period 2015 to 2022

- The construction of a new storage ring, inside the existing structure, with performance increased by a factor of 100
- The construction of new state-of-the-art beamlines
- An ambitious instrumentation programme (optics, high-performance detectors)
- An intensified big data strategy, designed in order to exploit the enhanced brilliance, coherent flux and performances of the new X-ray synchrotron source